

République Algérienne Démocratique et Populaire
Ministère de l'Enseignement Supérieur et de la Recherche Scientifique
Ecole Nationale Polytechnique



Département d'Elctrotechnique
Centre de Développement des Energies Renouvelables

End-of-study project dissertation for obtaining the State Engineer's
degree in Electrotechnics

Optimum DC-DC Buck Converter Used In Stand-Alone Photovoltaic Systems

Presented by :

Mr. BELLARBI Ali

Mr. RAHMOUNI Abdelhak

Under the direction of **Mr. Berkouk El Madjid Pr.**

Presented and defended publicly on : 26 June 2023

Composition of the jury :

President	Mr. Kamel BOUGHRARA	Pr. ENP
Examiner	Mr. Rabie BELKACEMI	Dr. ENP
Promoter	Mr. El Madjid BERKOUK	Pr. ENP
Promoter	Mr. Walid MERROUCHE	Dr. CDER

République Algérienne Démocratique et Populaire
Ministère de l'Enseignement Supérieur et de la Recherche Scientifique
Ecole Nationale Polytechnique



Département d'Elctrotechnique
Centre de Développement des Energies Renouvelables

End-of-study project dissertation for obtaining the State Engineer's
degree in Electrotechnics

Optimum DC-DC Buck Converter Used In Stand-Alone Photovoltaic Systems

Presented by :

Mr. BELLARBI Ali

Mr. RAHMOUNI Abdelhak

Under the direction of **Mr. Berkouk El Madjid Pr.**

Presented and defended publicly on : 26 June 2023

Composition of the jury :

President	Mr. Kamel BOUGHRARA	Pr. ENP
Examiner	Mr. Rabie BELKACEMI	Dr. ENP
Promoter	Mr. El Madjid BERKOUK	Pr. ENP
Promoter	Mr. Walid MERROUCHE	Dr. CDER

République Algérienne Démocratique et Populaire
Ministère de l'Enseignement Supérieur et de la Recherche Scientifique
Ecole Nationale Polytechnique



Département d'Electrotechnique
Centre de Développement des Energies Renouvelables

Mémoire de Projet de fin d'Etudes
Pour l'obtention du Diplôme d'Ingénieur d'Etat en Electrotechnique

**Convertisseur DC-DC Buck Optimal Utilisé
Dans Les Systèmes Photovoltaïques Autonomes**

Présenté par :
M. BELLARBI Ali
M. RAHMOUNI Abdelhak

Sous la Direction de M. Berkouk El Madjid Pr.
Présenté et soutenue publiquement le : 26 Juin 2023

Composition du jury :

Président	M. Kamel BOUGHRARA	Pr. ENP
Examineur	M. Rabie BELKACEMI	Dr. ENP
Promoteur	M. El Madjid BERKOUK	Pr. ENP
Promoteur	M. Walid MERROUCHE	Dr. CDER

ملخص

في هذا العمل، درسنا نظامًا ضوئيًا مستقلًا. أجريت الدراسة على النمذجة والتحكم وتحسين كفاءة محول باك في هذا النظام، ويتألف من نظام تخزين قائم على البطارية، ومولد ضوئي. تم إجراء دراسة نظرية ومحاكاة باستخدام أداة مطلب /سيميلينك وبرنامج البروتوس. يتم استخدام تقنية البحث عن نقطة الطاقة القصوى للحصول على التشغيل الأمثل لقوة النظام الضوئي. بالإضافة إلى ذلك، سمحت محاكاة النظام العام باستخدام برنامج مطلب بمراقبة الدور الحاسم للبطارية في النظام الكهروضوئي لتخزين الطاقة وتحسين عملية التحكم في النظام بأكمله.

المساهمة الرئيسية لهذا المشروع هي محاولة إعطاء التصميم الأمثل لمحول باك من خلال دراسة واختبار العوامل المختلفة التي يمكن أن تؤثر على كفاءته مثل تأثير جهاز التبديل وأخيرًا قدمنا نتائج الدراسة.

كلمات مفتاحية خلية ضوئية، نظام مستقل، متحكم، محاكات، تصميم، بطارية، محول باك، مردود.

Résumé

Dans ce travail, nous avons étudié un système photovoltaïque autonome. L'étude a été menée sur la modélisation, le contrôle et l'amélioration de l'efficacité du convertisseur buck dans ce système, composé d'un système de stockage à base de batterie, d'un générateur photovoltaïque. Une étude théorique et une simulation ont été réalisées à l'aide de l'outil MATLAB / SIMULINK et du logiciel proteus. La technique MPPT est utilisée pour obtenir un fonctionnement optimal de la puissance du GPV. En outre, une simulation du système global avec MATLAB a permis d'observer le rôle crucial de la batterie dans le système photovoltaïque pour le stockage de l'énergie et d'améliorer le processus de contrôle de l'ensemble du système. La principale contribution de ce projet est d'essayer de donner une conception optimale pour un convertisseur buck en étudiant et en testant les différents facteurs qui peuvent affecter son efficacité, comme l'effet de l'appareil de commutation et finalement nous avons donné les résultats de l'étude.

Mots clés: PV, autonome, MPPT, contrôle, Simulink, Proteus, conception, batterie, convertisseur abaisseur, efficacité.

Abstract

In this work, we studied an autonomous photovoltaic system. The study was carried out on modeling, control and enhancing the efficiency of buck converter in this system, consisting of a battery-based storage system, a photovoltaic generator. A theoretical study and simulation was done using the MATLAB / SIMULINK tool and proteus software. The MPPT technique is used to have optimal GPV power operation. Furthermore A simulation for the global system with matlab to observe the crucial role of the battery in the PV system for storing the energy and to enhance the control process of the whole system. The main contribution of this project is to try to give an optimum design for a buck converter by studying and testing the different factors that can affect its efficiency, As the effect of the switching device and eventually we gave the results of the study.

Keywords : PV, Stand-Alone, MPPT, Control, Simulink, Proteus, Design, Battery, Buck Converter, Efficiency.

Special thanks

Above all, we thank Almighty Allah for having given us the courage, willpower will, patience and health over all these years, and thanks to Him this work has been possible. We would also like to express our deepest gratitude to our promoters **Pr. EM. BERKOUK** and **Dr.W.MERROUCHE** for having proposed this subject, there patience, there unlimited help throughout our work, there rich advice and also for there kindness.

We would also like to thank the members of the jury for their interest in our work by agreeing to examine it.

We warmly thank our families and all our friends for their support and encouragement.

We'd also like to thank all the teachers for the quantity and quality of the knowledge and intellectual skills they passed on to us during these three years.

Finally, We would like to thank all the people who contributed in any way to the realization of this work.

Contents

List of figures

List of tables

General introduction	11
1 General overview on photovoltaic systems	12
1.1 Introduction	13
1.2 Photovoltaic generators	13
1.2.1 PV characteristics	15
1.2.2 Series and parallel connection of photovoltaic modules	15
1.3 Modeling a photovoltaic generator	17
1.3.1 Modeling a photovoltaic cell	17
1.3.2 I(V) and P(V) Characteristics	18
1.4 PV system applications	19
1.4.1 Stand-alone systems	19
1.4.2 Grid-connected systems	19
1.5 Command and control electronics	20
1.5.1 DC/DC converter	21
1.5.2 DC/AC converter	21
1.5.3 Charge controller	21
1.5.4 Batteries	21
1.5.5 Maximum power point search techniques MPPT	22
1.6 Conclusion	24
2 DC-DC converters	25
2.1 Introduction	26
2.2 Basic structure of DC-DC converters	26
2.3 DC-DC converter components	27
2.3.1 MOSFET transistor	27
2.3.2 Schottky diode	28
2.3.3 Capacitor	28
2.3.4 Inductance	29
2.4 Different types of DC-DC converters	30
2.5 Operating modes of DC-DC converters	30
2.6 Sizing and converter operating concept (BUCK)	31
2.6.1 Structure	31
2.6.2 Continuous conduction mode CCM	31
2.6.3 Discontinuous conduction mode DCM	37
2.7 DC-DC buck converter control	42
2.7.1 PWM control	42
2.7.2 Proportional-Integral (PI) linear control	44

2.8	Conclusion	47
3	Control and simulation of Buck converter	48
3.1	Introduction	49
3.2	Assumptions :	49
3.3	Buck converter sizing	50
3.4	Component selection and calculation :	50
3.5	Simulation and Observation	51
3.5.1	Matlab Simulation :	51
3.5.2	Proteus Simulation:	63
3.6	Global system simulation:	69
3.7	Conclusion	77
4	Design and realization of the power circuit (Buck converter)	78
4.1	Introduction:	79
4.2	Testing and observing the results for the tested buck converter:	79
4.2.1	Description of the board :	79
4.3	Choice and description of board components:	86
4.3.1	« MOSFET » switch	86
4.3.2	Diode	86
4.3.3	Ferrite core coil	87
4.3.4	Capacitors	87
4.3.5	MOSFET-DRIVER «IR2112»	88
4.4	Power Losses and Efficiency of the Buck Converter:	91
4.5	Conclusion	93
	Conclusion and perspectives	94
	Bibliography	96

List of Figures

1.1	Semi-conductor material doping and the photovoltaic effect [2].	13
1.2	Construction of a photovoltaic generator [3].	14
1.3	Placement of bypass and non-return diodes [2].	14
1.4	Current-voltage characteristic of N_s series cell [4].	16
1.5	Current-voltage characteristic of N_p parallel cell [4].	17
1.6	Equivalent diagram of a real photovoltaic cell [5].	17
1.7	Caractéristique I(V) d'une cellule photovoltaïque [4].	18
1.8	Caractéristique P(V) d'une cellule photovoltaïque [4].	18
1.9	Stand-alone photovoltaic system [6].	19
1.10	Grid-connected photovoltaic system [6].	20
1.11	General scheme for stand-alone photovoltaic system [7].	20
1.12	Controlling the charging and discharging operation of the battery [6]	21
1.13	Primary: Alkaline batteries.	22
1.14	Secondary: Lead Acid batteries [6]	22
1.15	Perturb and observe method technique operation[6].	23
1.16	behavior of the PO algorithm under a change in illuminance	24
2.1	Converter dc dc schematic diagram	26
2.2	Symbolic representation and notation for the N-channel MOSFET	27
2.3	Structure of a low-power MOSFET cell.	27
2.4	power diode	28
2.5	simple inductance L	29
2.6	Coil current waveforms: (a) CCM, (b) DCM .[14]	30
2.7	Buck converter circuit [14].	31
2.8	Equivalent circuit during $(0 \leq t \leq d.T)$ [14].	31
2.9	Equivalent circuit during $(dT \leq t \leq T)$ [14].	32
2.10	Form of current and voltage in the inductor during continuous conduction [15].	34
2.11	Form of current and voltage in the Sw switch [15].	35
2.12	Form of current and voltage in Diode D [15].	36
2.13	Waveform of current $I_{L(t)}$ and voltage $V_{s(t)}$ [14].	37
2.14	Equivalent circuit during $(0 \leq t \leq d.T)$ [14].	38
2.15	Form of inductance current and voltage [15].	39
2.16	Form of switch current and voltage Sw.[15]	40
2.17	Form of diode current and voltage D [15].	41
2.18	Signal form generated by the PWM technique [14].	42
2.19	PWM signal waveform [17].	43
2.20	Schematic diagram of direct duty cycle control.[22]	46
2.21	Diagram of Buck converter regulated in VMC [22].	47

3.1	Matlab-level task representation [24].	52
3.2	Bode diagram of the voltage loop transfer function.	53
3.3	System response no corrected in closed loop	54
3.4	Bode diagram of the voltage loop transfer function.	55
3.5	Response of a closed-loop corrected system	56
3.6	Simulation of buck converter	57
3.7	Control signal generation for $V_{ref} = 12V$	57
3.8	Control signal	58
3.9	Voltage curve Vs	58
3.10	Load current Is	58
3.11	Control signal generation for $V_{ref} = 6V$	59
3.12	Control signal	59
3.13	Voltage curve Vs	59
3.14	Load current Is	60
3.15	Control signal generation for $V_{ref} = 18V$	60
3.16	Control signal	60
3.17	Voltage curve Vs	61
3.18	Load current Is	61
3.19	Efficiency vs the duty cycle d	61
3.20	PROTEUS interface.[25]	63
3.21	Buck Converter circuit diagram	64
3.22	PWM script code	64
3.23	The control signal	65
3.24	Voltage curve Vs(red) ,current Is(green)	65
3.25	The control signal	66
3.26	Voltage curve Vs(red) ,current Is(green)	66
3.27	The control signal	67
3.28	Voltage curve Vs(red) ,current Is(green)	67
3.29	Efficiency vs the duty cycle d	68
3.30	Global system simulation block	69
3.31	SIMULINK model of the photovoltaic panel	69
3.32	Different radiation values at a given time.	70
3.33	I-V (current-voltage) and P-V (power-voltage) characteristics.	70
3.34	P&O Flowchart algorithm [26].	71
3.35	PV Voltage Evolution (in V).	72
3.36	PV Current Evolution (in A).	72
3.37	PV Power Evolution (in W)	72
3.38	Battery Voltage Evolution (in V).	73
3.39	Battery Current Evolution (in A).	73
3.40	Battery Power Evolution (in W)	73
3.41	State of charge of the battery.	74
3.42	Global system simulation with a resistive load.	74
3.43	PV Voltage Evolution (in V).	75
3.44	PV Current Evolution (in A).	75
3.45	PV Power Evolution (in W)	75
3.46	Load Voltage Evolution (in V).	76
3.47	Load Current Evolution (in A).	76
3.48	Load Power Evolution (in W)	76

4.1	TLP250-Buck converter schematic, PCB and 3D view	80
4.2	MOSFET IRFP140N [27]	81
4.3	Efficiency vs duty cycle for IRFP140N	82
4.4	MOSFET IRFZ44N [28].	82
4.5	Efficiency vs duty cycle for IRFZ44N	83
4.6	MOSFET IRF2807 [29].	84
4.7	Efficiency vs duty cycle for IRF2807N	84
4.8	Average Efficiency Comparison for IRFP140N ,IRFZ44N , IRF2807	85
4.9	MOSFET IRF2807 [29].	86
4.10	Schottky Diode MBR3060PT [31].	87
4.11	Ferrite core coil	87
4.12	Capacitor $330\mu F - 63V$	88
4.13	IR2112 Functional Block Diagram [32]	88
4.14	IR2112-DRIVER overview [32].	89
4.15	Diode UF4007 [33].	90
4.16	Buck converter schematic, PCB and 3D view	90
4.17	Realized buck converter overview	92
4.18	Experimental platform	92
4.19	Efficiency vs duty cycle for the realization buck converter	93

List of Tables

- 3.1 Design specification 50
- 3.2 Component specification 63

- 4.1 Components specification 80
- 4.2 IRFP140N results 81
- 4.3 IRFZ44N results 83
- 4.4 IRF2807N results 84
- 4.5 Testing results 93

General introduction

Renewable energies are generated by regular or constant natural phenomena caused mainly by the Sun, Moon, wind, water and Earth . For these inexhaustible energy resources, the issues of the day are design, optimization and implementation. So the techniques for generating electricity from these resources require further study, with the aim of maximizing the power extracted from these sources, plus lower costs (of manufacture, use and recycling). The use of PV energy would make it possible to supply electricity to sites isolated from the grids and avoid the need to build new power lines, which are generally investment. Photovoltaic systems use cells to convert solar radiation into electricity, and they are responsible for the energy conversion[1].

The aim of our project is to study one type of PV system, and to design and control one of its components, the buck Converter.This project is divided into four chapters:

First of all, we need to mention a few general facts about PV generators and its characteristics. followed by a look at the techniques for using this energy. The principle of converting solar power into electrical power, We talk about PV systems and the different applications involved. we will take a look at the different components of the stand alone system and specify its rules in the system.

The second chapter is concerned about DC-DC converters, with different types ,basic structure , the electronics components for there design , the two operating modes(Continuous conduction mod(CCM) and discontinuous conduction mod(DCM)) . And to give a detailed operating concept analysis for the buck converter in the two CCM and DCM modes,and a definition and concept for the PWM control method.

In the next chapter we will try to do a simulation for the buck converter with matlab and proteus softwars,for a specific assumptions and characteristics.and observe the circuit performance as each component contributes to overall performance.

Also a simulation for the global system with matlab for seeing the crucial role for the battery in the pv system for storing the energy and enhance the control process of the whole system.

The last chapter,we try to give an optimum design for a buck converter by studying and testing the different factors that can affect its efficiency , In particular the effect of the switching device then we give the results of the study.

Lastly this work will conclude with a general conclusion, and a bibliography that brings together all the documents consulted in the course of the work.

Chapter 1

General overview on photovoltaic systems

1.1 Introduction

Solar energy is available everywhere on the planet, and it is completely renewable. Its contribution varies depending on the days and seasons, but it is relatively predictable. Photovoltaic systems do not require any external supply of fuel, and furthermore, the generator itself does not contain any moving parts and therefore requires very little maintenance. As a result, the recurring costs of operation and maintenance are relatively low. Photovoltaic solar energy is increasingly being used to power various terrestrial applications such as lighting, telecommunications, refrigeration, and pumping[1].

1.2 Photovoltaic generators

The photovoltaic generator is the unit that produces electrical energy from solar radiation in direct current. The photovoltaic cell is the generator's basic unit, responsible for converting sunlight into electricity using the photoelectric effect.

Photovoltaic cells, which convert sunlight directly into electricity, are made from semiconductor materials. The voltage generated by a photovoltaic cell is therefore limited to the gap value of the material used, which is 0.6 V for crystalline and amorphous cells.

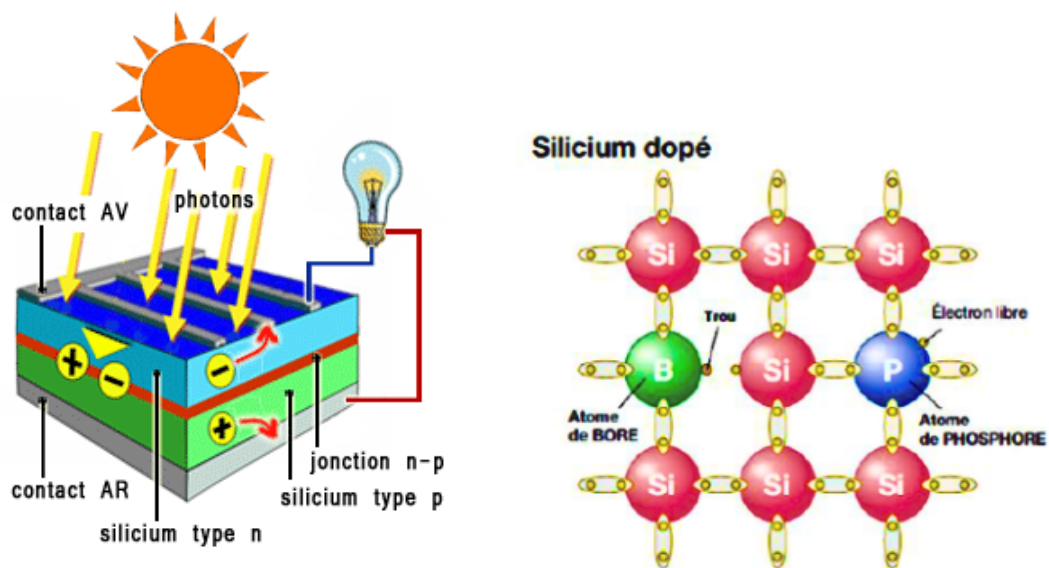


Figure 1.1: Semi-conductor material doping and the photovoltaic effect [2].

The current depends on the cell's surface area, but is also influenced by its efficiency. Monocrystalline cells have an efficiency of around 15 to 22%, while multicrystalline cells have an efficiency of around 10 to 15 % [2].

To form a photovoltaic module, cells are grouped in series and in parallel. This enables higher voltage and current to be obtained, adapted to the needs of larger-scale electricity production.

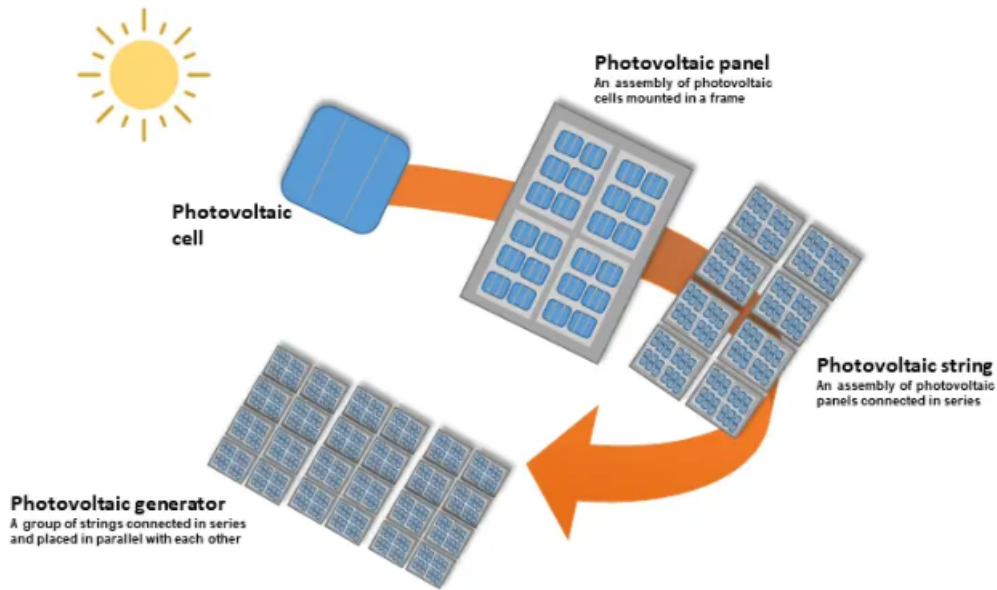


Figure 1.2: Construction of a photovoltaic generator [3].

The cells are grouped in series and in parallel to form a photovoltaic module (from 36 to 72 cells) to deliver the desired final power, reflected by a current and voltage. characterizing the module’s operating point. In order to further increase power, several modules are connected in series to form arrays which, in turn, are assembled in parallel. These,are connected in parallel to form a PV field or generator. In addition to mechanical protection (aluminum frame, glass encapsulation...) against adverse weather conditions, the modules can also be used to generate electricity. meteorological conditions, bypass diodes and anti-reverse diodes are used to protect against the effects of dissipation and reverse currents caused by, among other things dissymmetry and shading[2].

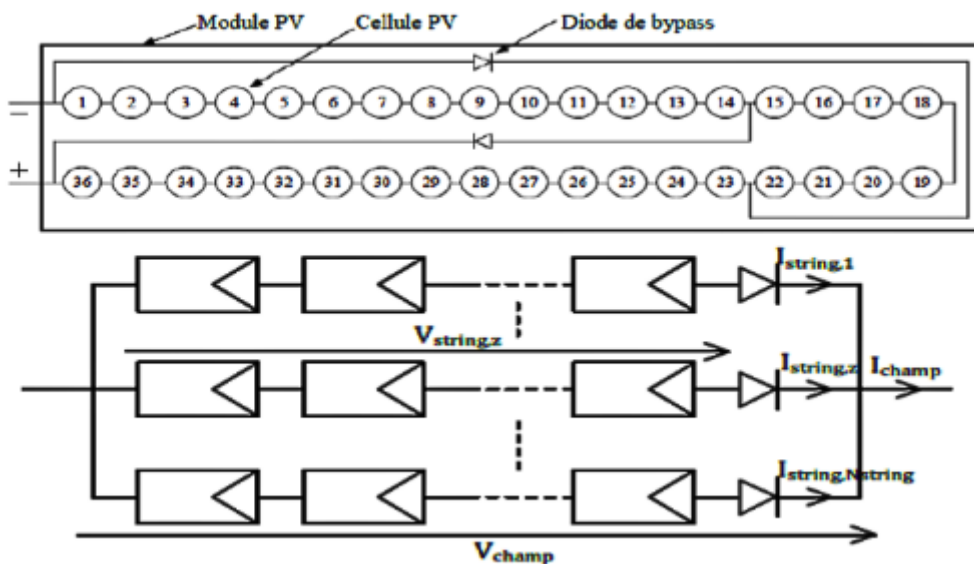


Figure 1.3: Placement of bypass and non-return diodes [2].

1.2.1 PV characteristics :

Peak power P_c :Maximum electrical power that the module can supply under standard conditions (25^{deg}C and an illumination of 1000 W/m^2).

Characteristic $I = f(V)$:Curve showing the current I delivered by the module as a function of the voltage at its terminals.

Open circuit voltage V_{co} :Voltage at module terminals in the absence of any current, for "full sun" illumination. It is equal to 0.6 V for the crystalline cell.

Short-circuit current I_{cc} :This is the current obtained by short-circuiting the cell terminals. (by taking $V = 0$ in the equivalent diagram). It increases linearly with cell illumination intensity, and depends on the illuminated surface, radiation wavelength, carrier mobility and temperature.

Optimum operating point $P_m(V_m, I_m)$: When peak power is at its highest in full sunlight, $P_m = V_m \cdot I_m$.

Efficiency : Efficiency is given by the ratio of maximum electrical power generated to the power of incident solar radiation.

$$\eta = \frac{V_{\text{max}} \cdot I_{\text{max}}}{P_{\text{solaire}}} \quad (1.1)$$

Form factor : Ratio between optimum power P_m and maximum power that the cell can deliver: $V_{co} \cdot I_{cc}$

1.2.2 Series and parallel connection of photovoltaic modules :

Both types of grouping, series and parallel, are commonly used to obtain the desired output voltage and current values. For N_s cells in series, constituting branches themselves N_p in parallel. The power available at the output of the PV generator is given by the equation (1.2).

$$P_{pv} = N_s \cdot V_{pv} \cdot N_p \cdot I_{pv} \quad (1.2)$$

With:

- P_{pv} : Available power at GPV output.
- V_{pv} : Voltage at GPV output.
- I_{pv} : GPV output current.

Association in series :

Equation (1.3) summarizes the electrical characteristic of a series association of N_s cells. The current-voltage of N_s series cell :

$$V_{pv} = N_s \cdot V_{CO} \quad (1.3)$$

$$I_{pv} = I_{CC} \quad (1.4)$$

With :

- V_{pv} : The voltage generated by a photovoltaic module with N_s cells in series.
- I_{pv} : The current across the photovoltaic module of N_s cells in series.

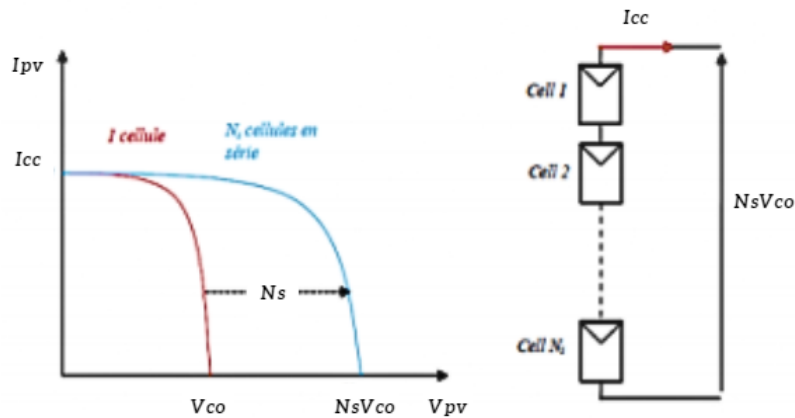


Figure 1.4: Current-voltage characteristic of N_s series cell [4].

Association in parallel :

Equation (1.6) summarizes the electrical characteristics of a parallel association of N_p cells.

The current-voltage of N_p parallel cell is defined by the following equation:

$$V_{pv} = V_{CO} \quad (1.5)$$

$$I_{pv} = N_p \cdot I_{CC} \quad (1.6)$$

A parallel combination of N_p A parallel combination of N_p cells is possible, and allow increasing the generator's output current.

When a group of identical cells is connected in parallel, all cells are subjected to the same voltage. The resulting grouping characteristic is obtained by summing the currents of the individual cells.

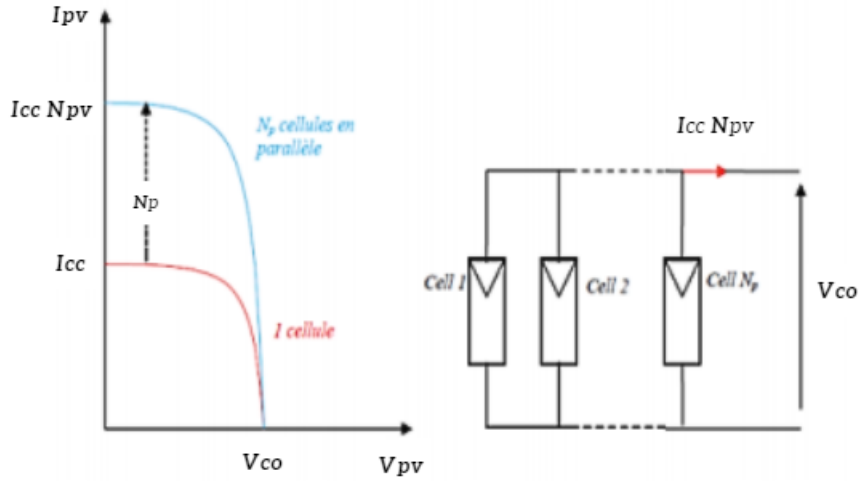


Figure 1.5: Current-voltage characteristic of N_p parallel cell [4].

1.3 Modeling a photovoltaic generator

1.3.1 Modeling a photovoltaic cell :

The performance of a solar cell is limited by the influence of two physical phenomena that can be linked to two resistances R_s and R_p . R_s : Series resistance, mainly due to Joule-effect losses through collector grids and the resistance of semiconductors, as well as poor contacts (semiconductor, electrodes). R_p : Parallel resistance, known as "Shunt", results from recombination losses due mainly to thickness, surface effects and the non-ideality of the junction[5].

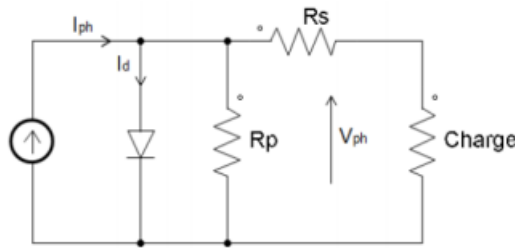


Figure 1.6: Equivalent diagram of a real photovoltaic cell [5].

$$I = I_{ph} - I_D - I_{R_p} \tag{1.7}$$

I_D :The junction current I_D given by :

$$I_D = I_0 \left(\exp \left(\frac{V + R_s \cdot I}{V_T} \right) - 1 \right) \tag{1.8}$$

The current in the resistor R_p is given by :

$$I_{R_p} = \frac{V + R_s \cdot I}{R_p} \quad (1.9)$$

Replacing equations (1.8) and (1.9) in (1.7), the characteristic equation becomes :

$$I = I_{ph} - I_0 \left(\exp \left(\frac{V + R_s \cdot I}{V_T} \right) - 1 \right) - \frac{V + R_s \cdot I}{R_p} \quad (1.10)$$

1.3.2 I(V) and P(V) Characteristics

When considering irradiance, temperature and specific cell parameters, the relationship between current and voltage is defined, which is an implicit non-linear equation requiring numerical resolution. Typical current-voltage and power-voltage characteristics described by this equation are illustrated in Figure 1.7,1.8.

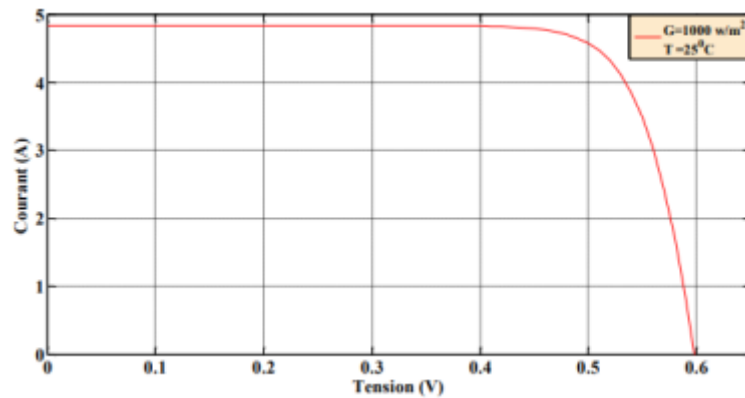


Figure 1.7: Caractéristique I(V) d'une cellule photovoltaïque [4].

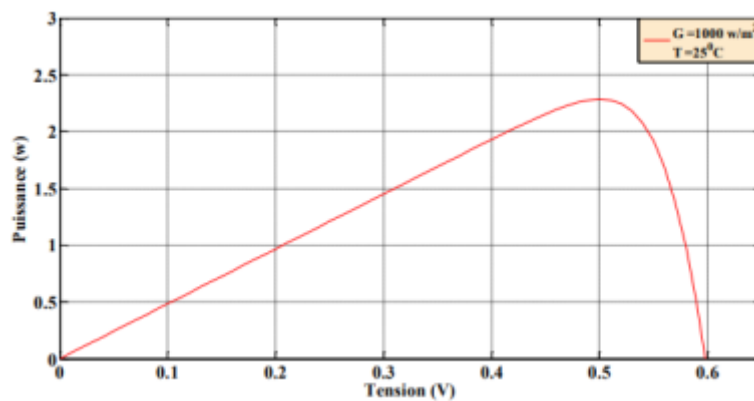


Figure 1.8: Caractéristique P(V) d'une cellule photovoltaïque [4].

1.4 PV system applications :

The following broad categories of applications stand out as being most likely to be powered by photovoltaic energy :

Stand-alone production systems to supply isolated sites or equipment not connected to the electricity grid.

Generation systems connected to the distribution grid.

Hybrid systems, which combine photovoltaic energy with another source, such as wind power.

1.4.1 Stand-alone systems :

This system operates independently of any other energy source. In most cases, it is used in isolated locations. In these locations, the photovoltaic field is sized to supply the electrical energy required to operate specific loads such as lighting and domestic equipment. A control system and a battery are used to store electrical energy for use in the absence of sunlight [6].

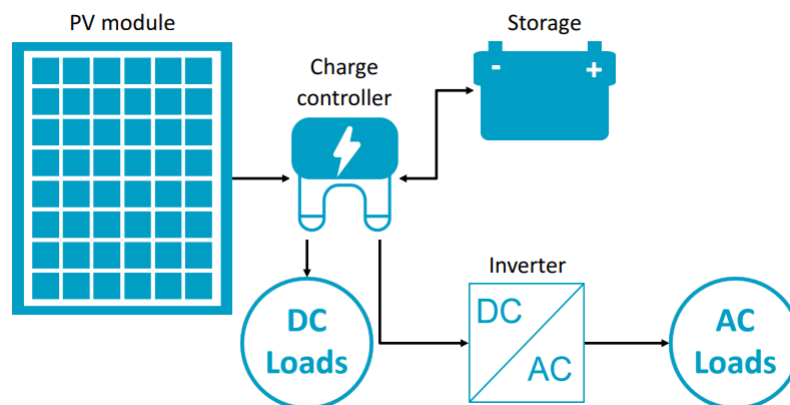


Figure 1.9: Stand-alone photovoltaic system [6].

1.4.2 Grid-connected systems :

The photovoltaic field is connected to the grid via an inverter, whose main role is to feed the electricity produced into the grid. Individuals can resell all or part of the electricity they produce. In this case, energy storage batteries are not required [6].

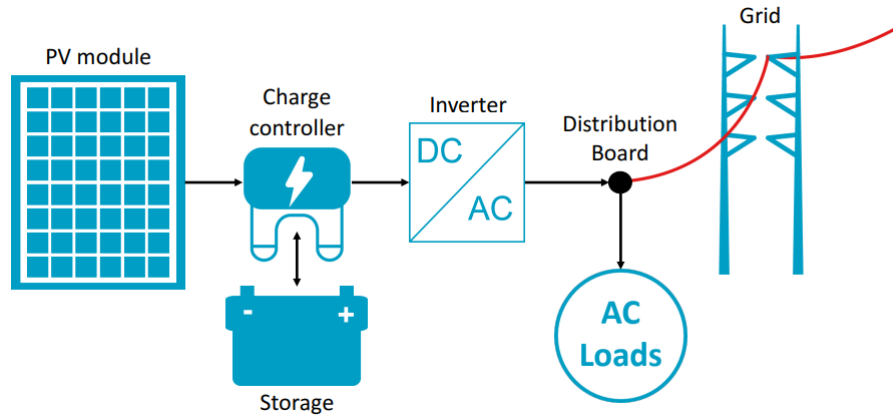


Figure 1.10: Grid-connected photovoltaic system [6].

1.5 Command and control electronics :

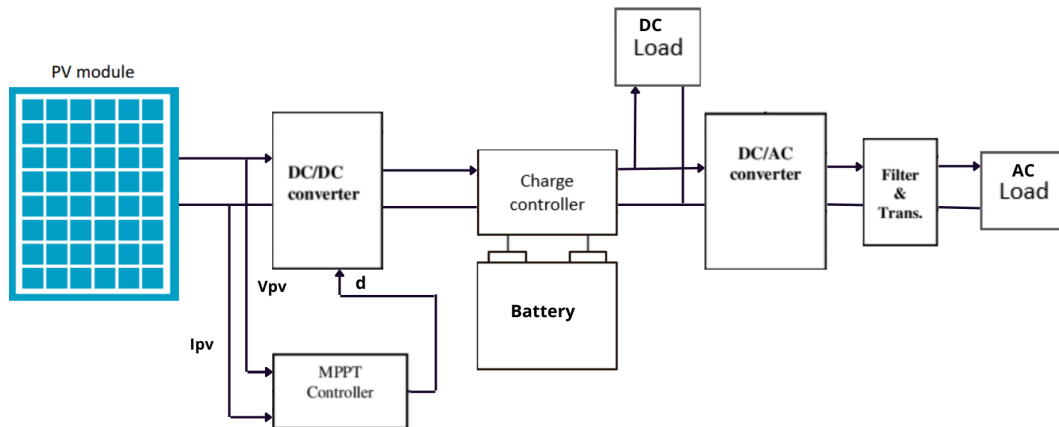


Figure 1.11: General scheme for stand-alone photovoltaic system [7].

As shown in Figure 1.11, the standalone system is composed of various components and blocks, which are :

- DC/DC converters
- Charge controller
- MPPT controller
- Storage battery
- DC/AC converters

An energy converter is a piece of equipment that is generally placed either between the photovoltaic field and the DC load (without storage, it's called a DC-DC converter), or between the battery and the AC load (after storage, it's called an inverter or DC-AC converter).

The converter performs the following functions :

Optimization of the DC voltage so that the module array operates under optimum power conditions.

Conversion of direct current to alternating current compatible with mains voltage network.

1.5.1 DC/DC converter

To maximize the power available from the photovoltaic generator (GPV) and deliver it efficiently to the load, it is common practice to use a matching stage. This stage acts as an interface between the GPV and the load, and ensures, by means of a duty cycle-controlled control, the transfer of the maximum power supplied by the generator, in order to get as close as possible to the maximum power available [8].

1.5.2 DC/AC converter

In a photovoltaic system, the connection between the photovoltaic generator and the AC load is provided by an inverter. The DC/AC converter ensures optimum power transfer from the solar generator to the the AC load group [9].

1.5.3 Charge controller

The charge controller is principally established in the battery connected systems. The charge controller is generally connected to PV modules. It is also connected to the battery and other loads of the system. The charging rate of the battery fluctuates and may, under some illumination conditions, exceed the rated current of the battery which would be harmful to the battery. To prevent this situation from happening, the device that is inserted in the PV system is the charge controller [6].

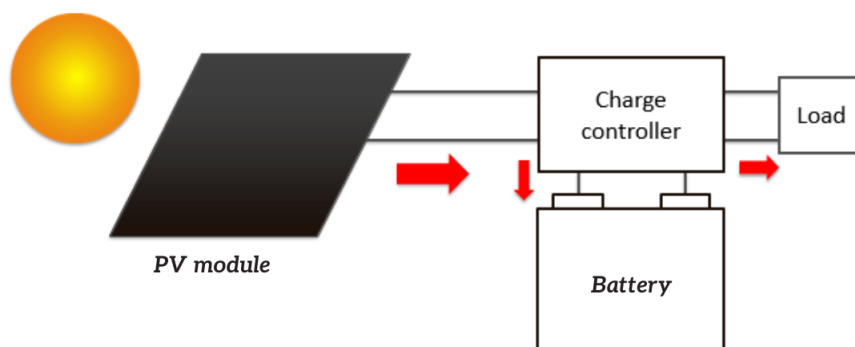


Figure 1.12: Controlling the charging and discharging operation of the battery [6] .

1.5.4 Batteries

Batteries are typically used in off-grid PV systems. The PV Modules are connected to a charge controller. This charge controller then connects to the battery as well as the inverter and DC

Loads. So the battery is connected on the DC side of the PV system. Basically, current from the PV modules will either flow into the battery or go to the loads, The standalone PV system needs a battery and we just cant power the loads with solar energy directly for One major reason is the mismatch between supply and demand. There are two types of batteries :

- Primary batteries. These are batteries such as zinc carbon and alkaline batteries.
- Secondary batteries, can take energy in. They are also called “rechargeable” batteries. These are the only batteries of interest for PV systems. Secondary batteries such as lead-acid and lithium ion batteries are commonly used[6].



Figure 1.13: Primary: Alkaline batteries.



Figure 1.14: Secondary: Lead Acid batteries [6] .

1.5.5 Maximum power point search techniques MPPT :

Photovoltaic cells are widely used to supply energy in many electrical applications. To optimize the power supplied by the solar panel, a device called Maximum Power Point Tracking (MPPT) is used to regulate variations in the cells' current-voltage characteristic. MPPT (Maximum Power Point Tracking) is a mechanism (whose operation needs to be determined) that positions itself on the maximum point of a photovoltaic cell's power characteristic, and remains there despite variations in temperature, sunlight or other factors.

Maximum Power Point Tracking (MPPT) was developed to ensure the best possible connection between the photovoltaic generator and the load, and to produce the best possible power. since 1968, these types of controllers force the generator to work at its Maximum Power Point (MPP), resulting in improved system efficiency [10].

In the literature, several tracking methods have been proposed, but the most widely most widely used and least expensive :

- Perturber and Observer algorithms (P O).

- Conductivity Increase Algorithms (INC: Incremental Conductance).
- Constant Voltage (CV) algorithms.
- Parasit Capacitance (PC) algorithms.

The efficiency of an MPPT module is defined by :

$$\eta = \frac{\int_0^t P_m(t) \cdot dt}{\int_0^t P_{max}(t) \cdot dt} \tag{1.11}$$

With :

P_m : Measured power produced by the PV panel under MPPT control.

P_{max} :Maximum power they could produce under the same temperature and the same Sunshine.

Perturbation and observation method :

This method is quite simple and straightforward. Basically, the MPPT continuously makes incremental changes to the voltage and monitors changes in power.

- If $\Delta P > 0$ then the voltage perturbation moves the operating point closer to the MPP and we continue to perturb the voltage in the same direction, this will move the operating point until the MPP is reached..

- If $\Delta P < 0$ the operating point is moving away from the MPP so we perturb the voltage with an algebraic sign opposite to the previous sign to move the operating point until the MPP is reached.

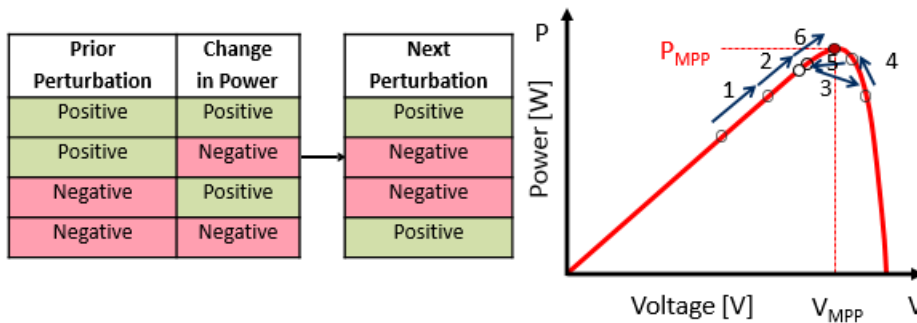


Figure 1.15: Perturb and observe method technique operation[6].

In figure 1. 16 we consider that the operating point is on curve (1), the MPPT oscillates around the MPP from point A_2 to point A then back to point A_1 and vice versa, if the value of the illuminance increases, the curve $P(V)$ of the panel moves towards curve (2) then the MPPT disturbs the operating point from point A to point B_1 which leads to $\Delta P > 0$ with $[\Delta P = P(K) - P(K - 1)]$ and the MPPT continues to perturb the voltages in the same direction, i.e. towards the B_2 point.

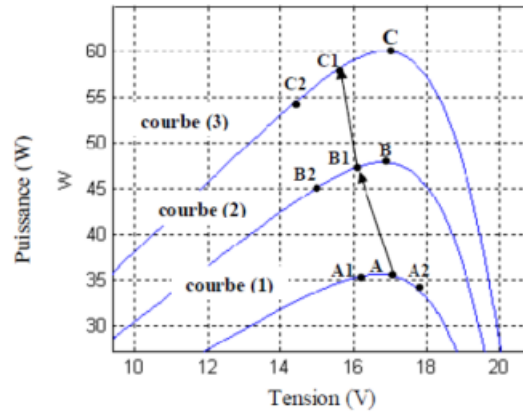


Figure 1.16: behavior of the PO algorithm under a change in illuminance

If the illuminance still increases, the operating point moves to the point C_1 on curve (3) instead of the point B_2 on curve (2), then the MPPT still has $\Delta P > 0$ and moves the operating point to the point C_2 . From the points $A \rightarrow B_1 \rightarrow C_1 \rightarrow C_2$ the algorithm P&O continues to move away from the MPP which gives a power that will be lost and the efficiency decreases.

1.6 Conclusion

In this chapter, we have reviewed the principle of converting and exploitation of solar energy into usable (electrical) energy, In addition the characteristics of photovoltaic cells and the various structures of a PV installation, specifically the structures for an off-grid installation, with all the components composing it and its purpose. In the next chapter, we'll look at DC-DC converters, which can convert the low-amplitude from PV panels into a useful voltage.

Chapter 2

DC-DC converters

2.1 Introduction

A chopper, also known as a DC-DC converter, is a power electronic device that changes the voltage value of a high-efficiency DC voltage source using one or more controlled switches. The conversion is performed at high frequency. If the output voltage is lower than the input voltage, the device is referred to as a buck converter. If the output voltage is higher than the input voltage, we speak of a "boost" chopper. Some choppers can operate in both directions (boost and buck). In some applications, choppers are also reversible, meaning they can supply power to the load. A DC motor is often used in this type of application, or a device derived from it can be used to brake the machine [11].

There are different classifications of DC-DC converters, one of which depends on the insulating properties of the primary and secondary sections. This isolation is generally implemented using a transformer, which has a primary section on both the input and output sides. The control loop is implemented using another transformer. In this way, the output is galvanically isolated from the input.

However, this isolation is costly, which is why some DC-DC converter applications prefer not to have galvanic separation between input and output.

Buck and boost DC-DC converters are widely used in photovoltaic systems to adjust voltages and currents as required. They consist only of reactive elements such as inductors and capacitors, which ideally consume no energy. This is why they are so efficient [12].

2.2 Basic structure of DC-DC converters

In the study of chopper converters, we assume that the input source of the converter is a DC voltage V_e and that the output is also a DC voltage V_s . We also consider that the load can be represented by a resistor R .

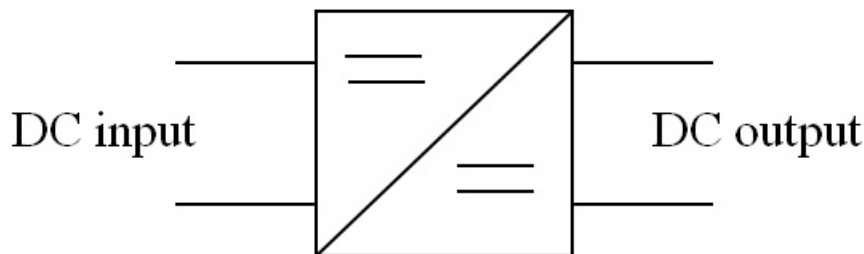


Figure 2.1: Converter dc dc schematic diagram

The DC-DC converter consists mainly of transistors, diodes, inductors, capacitors and other passive components. Under ideal conditions, these devices dissipate no active power, which explains the high efficiency of these converters.

2.3 DC-DC converter components

2.3.1 MOSFET transistor :

The MOSFET is a metal-oxide semiconductor field-effect transistor. Its usual symbolic representation is given in figure (2.2.a), with an arrow indicating the forward direction of the two junctions substrate-source and substrate-drain, starting from the terminal connected to the substrate (bulk). In general, the substrate and source are connected, as shown in figure (2.2.b), which also shows the notations used.

To manufacture a MOSFET, a P-type semiconductor (Fig. 2.3) is doped with two N-type zones, to which the source (S) and drain (D) contacts are soldered. An oxide layer is deposited on the P zone between source and drain, and the gate contact (G) is welded to this layer. The prefix MOS is used to characterize this type of transistor because of the Metal-Oxide-Semiconductor sequence.

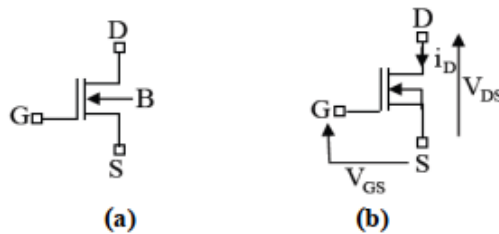


Figure 2.2: Symbolic representation and notation for the N-channel MOSFET

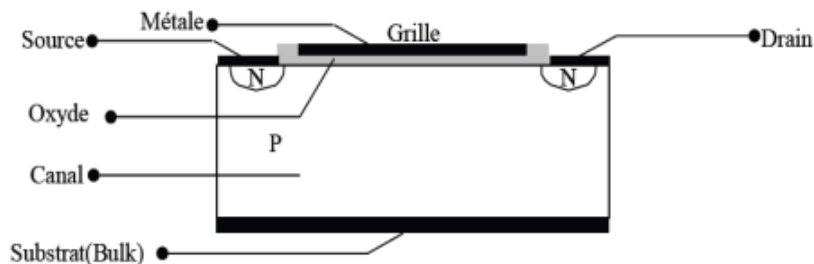


Figure 2.3: Structure of a low-power MOSFET cell.

The MOSFET offers several advantages as a power transistor, including :

- low on-state resistance (R_{DSon}) to minimize ohmic losses and improve efficiency.
- high switching capacity for fast, precise switching.
- galvanic isolation between source and grid, avoiding reverse conduction and noise problems.
- no gate current, reducing switching losses and facilitating control circuit design [13].

2.3.2 Schottky diode :

Schottky diodes offer two advantages over conventional diodes :

- electrical characteristic: 600 V blocking voltage .
 - lower threshold voltage ($V_F \approx 0.3V$).
- Schottky diodes have very short reverse recovery times (t_r from 0.15 to 0.35 μs).

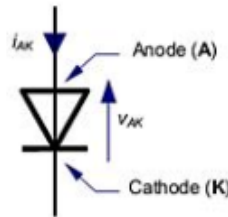


Figure 2.4: power diode

Schottky diode applications :

Schottky diodes are used at low voltages in circuits requiring high switching speed, for example in the high-frequency chopper circuits found in chopper circuits ,found in switch-mode power supplies [13].

2.3.3 Capacitor :

In switch-mode power supplies, capacitors play two distinct roles: they supply energy during variations in control or load, and they also act as switching or filter capacitors to ensure smooth high-frequency operation of the power supply. Low series resistance electrolytic capacitors, also known as chemical capacitors, are commonly used for this function, as they offer high capacitance and excellent frequency response. Capacitors are characterized by physical quantities that define their fields of application. The capacitance of a capacitor is equal to the ratio of the electrical charge Q stored to the voltage V applied across its electrodes.

$$C(F) = Q(C)/V(V)$$

The expression of capacitance for a capacitor with plane-parallel plates is simplified and given by the equation :

$$C = \epsilon_r \epsilon_o S / e$$

With:

ϵ_o : Permittivity of vacuum.

ϵ_r : Relative permittivity (2 to 20000) of the dielectric.

e : dielectric thickness .[13]

2.3.4 Inductance :

Inductors store electrical energy in magnetic form and release it later. Air coils can be used for this function, but the use of magnetic circuits offers two important advantages :

- 1-smaller footprint with equivalent inductance value
- 2-limitation of stray radiation by confining magnetic flux to a small area.

Inductors are mainly used for filtering, power conversion (e.g. in switch-mode power supplies), and magnetic switches (using saturable inductors). The equivalent circuit diagram of a simple L inductor is as follows :

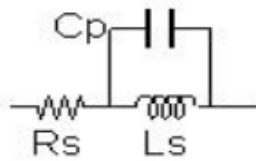


Figure 2.5: simple inductance L

where R_s represents the series resistance of the wound wire and C_p the inter-turn parasitic capacitances. The value of the inductance is obtained by:

$$L = \mu_o \mu_e \frac{S_e}{l_e} N^2$$

With : $\mu_o = 4\pi 10^{-7}$ (SI)

μ_e : relative permeability (including between possible iron)

S_e : effective magnetic cross-section of the core (average cross-section)

l_e : Effective magnetic length (average magnetic circuit length))

N : number of turns [13].

2.4 Different types of DC-DC converters

There are various types of DC-DC converters, which can be divided into two categories: converters with galvanic isolation between input and output, and converters with a common terminal between input and output.

Energy storage converters can be divided into three types of static converters :

- The boost converter
- Buck converter
- The Buck-Boost converter

In this project our concern is the buck converter, The Buck chopper series is a static step-down converter that converts a fixed DC voltage conversion of a fixed DC voltage to a user-adjustable low voltage, consisting of a dual-control power switch, a diode, an inductor and a capacitor.

2.5 Operating modes of DC-DC converters

DC-DC converters can be roughly classified into two operating modes: Continuous Conduction Mode (CCM) and Discontinuous Conduction Mode (DCM). In CCM mode, the current through the coil does not cancel during an operating period, as shown in Figure (2.6.a). In DCM mode, on the other hand, the current through the coil cancels out before the end of the operating period, as shown in Figure (2.6.b).

It should be noted that the CCM or DCM modes depend directly on the operating point of the converter and can be represented by a continuous or discrete model. In the remainder of this study, only the continuous conduction mode will be considered.

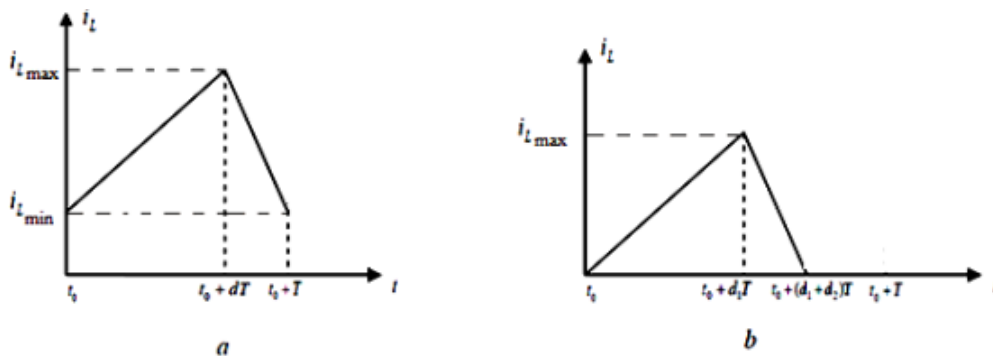


Figure 2.6: Coil current waveforms: (a) CCM, (b) DCM .[14]

2.6 Sizing and converter operating concept (BUCK)

2.6.1 Structure :

The electrical circuit of the Buck converter is shown in figure (2.7). :

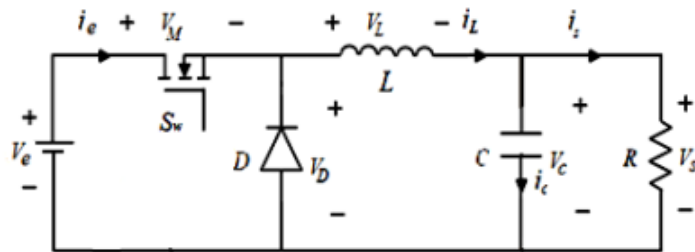


Figure 2.7: Buck converter circuit [14].

In a Buck converter, the input source is a DC voltage source and the load is a current source.

2.6.2 Continuous conduction mode CCM :

First conduction sequence ($0 \leq t \leq d.T$)

At the start of the operation in question, at $t=0$, switch S is closed and diode D is blocked, giving the following equivalent circuit:

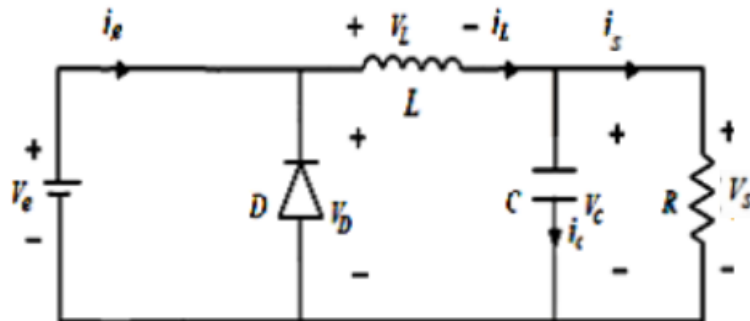


Figure 2.8: Equivalent circuit during ($0 \leq t \leq d.T$) [14].

In this phase, the current variation in the inductor is given by the following equation :

$$v_e(t) = v_L(t) + v_{S_w}(t) + v_s(t)$$

In the case of an ideal switch, we have :

$$v_{S_w}(t) = 0 \Rightarrow v_e(t) = v_L(t) + v_s(t)$$

$$\Rightarrow v_L(t) = L \frac{di_L(t)}{dt} = v_e(t) - v_s(t) \quad (2.1)$$

We obtain the solution of the first-order equation using the following formula :

$$i_L(t) = \frac{V_e - V_s}{L}t + I_{L\min} \quad (2.2)$$

$i_L(0) = I_{L\min}$: minimum current

For $t = d.T$

$$i_L(dT) = \frac{V_e - V_s}{L}(dT) + I_{L\min} = I_{L\max} \quad (2.3)$$

The peak-to-peak current ripple ΔI_L can be determined by the following expression :

$$\Delta I_L = I_{L\max} - I_{L\min} = \frac{V_e - V_s}{L}(dT) \quad (2.4)$$

Second conduction sequence ($dT \leq t \leq T$)

At time $t = dT$, switch S is opened and the diode becomes conductive. The equivalent circuit diagram then becomes :

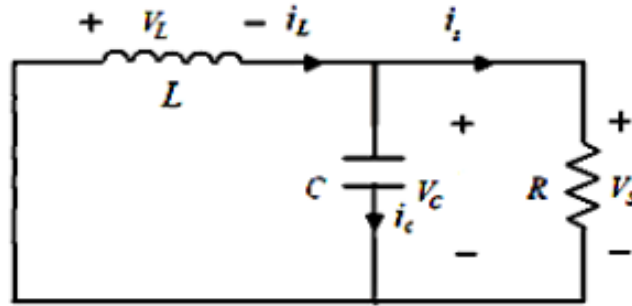


Figure 2.9: Equivalent circuit during ($dT \leq t \leq T$) [14].

In this phase, the current variation in the inductor is given by the following equation :

$$v_L(t) + v_D(t) + v_s(t) = 0$$

In the case of an ideal switch, we have : $v_D(t) = 0$

$$\Rightarrow v_L(t) = -L \frac{di_L(t)}{dt} = v_s(t) \quad (2.5)$$

From the solution of the first-order equation, we obtain :

$$i_L(t) = \frac{-V_s}{L}(t - dT) + A \quad (2.6)$$

For $t = dT$ $i_L(dT) = I_{L\max} = A$

So:

$$i_L(t) = \frac{-V_s}{L}(t - dT) + I_{L \max} \quad (2.7)$$

For $t=T$

$$I_L(T) = \frac{-V_s}{L}(T - dT) + I_{L \max} = I_{L \min} \quad (2.8)$$

The following expression is used to determine the peak-to-peak current ripple (ΔI_L) from equation eq(2.8):

$$\Delta I_L = I_{L \max} - I_{L \min} = \frac{V_s}{L}(1 - d)T \quad (2.9)$$

from eq 2.4 and 2.9 we deduce :

$$V_s = dV_e \quad (2.10)$$

Average inductance current and $I_{L \max}$, $I_{L \min}$ currents :

To ensure equality between the average current in the inductor and the DC current in the load, this can be expressed as follows :

$$I_{L \text{ moy}} = I_S = \frac{V_s}{R} \quad (2.11)$$

The expressions for the currents $I_{L \min}$ and $I_{L \max}$ in the inductor can now be rewritten as follows :

$$I_{L \max} = I_{L \text{ moy}} + \frac{\Delta I_L}{2} = \frac{V_s}{R} + \frac{V_s}{2L}(1 - d)T \quad (2.12)$$

$$I_{L \min} = I_{L \text{ moy}} - \frac{\Delta I_L}{2} = \frac{V_s}{R} - \frac{V_s}{2L}(1 - d)T. \quad [?] \quad (2.13)$$

Average inductance voltage :

$$V_{L \text{ moy}} = \frac{1}{T} \int_0^T v_L(t) dt = \frac{1}{T} \int_0^T L di_L = \frac{L}{T} [i_L(t)]_0^T = \frac{L}{T} [i_L(T) - i_L(0)] = 0 \quad [?] \quad (2.14)$$

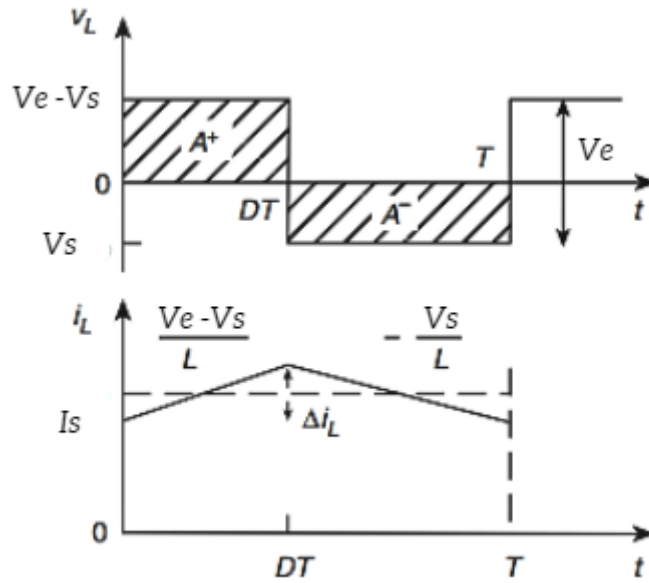


Figure 2.10: Form of current and voltage in the inductor during continuous conduction [15].

Source current $i_e(t)$ and switch $i_{Sw}(t)$:

During the first conduction phase ($0 \leq t \leq dT$) : $i_e(t) = i_{Sw}(t)$

L'expression du courant:

$$i_{Sw}(t) = \left(I_s - \frac{\Delta I_L}{2} \right) + \frac{\Delta I_L}{dT} t \quad (2.15)$$

So : $i_{Sw}^2(t)$ is :

$$I_{Sw(eff)}^2 = \frac{1}{T} \int_0^{dT} i_{Sw}^2(t) dt = \frac{1}{T} \left[\left(I_s - \frac{\Delta I_L}{2} \right)^2 t + \left(\frac{\Delta I_L}{dT} \right)^2 \frac{t^3}{3} + \frac{2\Delta I_L}{dT} \left(I_s - \frac{\Delta I_L}{2} \right) \frac{t^2}{2} \right] dT$$

$$I_{Sw(eff)} = \left[\left[\left(I_s - \frac{\Delta I_L}{2} \right)^2 + \frac{\Delta I_L^2}{3} + \Delta I_L \left(I_s - \frac{\Delta I_L}{2} \right) \right] d \right]^{1/2}$$

$$I_{Sw(eff)} = I_s \sqrt{d \left[\frac{1}{(1-d)^2} + \frac{1}{12} \left(\frac{\Delta i_L}{i_s} \right)^2 \right]} \quad (2.16)$$

Voltage at switch terminals :

when D is passing we have $V_{Sw \max} = V_{e \max}$

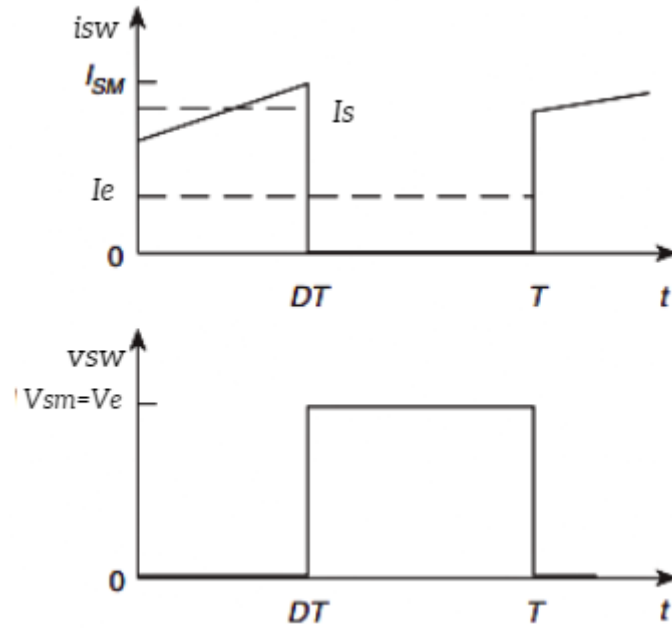


Figure 2.11: Form of current and voltage in the Sw switch [15].

Diode current $i_d(t)$:

During the second conduction phase ($dT \leq t \leq T$)

Current expression :

$$i_D(t) = \left(I_s + \frac{\Delta I_L}{2} \right) - \frac{\Delta I_L}{T - dT} (t - dT) \quad (2.17)$$

$$i_D^2(t) = \left(I_s + \frac{\Delta I_L}{2} \right)^2 + \left(\frac{\Delta I_L}{T - dT} (t - dT) \right)^2 - 2 \left(I_s + \frac{\Delta I_L}{2} \right) \left(\frac{\Delta I_L}{T - dT} (t - dT) \right)$$

The effective value is equal to :

$$I_{D(\text{eff})}^2 = \frac{1}{T} \left[\left(I_s + \frac{\Delta I_L}{2} \right)^2 (t - dT) + \left(\frac{\Delta I_L}{T - dT} \right)^2 \frac{(t - dT)^3}{3} - \frac{2\Delta I_L}{T - dT} \left(I_s + \frac{\Delta I_L}{2} \right) \frac{(t - dT)^2}{2} \right] T$$

$$I_{D(\text{eff})} = \left[(1 - d) \left[\left(I_s + \frac{\Delta I_L}{2} \right)^2 + \frac{(\Delta I_L)^2}{3} - \Delta I_L \left(I_s + \frac{\Delta I_L}{2} \right) \right] \right]^{1/2} \quad (2.18)$$

For the effective value of the current in the diode, we adopt the approximate value :

$$i_{D(\text{eff})} = i_s \sqrt{1 - d} \quad [16] \quad (2.19)$$

Diode terminal voltage :

when Sw is passing we have $|V_{D_{\max}} = |V_{e_{\max}}|$

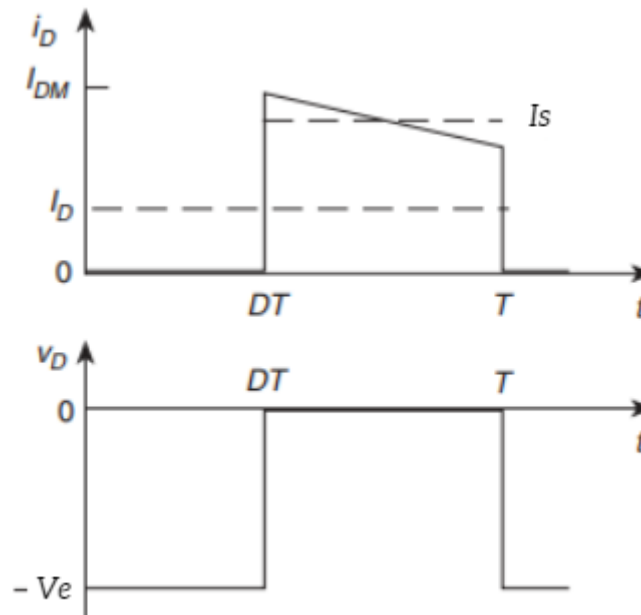


Figure 2.12: Form of current and voltage in Diode D [15].

Calculation of inductance L :

For a desired maximum ripple current, we can write $\Delta i_{L_{\max}}$:

According to eq(2.4)

$$L \geq \frac{V_e}{4\Delta i_{L(\max)}f} = \frac{V_s(V_e - V_s)}{\Delta i_L f V_e} \quad (2.20)$$

Calculation of capacitance C :

During t_{on} :

The relationship between the current I_c flowing through capacitor C, the current I_L flowing in inductor L and the output current I_s can be expressed as follows: $I_c = I_L - I_s$. The average value of this current is zero, as shown in Figure (2.13).

At moment t_1 , as shown in Figure (2.13), the voltage V_s is minimal. It then increases, reaching a maximum when the total surface area .

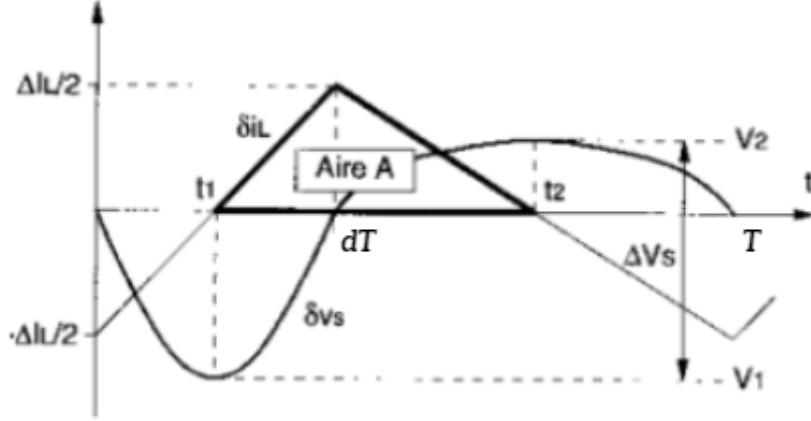


Figure 2.13: Waveform of current $I_{L(t)}$ and voltage $V_{s(t)}$ [14].

The ripple amplitude can be calculated as the area of this triangle.

$$\Delta V_s = \frac{\Delta Q}{C} = \frac{1}{C} \frac{1}{2} \frac{\Delta i_L T}{2} = \frac{\Delta i_L}{8Cf} = \frac{1}{8LCf^2} V_s \left(1 - \frac{V_s}{V_e}\right)$$

This gives the value of the capacitance C required to obtain a ripple in the output voltage. output voltage $\Delta V_s (\Delta V_s = \Delta V_c)$ if the capacitor is perfect:

$$C_{\min} \geq \frac{\Delta i_L}{8f\Delta V_s} = \frac{1}{8L\Delta V_s f^2} V_s \left(1 - \frac{V_s}{V_e}\right). \quad [16] \quad (2.21)$$

The size of the capacitor is inversely proportional to the square value of the switching frequency f . Therefore, by increasing the value of f , we can reduce the size of the capacitive filter. However, it's important to bear in mind that increasing f leads to a reduction in converter efficiency.

It is shown that the effective value of the current I_c can be expressed as follows.

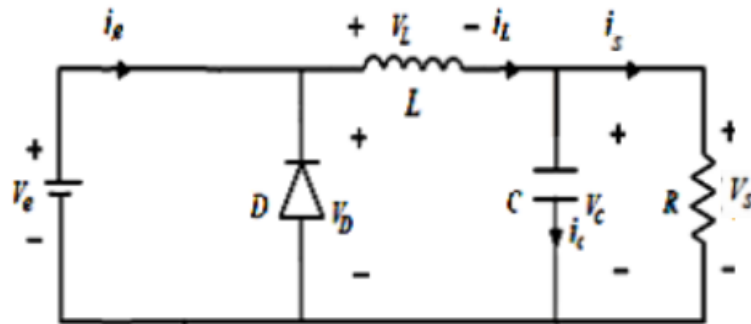
$$I_{c(eff)} = i_s \frac{\Delta i_L}{\sqrt{12}i_s} \quad (2.22)$$

In practice, capacitors are not perfect, and it is necessary to take into account their equivalent series resistances (ESR). These resistors introduce an additional ripple ΔV_{ESR} in phase with the current ripple Δi_L .

$$\Delta V_{ESR} = \Delta V_s = ESR\Delta i_L \quad (2.23)$$

2.6.3 Discontinuous conduction mode DCM :

First conduction sequence ($0 \leq t \leq d.T$)

Figure 2.14: Equivalent circuit during $(0 \leq t \leq d.T)$ [14].

In this phase, the current variation in the inductor is given by the following equation :

$$v_e(t) = v_L(t) + v_s(t) + v_{Sw}(t)$$

$$v_{Sw}(t) = 0 \Rightarrow v_L(t) = v_e(t) - v_s(t)$$

$$\Rightarrow L \frac{di_L(t)}{dt} = v_e(t) - v_s(t) \quad (2.24)$$

From the solution of the first-order equation, we obtain :

$$i_L(t) = \frac{V_e - V_s}{L} t + i_L(0) \quad (2.25)$$

$$i_L(0) = 0$$

$$\text{For } t = dT$$

$$i_L(dT) = \frac{V_e - V_s}{L} (dT) = I_{L \max} \quad (2.26)$$

Second conduction sequence $(dT \leq t \leq d_1T)$

d_1T : is the decay time of $i_L(t)$

(Origin in dT)

$$\Rightarrow i_L(t) = \frac{-V_s}{L} t + I_{L \max} \quad (2.27)$$

$$i_L(d_1T) = 0$$

$$\Rightarrow I_{L \max} = \frac{V_s}{L} (d_1.T) \quad (2.28)$$

From eq (2.25) and (2.27)

So :

$$\frac{V_e - V_s}{L} dT = \frac{V_s}{L} d_1T \Rightarrow \frac{V_s}{V_e} = \frac{d}{d + d_1}$$

$$\Rightarrow d_1 = d \frac{V_e - V_s}{V_s} \quad (2.29)$$

The following figure shows the current $i_{L(t)}$ and voltage $V_{L(t)}$:

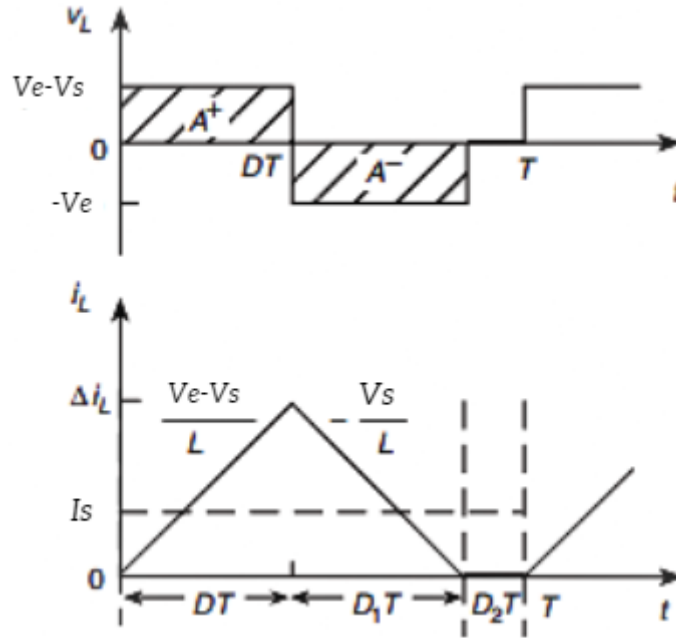


Figure 2.15: Form of inductance current and voltage [15].

On the other hand $I_s = I_{L(moy)}$

So :

$$I_s = \frac{1}{T} \left(\frac{1}{2} * I_{Lmax} dT + \frac{1}{2} * I_{Lmax} d_1 T \right)$$

$$\Rightarrow I_s = \frac{1}{2} I_{Lmax} (d + d_1) \quad (2.30)$$

Using eqs (2.25), (2.28), and (2.29) we obtain :

$$I_s = \frac{V_e - V_s}{2Lf} * d \left(d \frac{V_e}{V_s} \right)$$

$$\Rightarrow I_s = \frac{d^2}{2Lf} * \frac{V_e}{V_s} * (V_e - V_s) \quad (2.31)$$

$$V_s = V_e * \frac{1}{1 + \frac{2Lf I_s}{d^2 V_e}} \quad [13] \quad (2.32)$$

It can be seen that the expression for the output voltage is considerably more complex than that obtained using the (CCM) method. This is because the output voltage depends not only on the input voltage and the duty cycle

d, but also on the inductance L, the switching period T and the output current.

- **Source current $i_{e(t)}$ and switch $i_{Sw(t)}$:**

During the first conduction phase ($0 \leq t \leq dT$) : $i_e(t) = i_{Sw}(t)$

- **Voltage at switch terminals Sw : $V_{Sw(max)} = V_{e(max)}$**

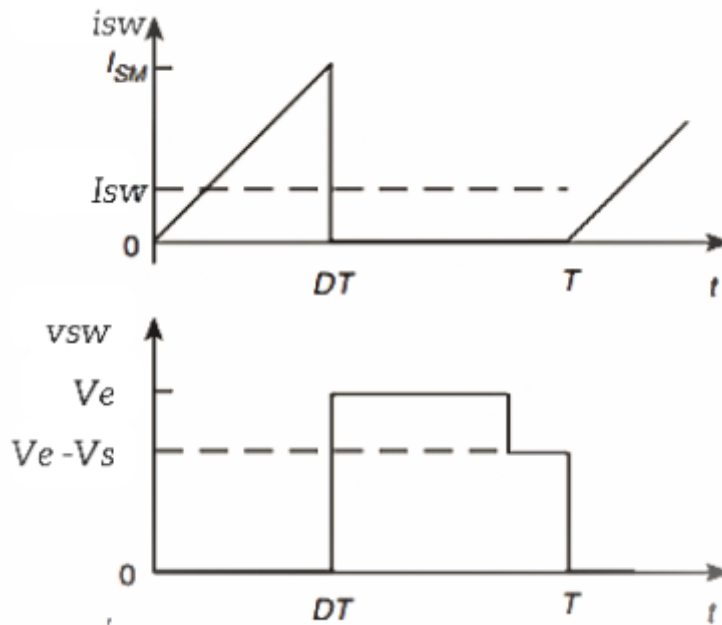


Figure 2.16: Form of switch current and voltage Sw.[15]

The current expression : $i_{Sw}(t) = \frac{I_{Lmax}}{dT}t$

So: $i_{Sw}^2(t)$ is : $i_{Sw}^2(t) = \left(\frac{I_{Lmax}}{dT}t\right)^2$

The effective value $I_{Sw(ef)}^2$ is equal to the value of $i_{Sw}^2(t)$, therefore :

$$I_{Sw(ef)}^2 = \frac{1}{T} \int_0^{dT} i_{Sw}^2(t) dt = \frac{1}{T} \left[\left(\frac{I_{Lmax}}{dT}\right)^2 * \frac{t^3}{3} \right]_0^{dT}$$

$$\Rightarrow I_{Sw(ef)} = \sqrt{\frac{d}{3}} I_{Lmax} \quad (2.33)$$

- **Diode current $i_{D(t)}$:**

During the second conduction phase ($dT \leq t \leq (d + d_1)T$) :

$$\text{Current expression: } i_D(t) = -\frac{I_{L\max}}{d_1T}(t - dT) + I_{L\max}$$

Therefor: $i_D^2(t)$ is :

$$i_D^2(t) = \left(\frac{I_{L\max}}{d_1T}(t - dT)\right)^2 + (I_{L\max})^2 - 2\left(\frac{I_{L\max}}{d_1T}(t - dT)\right)(I_{L\max})$$

The effective value $I_{D\text{eff}}$ is equal to the average value of $i_D^2(t)$, so :

$$\begin{aligned} I_{D\text{(eff)}}^2 &= \frac{1}{T} \int_{dT}^{dT+d_1T} i_D^2(t) dt \\ &= \frac{1}{T} \left[(I_{L\max})^2 (t - dT) + \left(\frac{I_{L\max}}{d_1T}\right)^2 \frac{(t-dT)^3}{3} - 2\left(\frac{I_{L\max}}{d_1T}\right)(I_{L\max}) \frac{(t-dT)^2}{2} \right]_{dT}^{dT+d_1T} \\ &= \frac{1}{T} (I_{L\max})^2 \left(\frac{d_1T}{3}\right) = I_{L\max} \sqrt{\frac{d_1}{3}} \end{aligned}$$

$$I_{D\text{(eff)}} = I_{L\max} \sqrt{\frac{d_1}{3}} \quad (2.34)$$

- **Diode terminal voltage D : $V_{D\max} = |V_e|$**

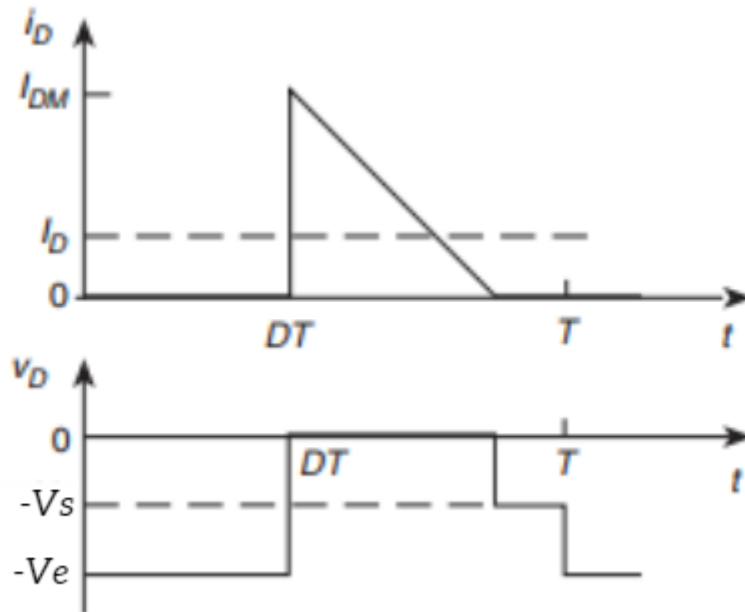


Figure 2.17: Form of diode current and voltage D [15].

2.7 DC-DC buck converter control

2.7.1 PWM control :

The Sw switch is controlled using the pulse-width modulation (PWM) technique. The control signal u is obtained by comparing a periodic triangular signal v_{ramp} of period T and amplitude 1. The duty cycle is represented by d (as shown in figure (2.18)). When $u = 0$, the switch will be in a blocked state, while when $u = 1$, the switch will be in a saturated state.

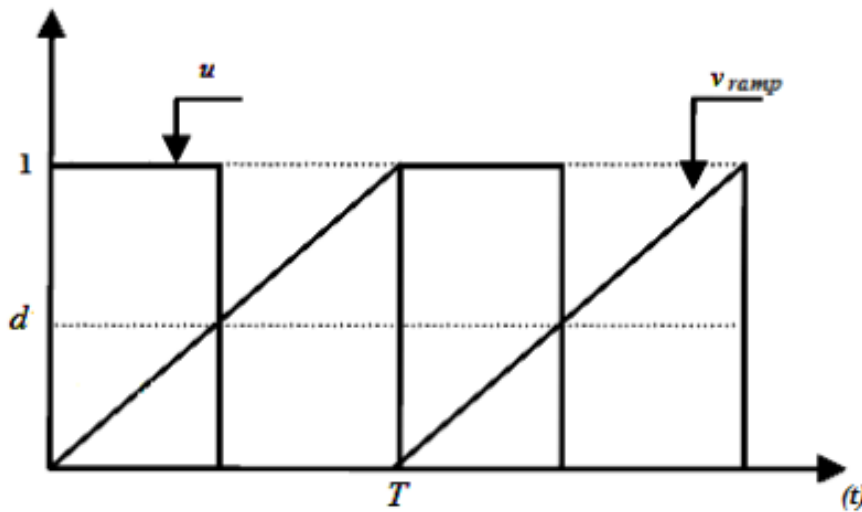


Figure 2.18: Signal form generated by the PWM technique [14].

- **PWM control principle :**

This technique can be seen as an extension of the chopping control principle, where pulse duration is not regular, but aims to eliminate low-rank harmonics that are difficult to filter out. It is mainly based on the chopping of a full rectangular wave, and its output voltage represents a succession of crenellations of amplitude equivalent to the DC supply voltage, with variable width [17].

A PWM signal is generally generated by comparing two signals :

- The reference signal, which is a continuous signal.
- The carrier signal, which represents the switching frequency of the converter's solid-state switches.

- The carrier signal is a high-frequency signal that is compared with the reference signal.
- The intersection of these two signals represents the switching times of the switches, as shown in Figure 2.19.

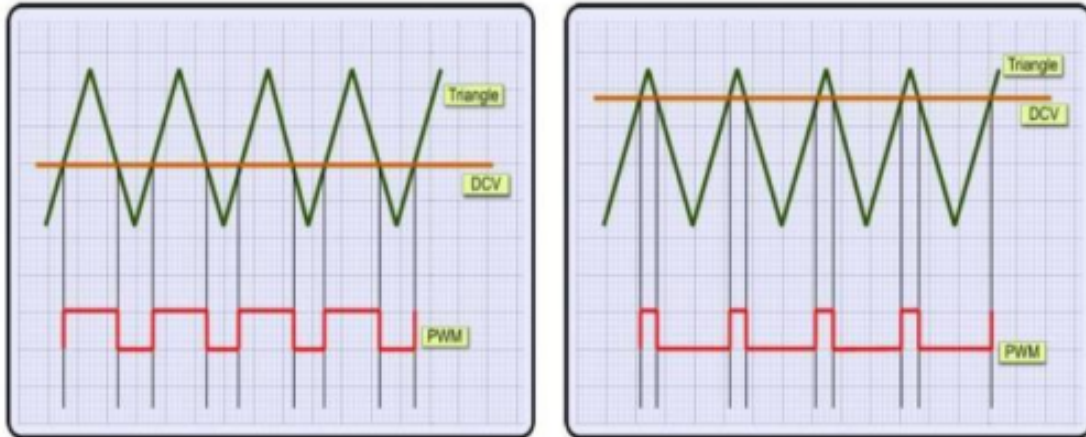


Figure 2.19: PWM signal waveform [17].

When reference and carrier signals cross :

- In increasing direction, the command opens the Sw switch.
- In descending direction, the command closes the Sw switch.

- **The advantages of PWM control :**

Good harmonic neutralization compared with square waves or single square waves :

- It simplifies filtering by shifting output voltage harmonics to higher frequencies.
- Allows variation of fundamental output voltage values.
- Allows several sets of inverters and induction motors to be powered from a single DC source.[17]

- **PWM command generation :**

This technology is characterized by the use of a constant-period signal and an adjustable duty cycle. It is commonly used in devices such as :

- Cycloconverters
- Inverters
- Rectifiers
- Choppers

This modulation has evolved significantly over the years, offering a wide range of applications in control systems and other functions. Thanks to this technique, the design of chopper control circuits has become more flexible and economical [18].

2.7.2 Proportional-Integral (PI) linear control :

Open-loop DC-DC converters may have poor accuracy, slow response time, excessive overshoot and high sensitivity to disturbances. . For this reason, it is necessary to correct their behavior using servo-control techniques. The servo system must include a controller, the aim of which is to respect the servo system's performance in terms of damping, overshoot and speed. The Proportional-Integral PI controller is widely used due to its because of its simplicity of implementation and its ability to achieve good dynamic response, A PI-type corrector improves accuracy, but reduces stability through phase loss and slows down the system through reduced speed. slows down the system by reducing bandwidth. The PI controller is known by a control law: $U(t) = K_p e(t) + K_i \int e(t) dt$ [19].

Proportional action P:

When K_p is high, correction is rapid, but this increases the risk of overshoot and oscillation in the output. On the other hand, when K_p is low, correction is slower, reducing the risk of oscillation.

Integral action I:

The integral action responds slowly to changes in error, allowing the set-point to be caught up progressively. As long as the positive (or negative) error continues, the $u(t)$ action increases (or decreases) until the error is cancelled.

Regulator features:

- **Stability** : A closed-loop system should only be stable if the feedback from the control system is energetically proportional to the error to be corrected. Excessive or delayed correction can lead to system instability [20].
- **Accuracy** : In control, precision is achieved by implementing integration in the loop [20].
- **Speed** : In general, a looped system must respond quickly to changes in its setpoint (tracking) and quickly clear disturbances (regulation). Reaction time is, of course, closely related to the inertia of the process itself [21].

Main transfer functions:

- **Transfer function of the PI corrector** : The PI corrector has a transfer function of the following type:

$$TC(p) = K_p + \left(\frac{K_i}{p}\right) \quad (2.35)$$

Buck converter transfer functions:

The general equation of the average model governing Buck converter operation is :

$$\begin{bmatrix} \frac{di_L}{dt} \\ \frac{dV_c}{dt} \end{bmatrix} = \begin{bmatrix} 0 & -\frac{1}{L} \\ \frac{1}{C} & -\frac{1}{RC} \end{bmatrix} \begin{bmatrix} i_L \\ V_c \end{bmatrix} + \begin{bmatrix} \frac{d}{L} \\ 0 \end{bmatrix} V_e$$

Using the average Buck converter model given by the previous equation and the following general law as follows:

$$\bar{\dot{x}} = \bar{A}\bar{x} + \bar{B}d$$

Where:

$$\bar{A} = \begin{bmatrix} 0 & -\frac{1}{L} \\ \frac{1}{C} & -\frac{1}{RC} \end{bmatrix}$$

and:

$$\bar{B} = \begin{bmatrix} \frac{d}{L} \\ 0 \end{bmatrix}$$

By performing the Laplace transform we obtain :

$$p\bar{x}(p) = \bar{A}\bar{x}(p) + \bar{B}d(p)$$

So:

$$\bar{x}(p) = (p\bar{I} - \bar{A})^{-1}\bar{B}d(p)$$

By substitution we have found the first transfer function linking the voltage V_s to d :

$$TS(p) = \frac{V_s}{d} = \frac{V_e}{LCp^2 + \frac{L}{R}p + 1} \quad (2.36)$$

Direct control of the Buck converter's duty cycle (Voltage Mode Control):

The representative diagram of the VMC control loop of a DC-DC converter with feedback using a PI is given in figure (2.20).

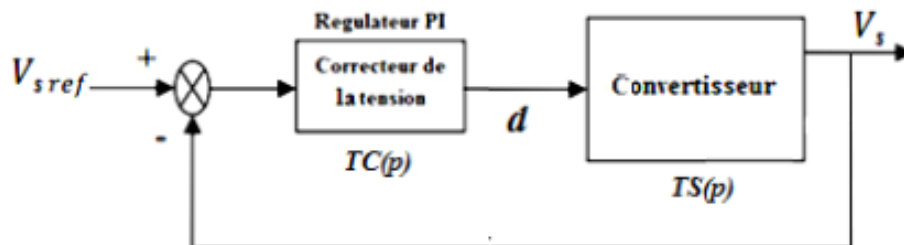


Figure 2.20: Schematic diagram of direct duty cycle control.[22]

The variable to be controlled (usually the output voltage) is compared with a reference value. The error signal is then corrected and compared with a sawtooth-shaped signal to generate the control signal.

This method is relatively simple to implement, and has the advantage of not requiring complex converter modeling.

A PI regulator is designed to increase gain at low frequencies and reduce the steady-state error between desired and actual output voltage, while maintaining a positive phase margin (PM) at a selected frequency [23].

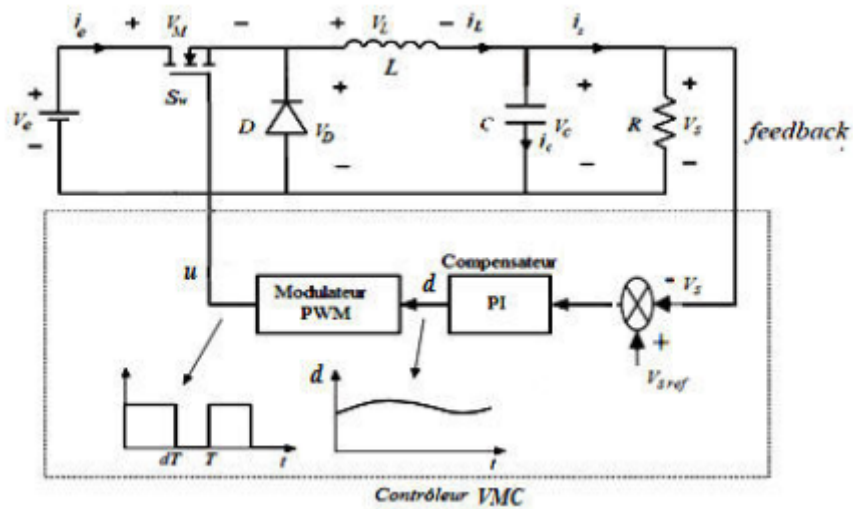


Figure 2.21: Diagram of Buck converter regulated in VMC [22].

2.8 Conclusion

In this chapter we have presented a theoretical study of a buck DC/DC converter for building an adjustable DC voltage source. We have detailed the study of the DC/DC converter in the two conduction modes to obtain the relationships between the various necessary converter parameters. We have seen also the types of command for the buck converter such as PI controller and PWM command. In the next chapter we are going to simulate the converter with two softwares matlab and proteus .

Chapter 3

Control and simulation of Buck converter

3.1 Introduction

Due to its speed and efficiency, circuit simulation is gaining in popularity as an alternative to prototyping, and is now seen as an additional tool for learning power electronics. Simulation involves transforming a circuit design into a software model, then subjecting it to input stimulations and observing the outputs to evaluate the performance of the new circuits and improve knowledge. More and more frequently, static converters are used in networks, particularly to connect decentralized renewable energy production sources. In system design, circuit performance is a crucial factor, as each component contributes to overall performance. In power electronics, it is crucial to focus on system evaluation, as output waveforms are affected not only by components, but also by junction capacitance and noise.

3.2 Assumptions :

The following assumptions will be taken into account in this theoretical study :

- All components are ideal, except capacitor ESR.
- The system is considered stable.
- The conduction mode is continuous.
- To calculate the input current, the input voltage is assumed to be constant, and the ripple of the output voltage with respect to its average value is ignored.
- To calculate the output voltage, the output current is considered constant, and the ripple of the input current with respect to its average value is ignored.
- The capacitance of the output capacitor is assumed to be sufficiently large for the voltage across it to be considered constant over the period.

3.3 Buck converter sizing

We are going to size the Buck converter components having ,the characteristics defined by the following specifications:

Topology	Specifications
Nominal input voltage (V_e)	20 V
Maximum input voltage ($V_{e(max)}$)	30 V
Rated output voltage (V_s)	12 V
Maximum output voltage ($V_{s(max)}$)	29 V
Maximum input current ($i_{e(max)}$)	15 A
Maximum input power ($P_{e(max)}$)	255 W
Minimum switching frequency (f)	20 kHz
Maximum inductance current ripple ($\Delta i_{L(max)}$)	5 %
Maximum output voltage ripple ($\Delta V_{s(max)}$)	2 %
Maximum output current ($i_{s(max)}$)	20 A

Table 3.1: Design specification

3.4 Component selection and calculation :

- **Load resistance :**

$$R_{min} = \frac{V_s}{I_s} = \frac{12}{10} \iff R_{min} = 0.6\Omega$$

- **The duty cycle d :**

$$d = \frac{V_s}{V_e} = \frac{12}{20} \iff d = 0.6$$

- **Operating period :**

$$T = \frac{1}{f} = \frac{1}{20 * 10^3} \iff T = 50\mu s$$

- **Current ripple Δi_L and choice of L :**

Maximum inductance current ripple: $\Delta i_{L(max)} = 5\%$ of I_s

$$\Delta i_{L(max)} = 0.05 * 20 = 1A$$

Minimum inductance value :

$$L \geq \frac{V_s(1-d)}{\Delta i_L f} = \frac{12(1-0.6)}{1(20 * 10^3)} \iff L \geq 240 \mu H$$

- **Output voltage ripple ΔV_s , choice of C:**

Maximum ripple of the output voltage: $\Delta V_{s(max)} = 5\%$ of V_s .

$$\Delta V_{s(max)} = 0.02 * 12 = 0.24V$$

The minimum value of C Capacitor:

$$C_{min} \geq \frac{\Delta i_L}{8f\Delta V_s} \geq \frac{0.5}{8(20 * 10^3)0.24} \iff C_{min} \geq 13.02 \mu F$$

- **Equivalent Series Resistances(ESR):**

$$ESR = \frac{\Delta V_s}{\Delta i_L} = \frac{0.24}{1} \iff ESR = 0.24 \Omega$$

- **Diode and MOSFET selection:**

The voltage and current requirements of the power MOSFET and the diode are as follows :

$$V_{M_{max}} = V_{D_{max}} = V_{e_{max}} = 30 \text{ V}$$

and

$$I_{M_{max}} = I_{D_{max}} = I_{s_{max}} + \frac{\Delta i_{L_{max}}}{2} = 20 + \frac{1}{2} = 20.5 \text{ A}$$

3.5 Simulation and Observation

3.5.1 Matlab Simulation :

MATLAB software is a matrix calculation tool with a simple syntax. Thanks to its specialized functions, it can be considered a programming language for scientific problems. As an interpreter, it executes instructions line by line. In addition, MATLAB has powerful graphics capabilities for presenting results and creating applications. Simulation of the Buck DC/DC converter can be efficiently carried out using MATLAB/SIMULINK software. Simulink is a graphical extension of MATLAB that lets you work with block diagrams to model and simulate systems[24].

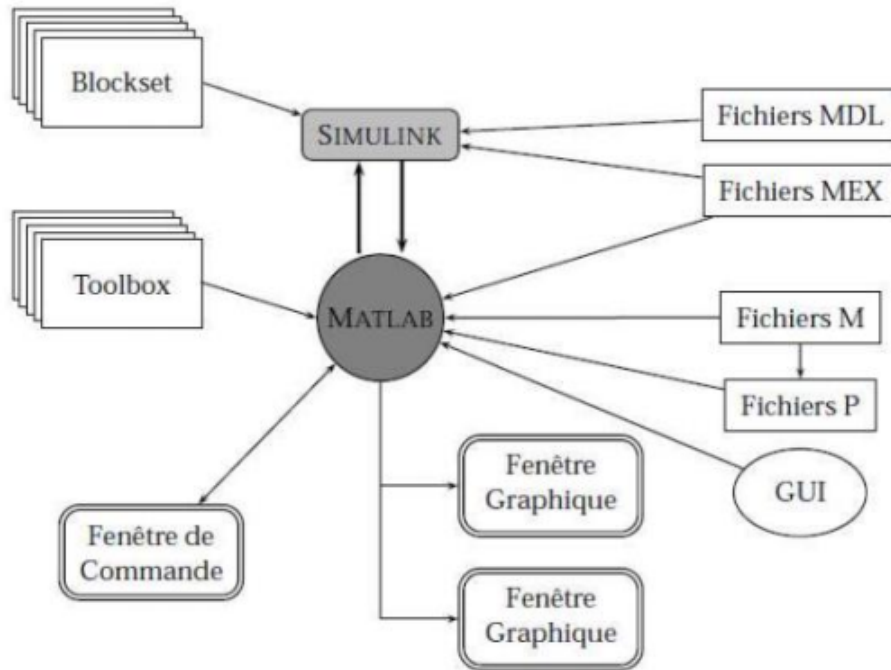


Figure 3.1: Matlab-level task representation [24].

We begin by analyzing the system represented by its transfer function $TS(p)$ given by (2.36). By numerical application, we obtain:

$$R = 0.6\Omega, L = 500\mu H, C = 330\mu F$$

$$TS(p) = \frac{20}{16.5 \cdot 10^{-8}p^2 + 83.33 \cdot 10^{-5}p + 1}$$

The Bode diagram of $TS(p)$ is given in figure (3.2).

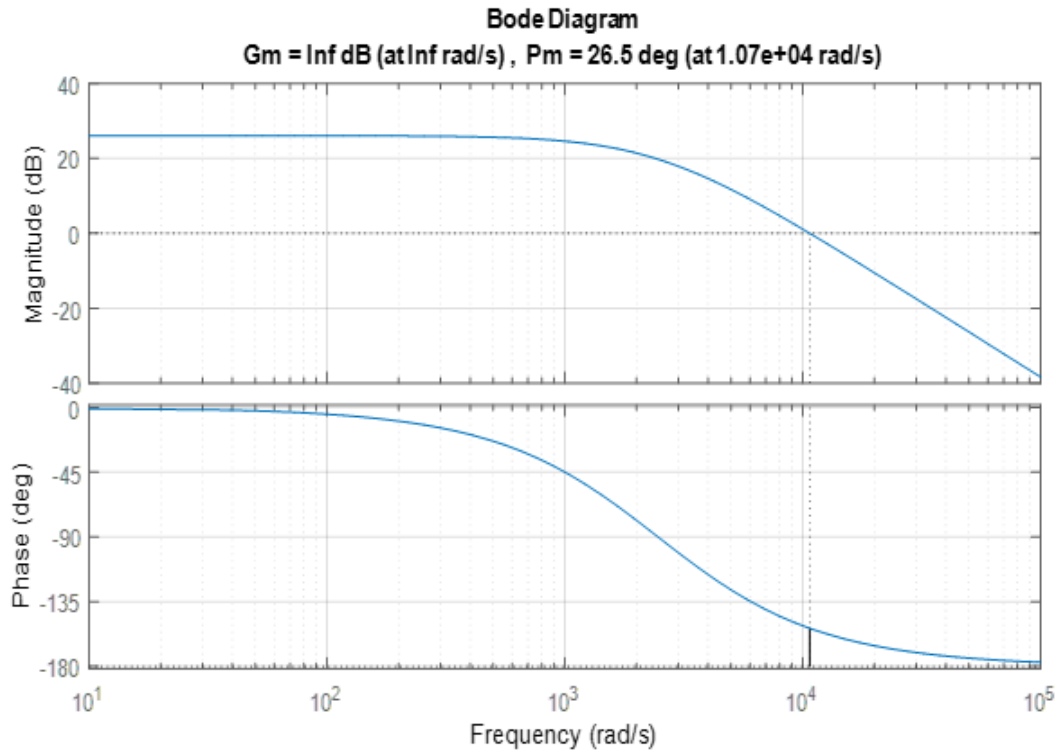


Figure 3.2: Bode diagram of the voltage loop transfer function.

No-corrected closed-loop system response:

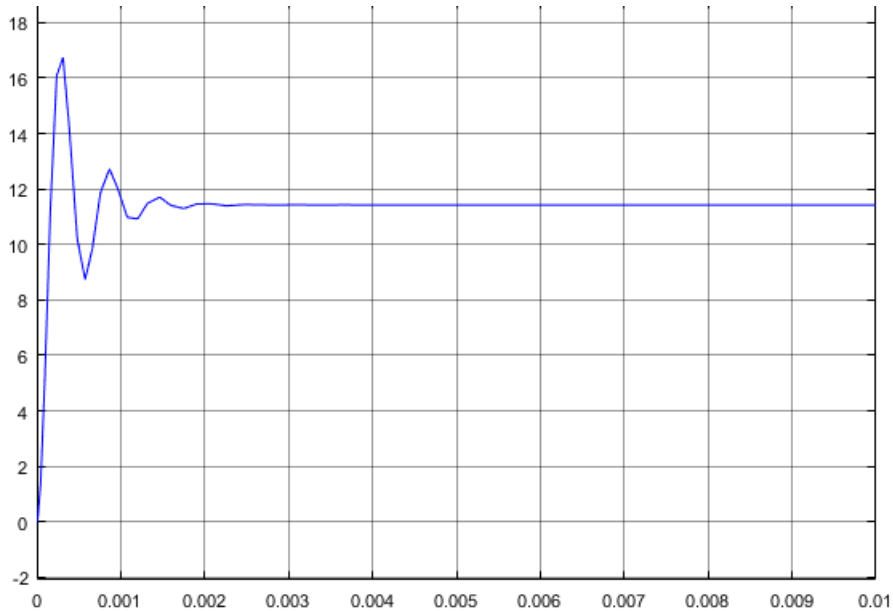
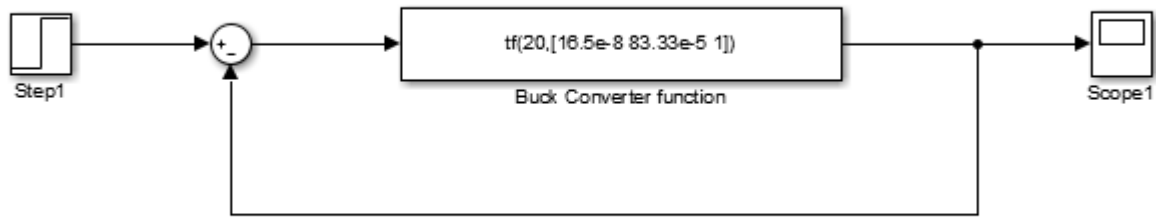


Figure 3.3: System response no corrected in closed loop

We note that the response is not robust, as there is a significant static error and excessive overshoot. As the minimum phase value is -180° , the gain margin is infinite. Now let's build the PI compensator to increase gain at low frequencies while maintaining a positive phase margin (PM) at a chosen frequency. The transfer function of the voltage corrector is as follows :

$$TC(p) = 0.1 + \frac{123.47}{p}$$

The open-loop transfer function is therefore written as follows :

$$T_{OL(\text{Buck})} = TC(p)TS(p) = \frac{1.974p + 2561}{16.5 \cdot 10^{-8} p^3 + 0.0008333 p^2 + p}$$

Figure (3.4) shows the Bode diagram of the corrected open-loop system:

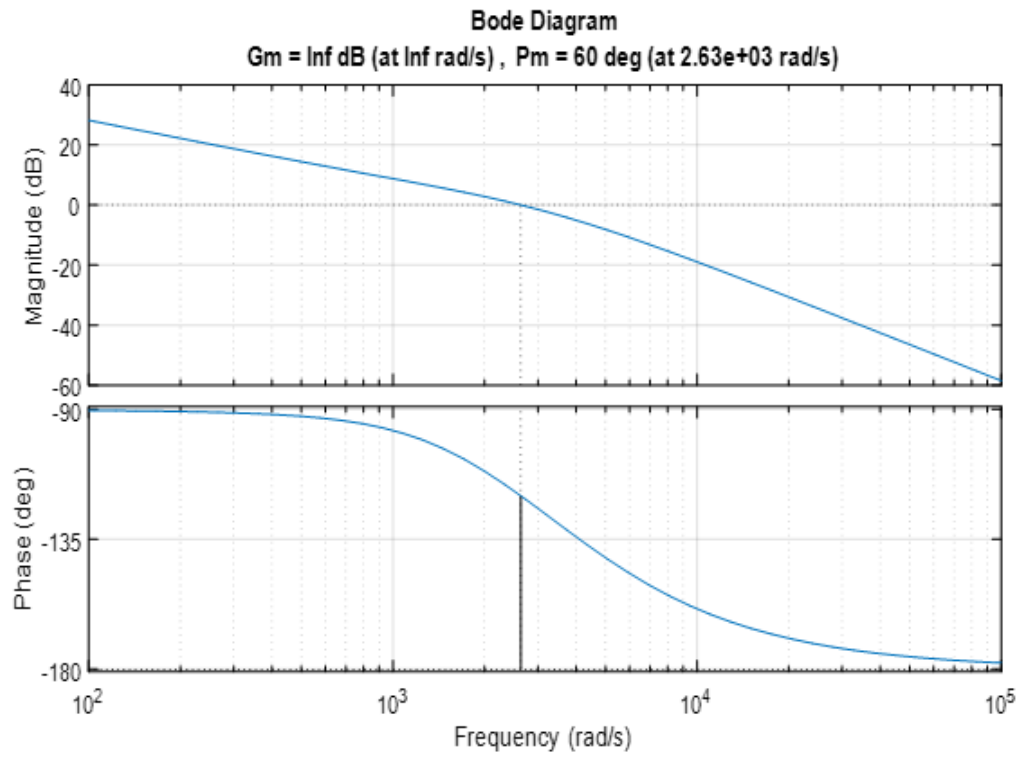


Figure 3.4: Bode diagram of the voltage loop transfer function.

The response of a closed-loop corrected system:

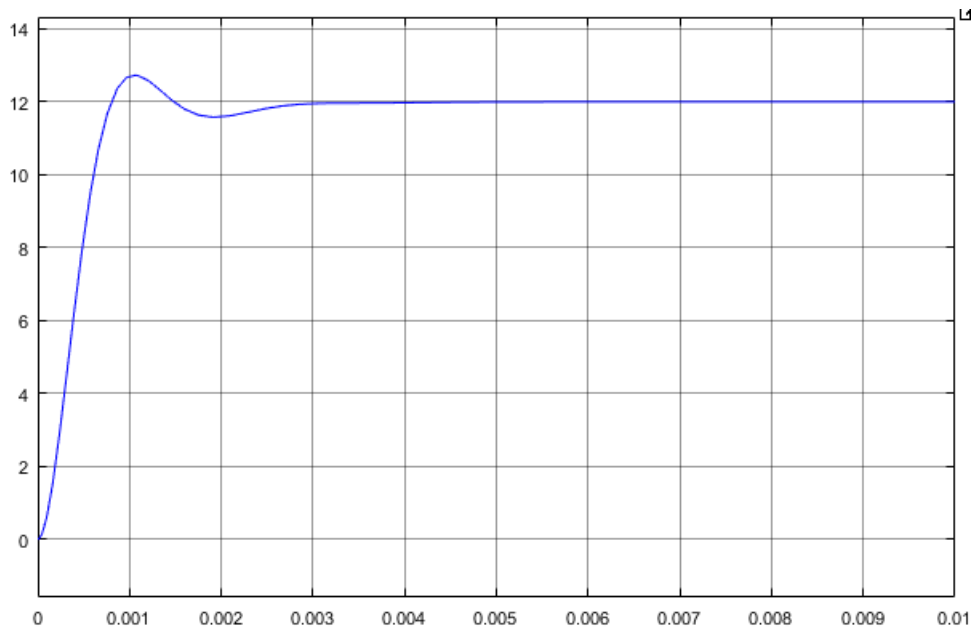
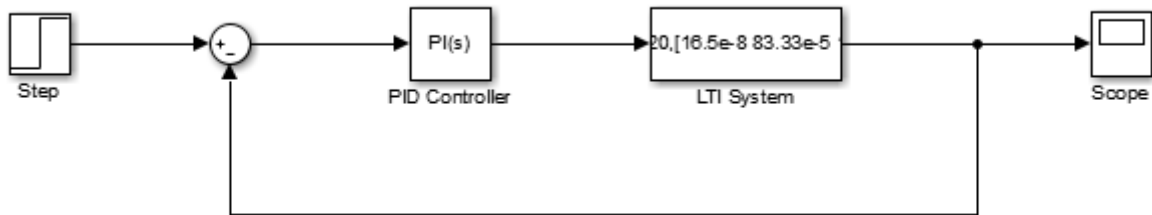


Figure 3.5: Response of a closed-loop corrected system

To simulate the buck correct operation with the calculated components, a simulation was run on the Matlab Simulink environment:

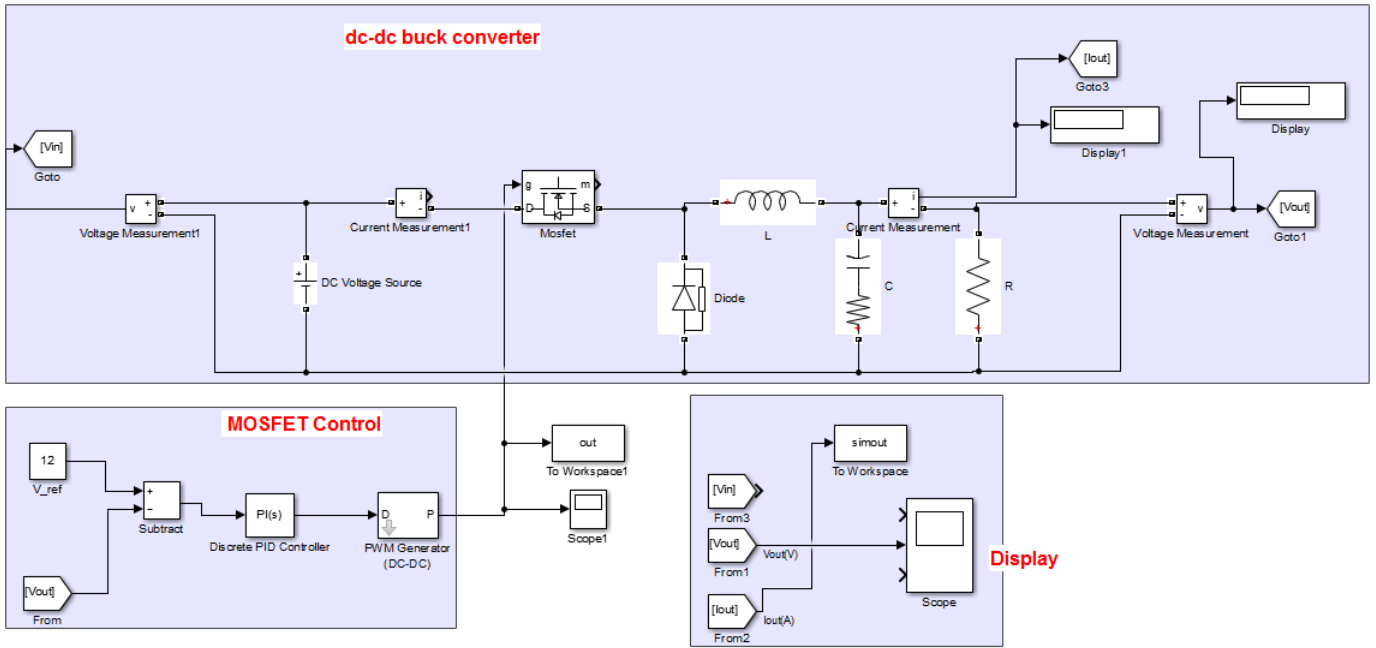


Figure 3.6: Simulation of buck converter

The simulation results are shown below:

- For $V_{ref} = 12V$, $R = 0.6\Omega$:

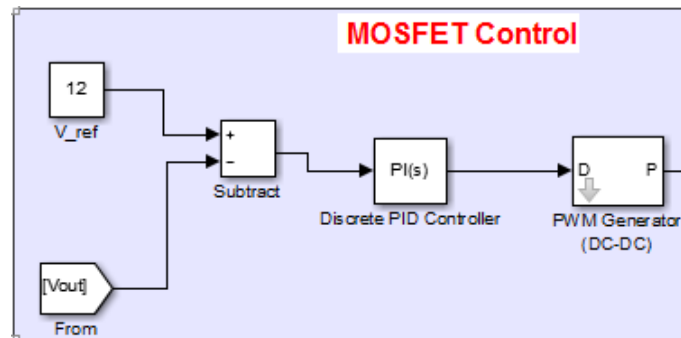


Figure 3.7: Control signal generation for $V_{ref} = 12V$

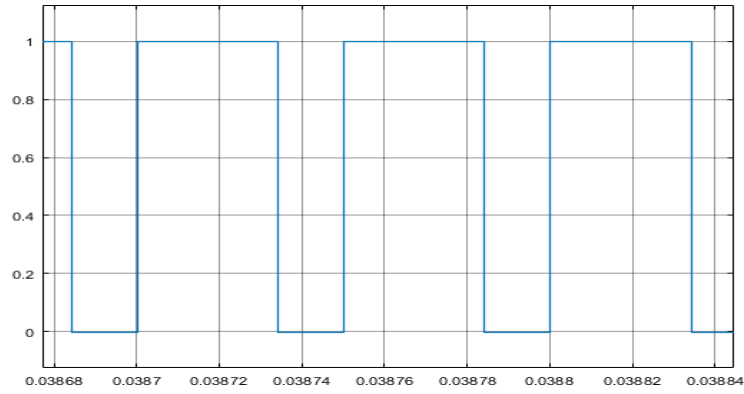
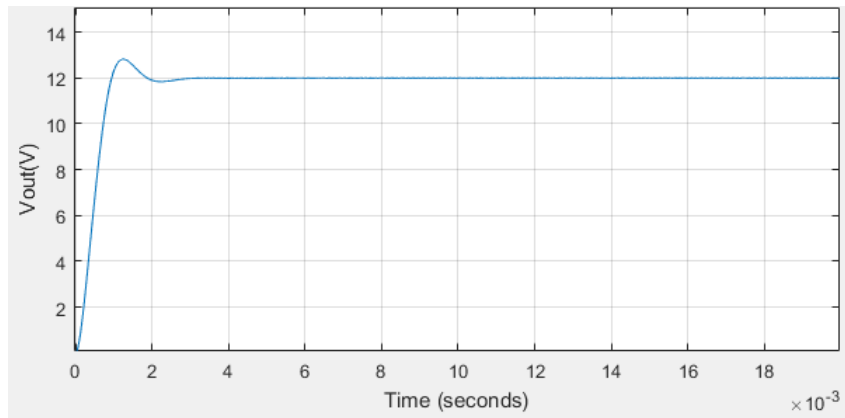
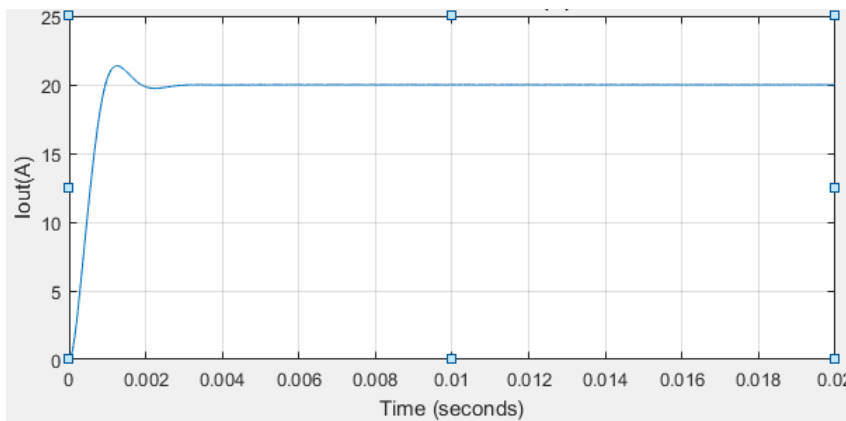


Figure 3.8: Control signal

The output voltage and load current curves are shown in figure 3.9 and figure 3.10 :

Figure 3.9: Voltage curve V_s Figure 3.10: Load current I_s

- For $V_{ref} = 6V$, $R = 0.6\Omega$:

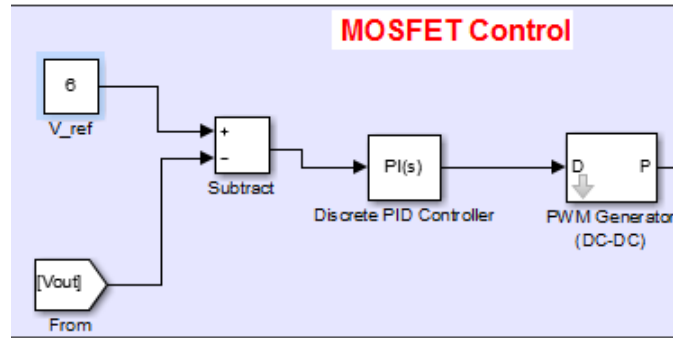


Figure 3.11: Control signal generation for $V_{ref} = 6V$

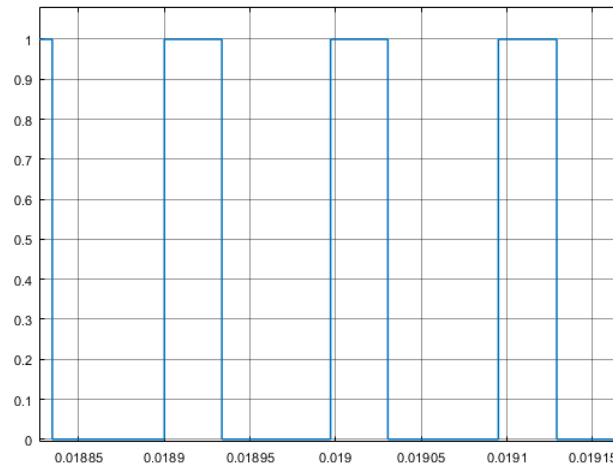


Figure 3.12: Control signal

The output voltage and load current curves are shown in Figure 3.13 and Figure 3.14. :

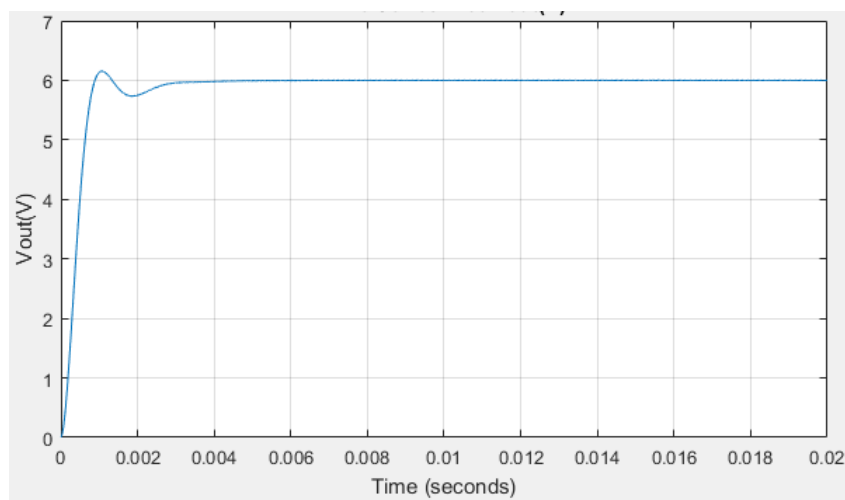


Figure 3.13: Voltage curve Vs

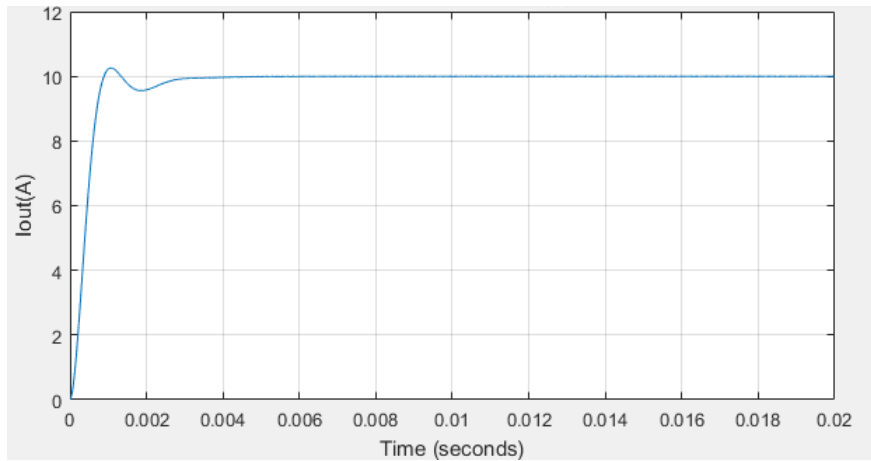


Figure 3.14: Load current I_s

- For $V_{ref} = 18V$, $R = 1.2\Omega$:

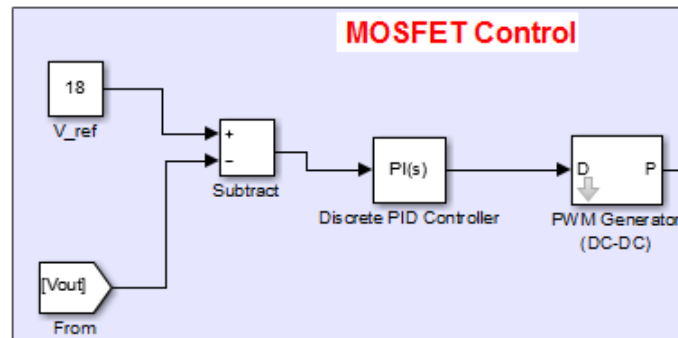


Figure 3.15: Control signal generation for $V_{ref} = 18V$

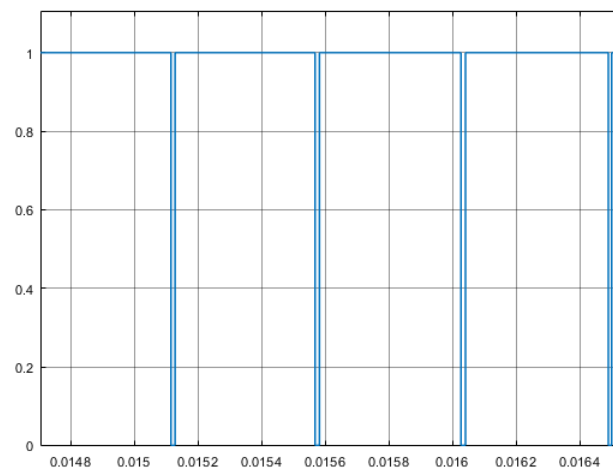


Figure 3.16: Control signal

- The output voltage and load current curves are shown in Figure 3.17 and Figure 3.18. :

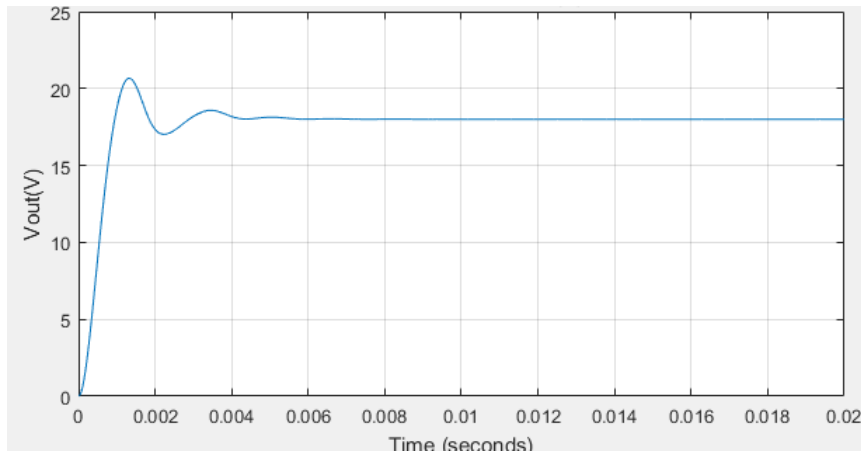


Figure 3.17: Voltage curve Vs

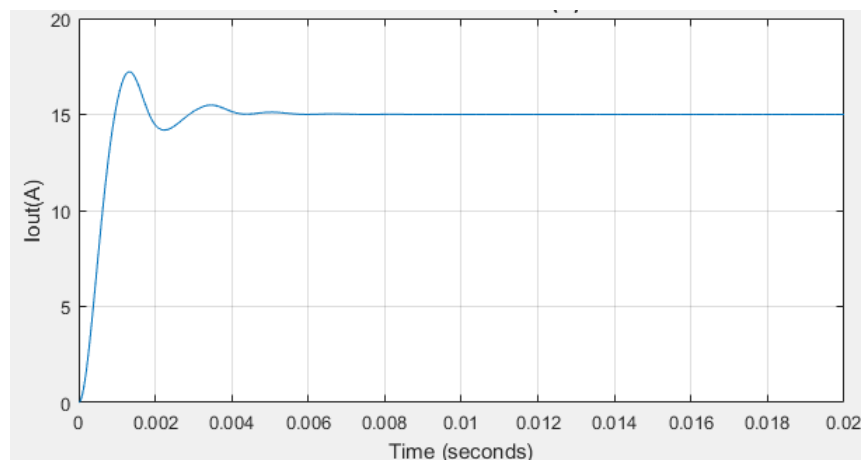


Figure 3.18: Load current Is

The efficiency vs the duty cycle is shown in figure 3.19 below

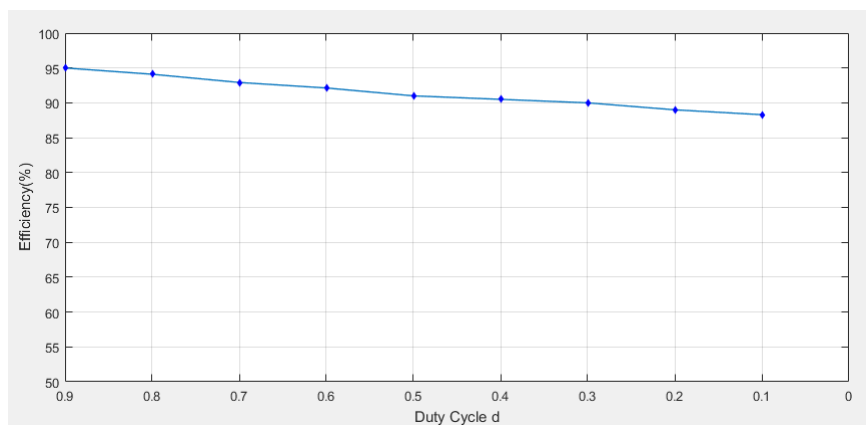


Figure 3.19: Efficiency vs the duty cycle d

- **Comments :**

The chopper output voltage is an adjustable voltage that can be varied from 12V to the desired value by controlling the duty cycle..

If the load varies, this may affect the converter output voltage and current.

The fixed-frequency control method can produce fluctuations in the output curves.

The selected switching frequency can also affect fluctuations. If the switching frequency is too high, this can lead to switching losses and disturbances in neighboring circuits..

It is also important to note that MATLAB simulations are based on mathematical models and do not take into account switching losses, conduction losses and other physical effects of the real circuit. Consequently, simulation results may differ slightly from actual experimental results.

3.5.2 Proteus Simulation:

PROTEUS allows you to enter electronic schematics (ISIS) in either single-page or hierarchical format. The input environment is fully customizable, and skins can be applied (ZUKEN or MENTOR, for example). PROTEUS is one of the simplest and most intuitive CAD programs available, yet it remains a powerful tool for creating complex assemblies and meeting industrial requirements in line with ISO and IPC standards[25].

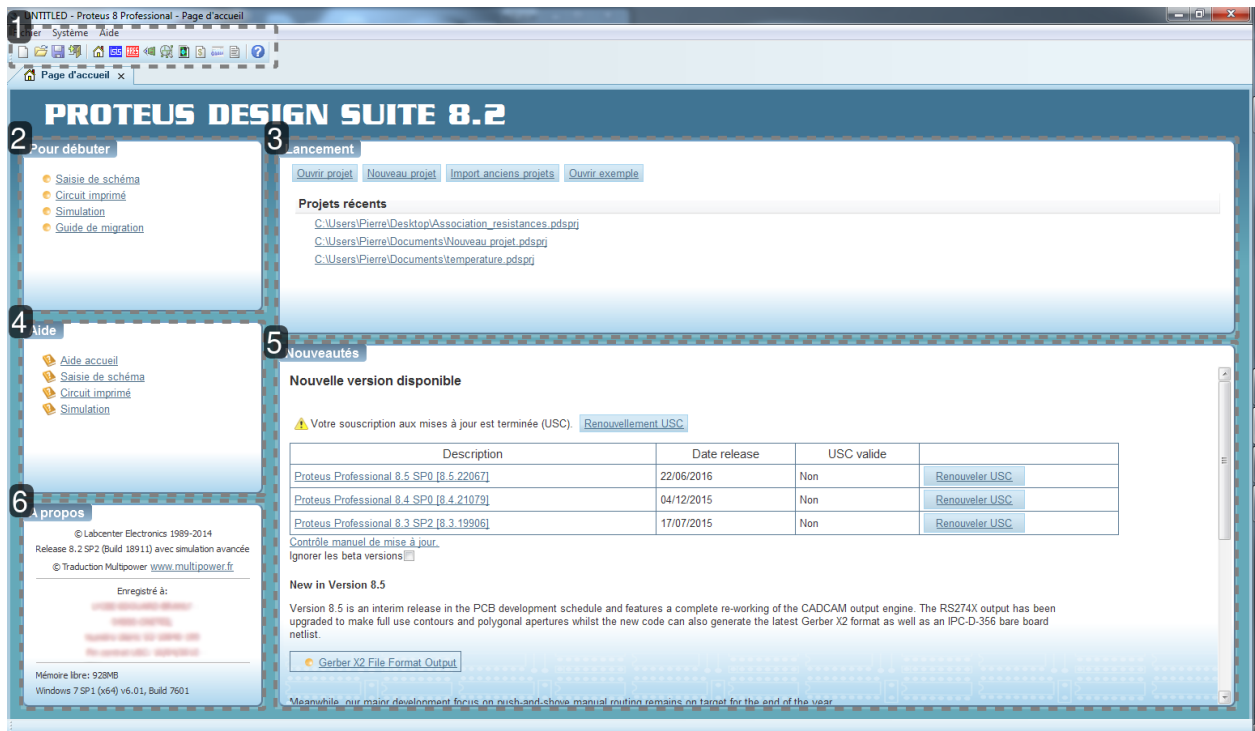


Figure 3.20: PROTEUS interface.[25]

- Choice of power and control circuit components :

Power circuit components	Specifications
MOSFET Switch M	IRF1415
Diode D	MBR6045WT
Inductance L	500 μH
Capacitor C	330 μF
ESR	10 m Ω
Load resistance R	1.2 Ω
Control circuit components	Specifications
Microcontroller	PIC16F877A
MOSFET-DRIVER	IR2112

Table 3.2: Component specification

- The components have been selected to meet the minimum conditions that have been calculated. The simulation is illustrated in figure 3.21.

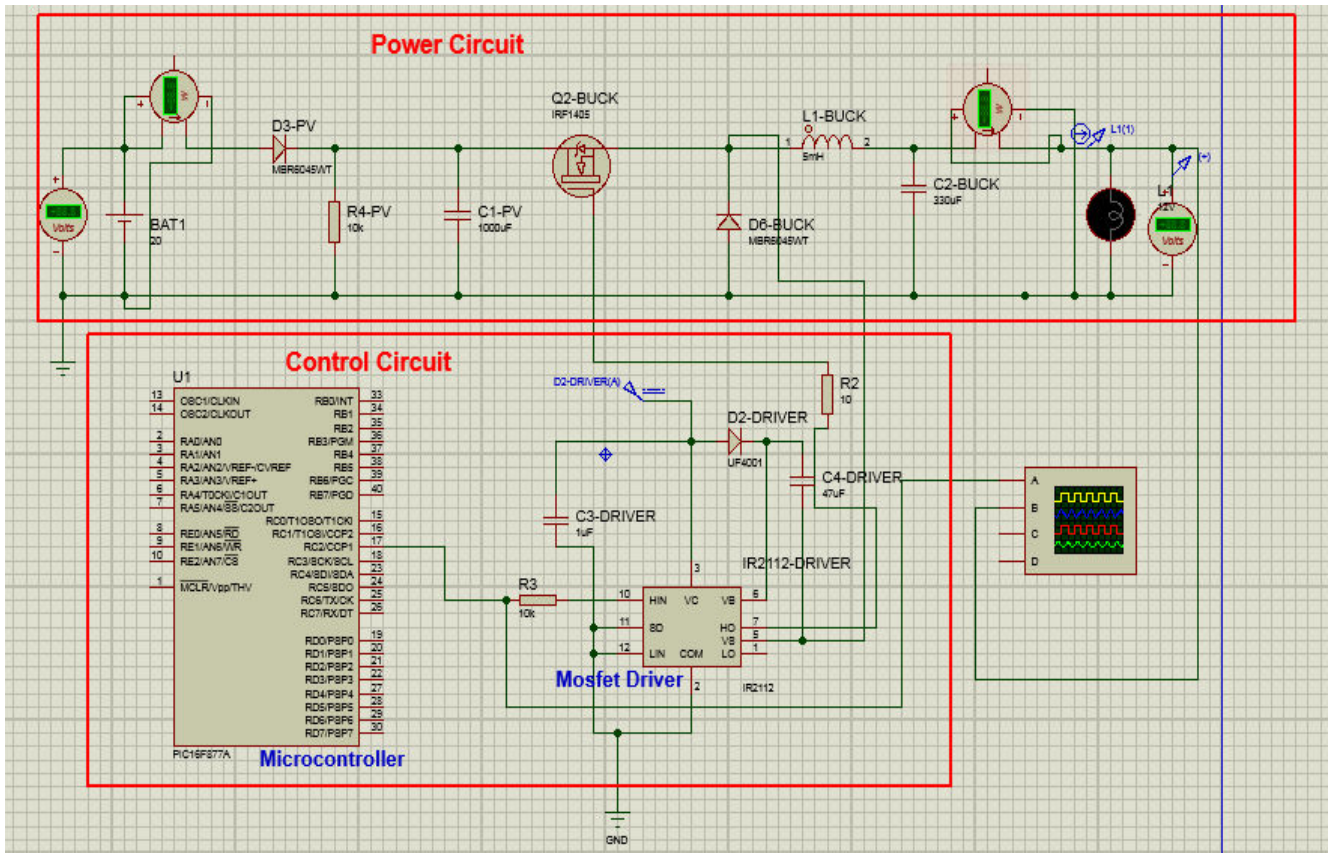


Figure 3.21: Buck Converter circuit diagram

- The control signal is generated by the microcontroller with script code under mikroC software.

```

void main()
{
    trisc = 0x00; // PORTC as output
    PWM1_Init(20000); // Initialize PWM1

    while (1) // endless loop
    {
        PWM1_Start(); // start PWM1
        PWM1_Set_Duty(153); //Change the duty cycle 60 %
        Delay_ms(1000);
    }
}
    
```

Figure 3.22: PWM script code

Simulation results are shown below :

- For $d=0.6$

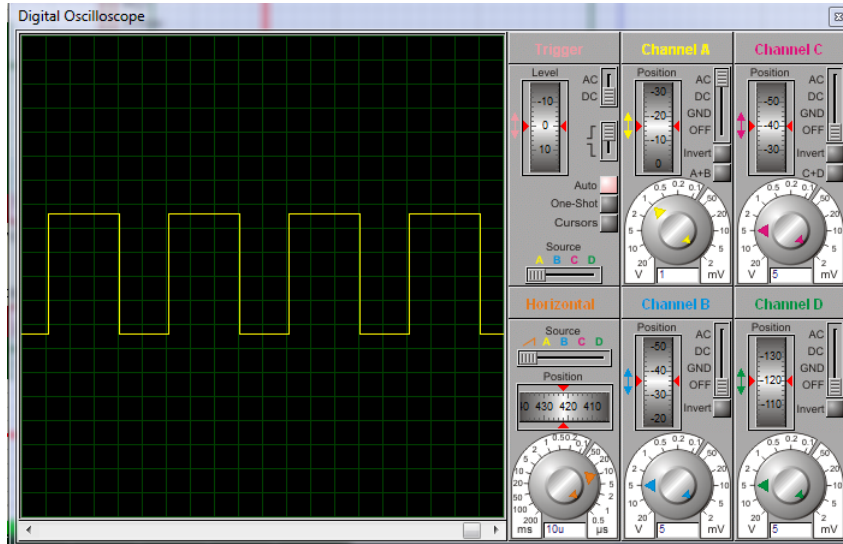


Figure 3.23: The control signal

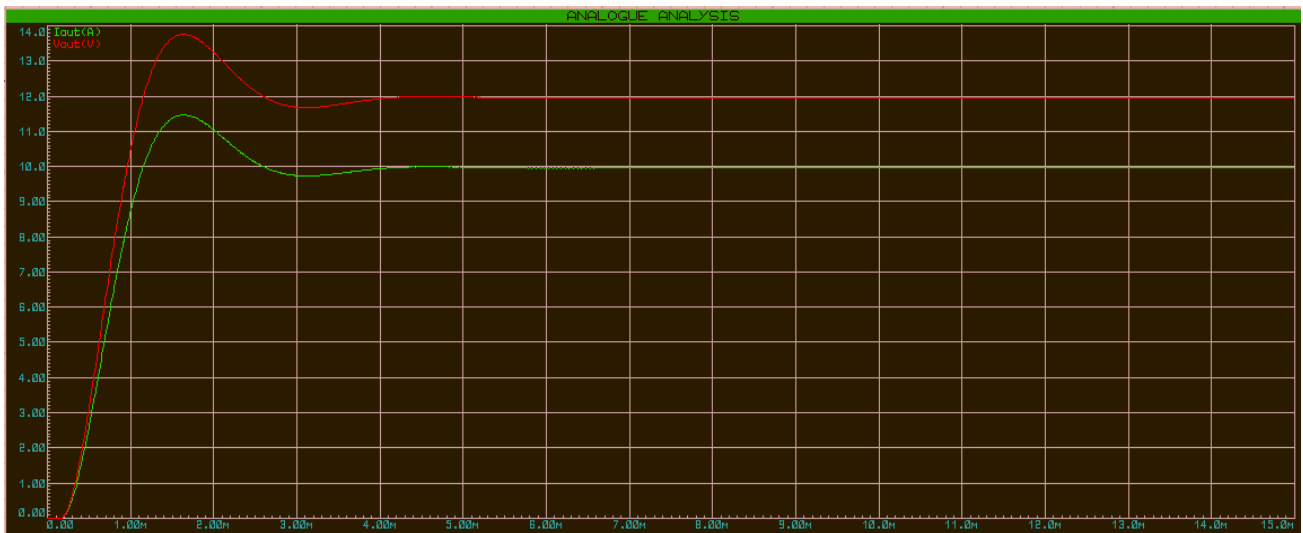


Figure 3.24: Voltage curve V_s (red) ,current I_s (green)

- For $d=0.3$

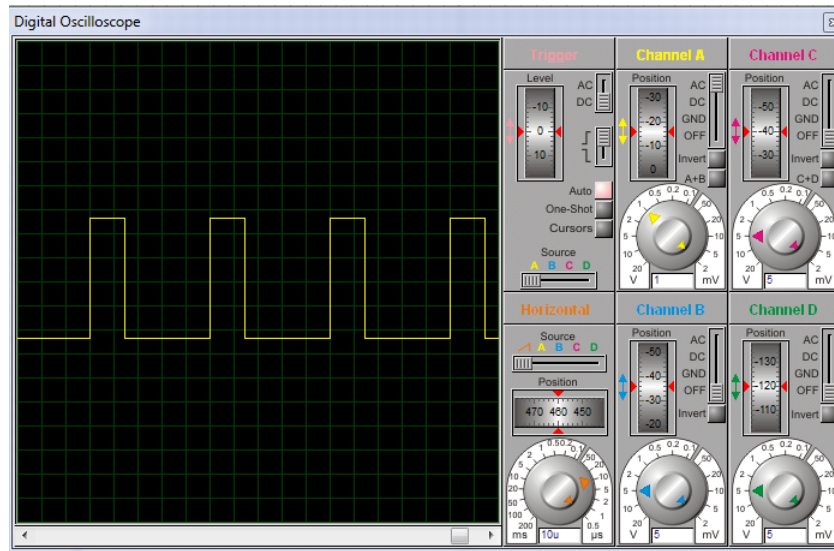


Figure 3.25: The control signal

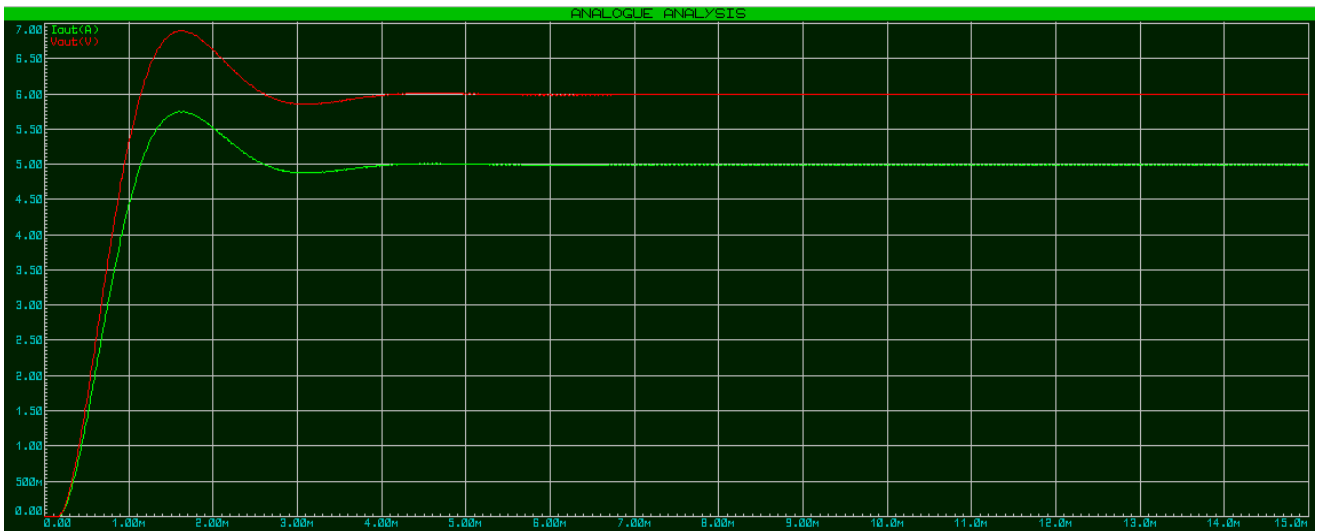


Figure 3.26: Voltage curve V_s (red) ,current I_s (green)

- For $d=0.9$

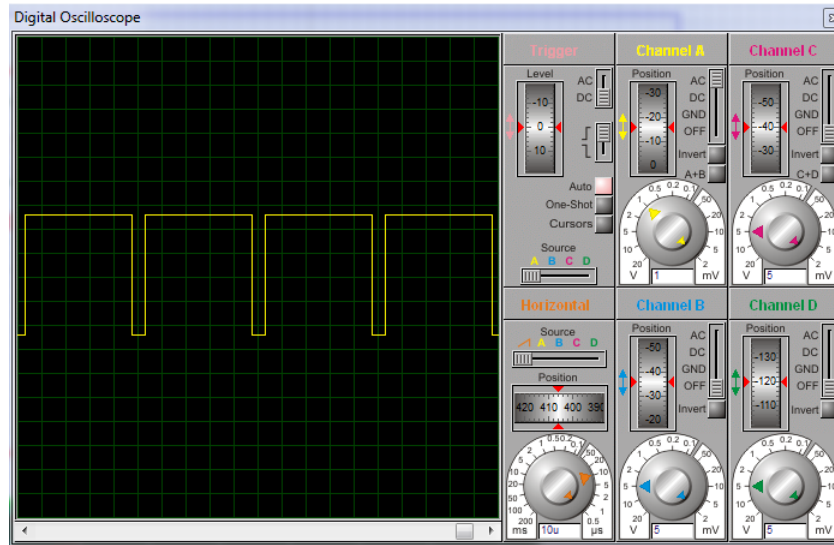


Figure 3.27: The control signal

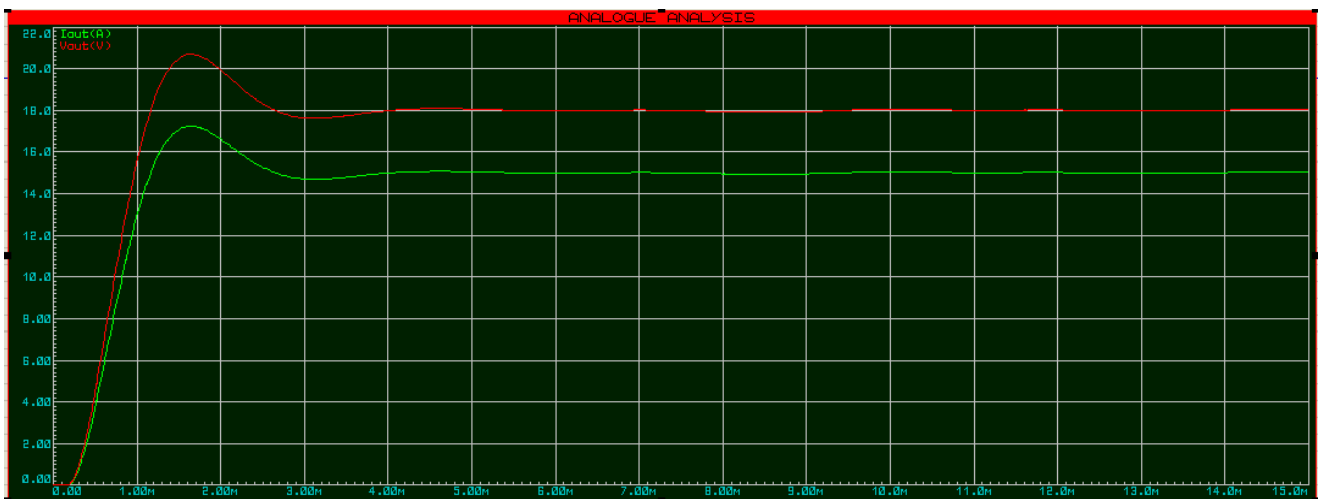


Figure 3.28: Voltage curve V_s (red) ,current I_s (green)

The efficiency vs the duty cycle for the simulated converter with the chosen components is shown in figure 3.29 below

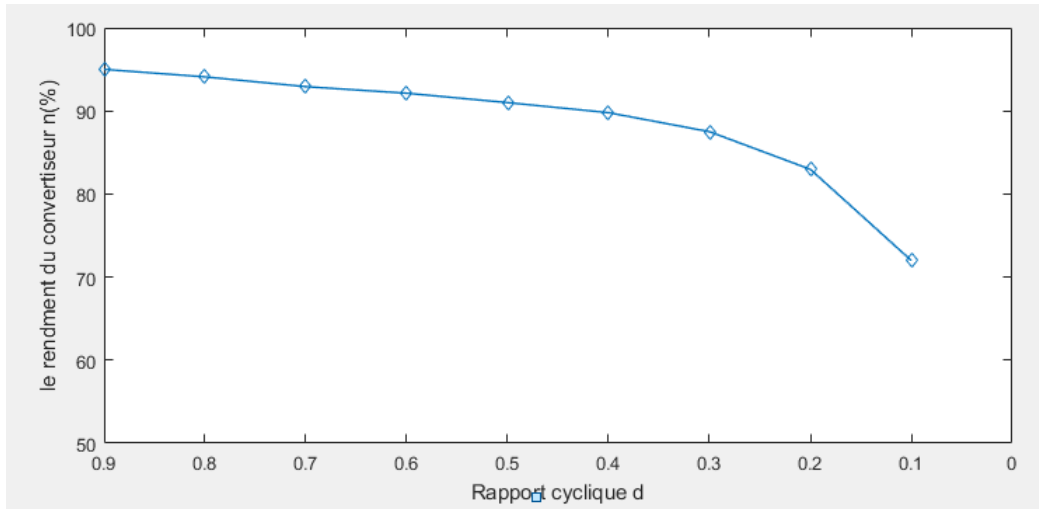


Figure 3.29: Efficiency vs the duty cycle d

- **Comments**

The quality of the inductor and components used can affect the stability of output voltage and current. Inductance losses and high ESR in capacitors can cause fluctuations in output voltage and current.

The rise and fall time of the output signal is important for fast switching applications. If the rise or fall time is too slow, this may indicate a problem with the components or the switching frequency.

Power transistor switching losses must be monitored to ensure that heat dissipation does not exceed permissible temperature limits. If switching losses are too high, this may indicate a problem with component selection or switching frequency.

3.6 Global system simulation:

After the simulation of the buck converter , this time we'll try to simulate the globale system with the PV Array as input source and a battery as output load using P&O Bloc for tracking the maximum power point and controlling the duty cycle for the buck converter.

The simulation of the overall system is shown in figure 3.30:

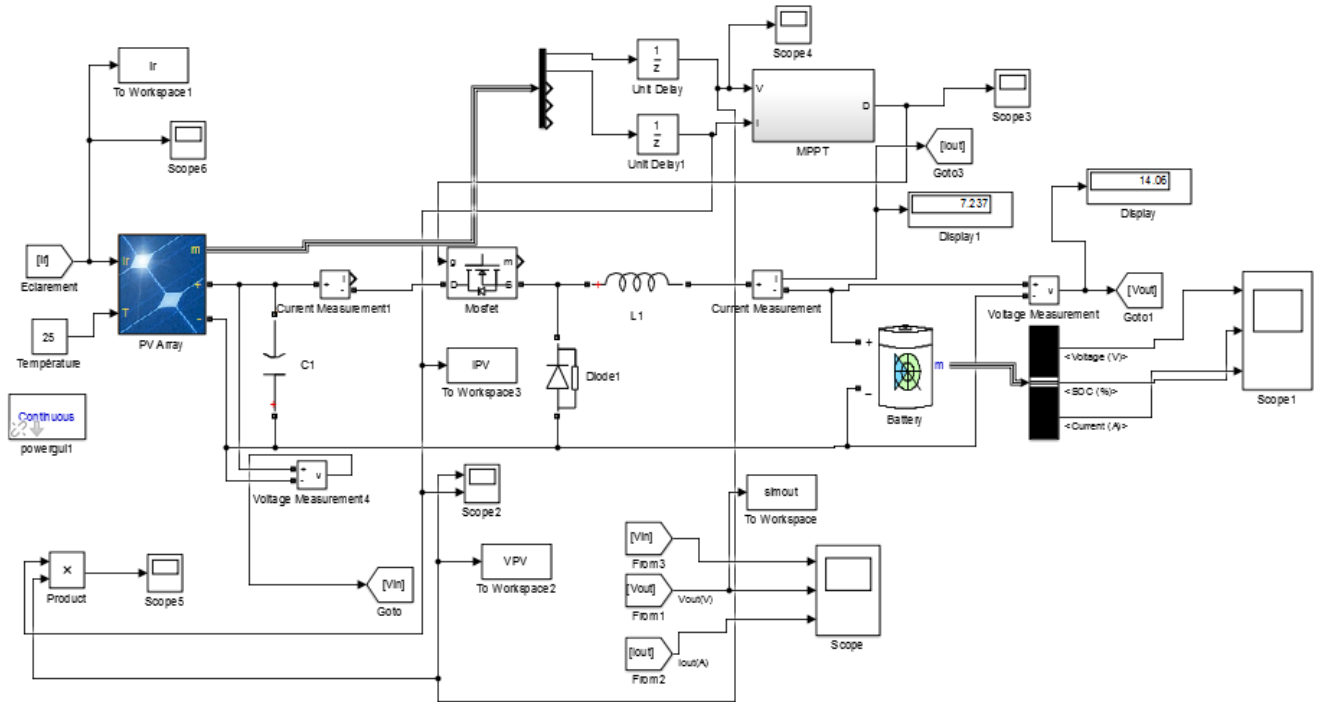


Figure 3.30: Global system simulation block

The PV block in Simulink is shown in figure 3.31 :

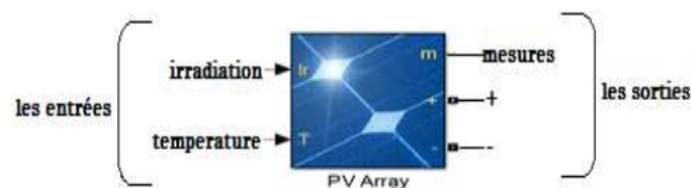


Figure 3.31: SIMULINK model of the photovoltaic panel

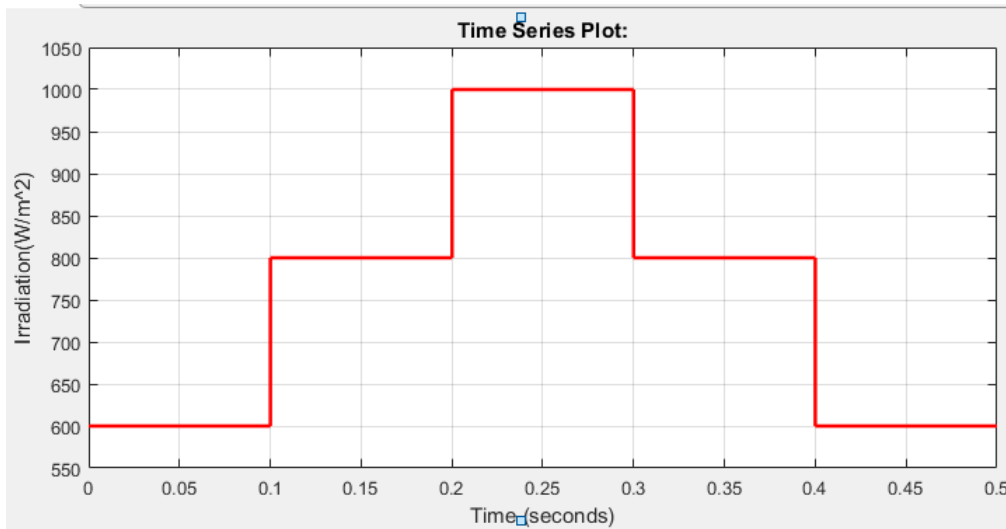


Figure 3.32: Different radiation values at a given time.

As shown in Figure 3.30, at any given time, different values of radiation are directed at the PV panel, starting at 600 W/m² of radiation, increasing to 1000 W/m² of radiation, then decreasing to 600 W/m² of irradiation.

The I-V (current-voltage) and P-V (power-voltage) characteristics for a specified irradiance in (W/m²) and a constant temperature (25°C) for a set of solar panels (PV) shown in figure 3.33.

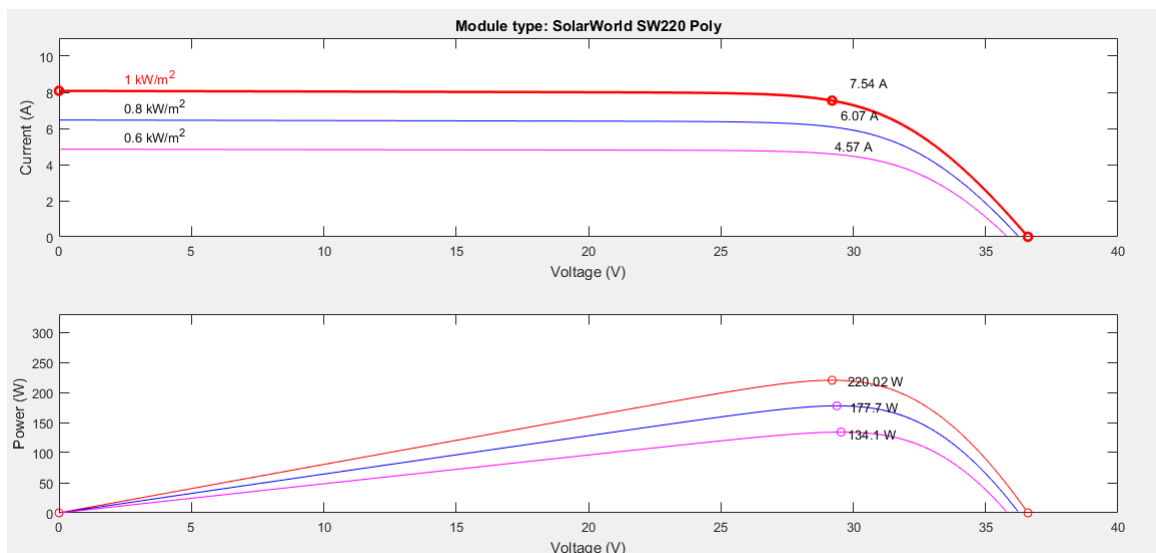


Figure 3.33: I-V (current-voltage) and P-V (power-voltage) characteristics.

In this simulation, the perturbation and observation method was used. The PO algorithm is widely used because it has the particularity of having a simple structure and few measurement parameters. To use it, we consider that the PV is operating at a point which is not necessarily the MPP. The PO method works by periodically disturbing the panel voltage V_{PV} and observing the variation in electrical energy delivered at the PV output.

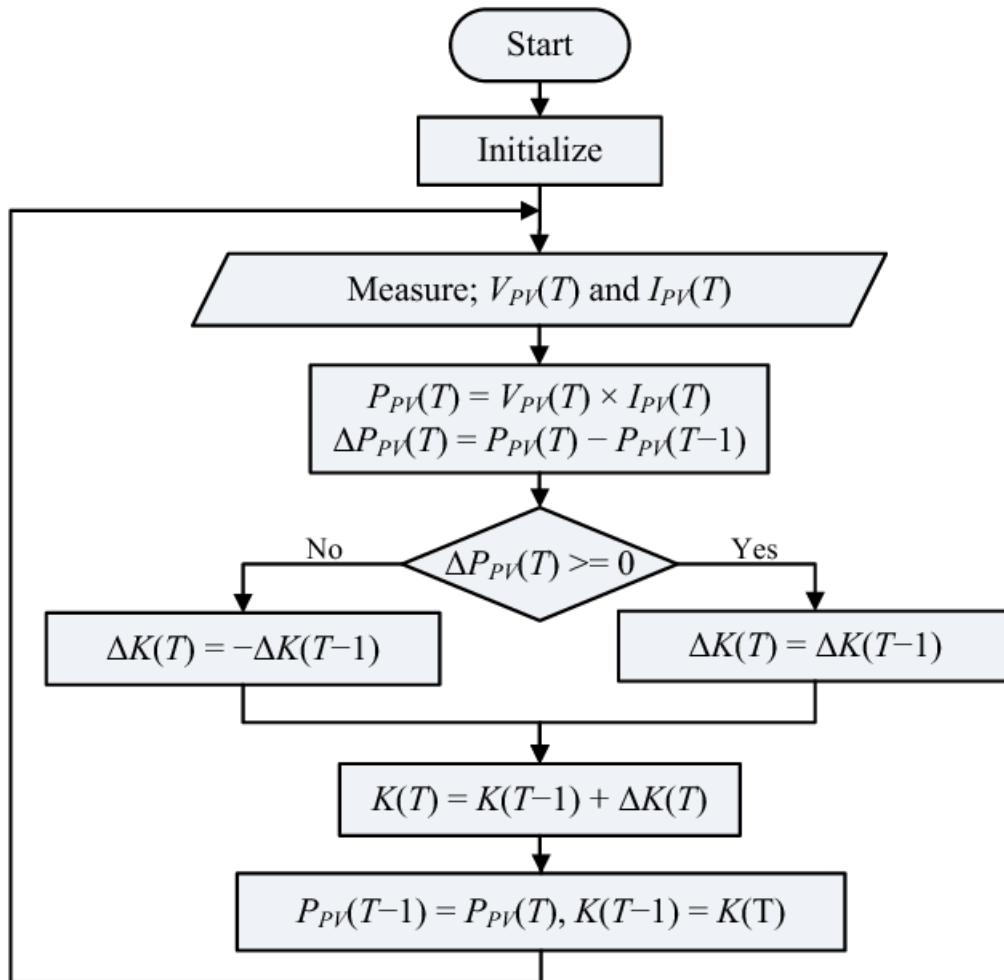


Figure 3.34: P&O Flowchart algorithm [26].

Simulation results are shown below:

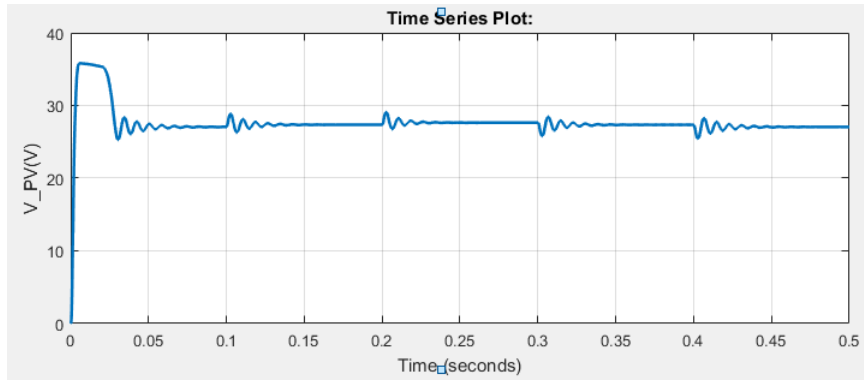


Figure 3.35: PV Voltage Evolution (in V).

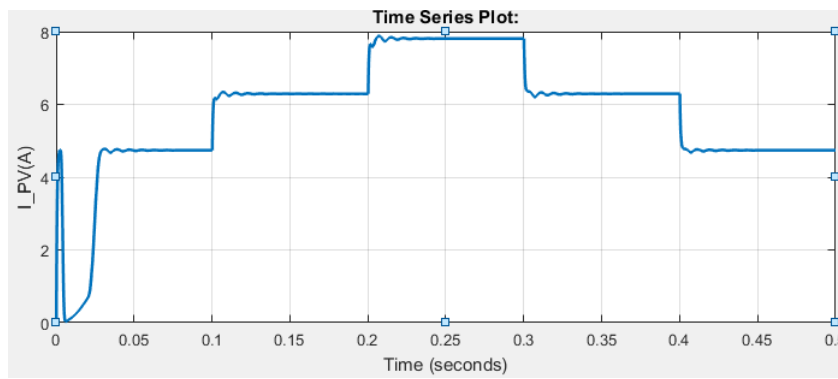


Figure 3.36: PV Current Evolution (in A).

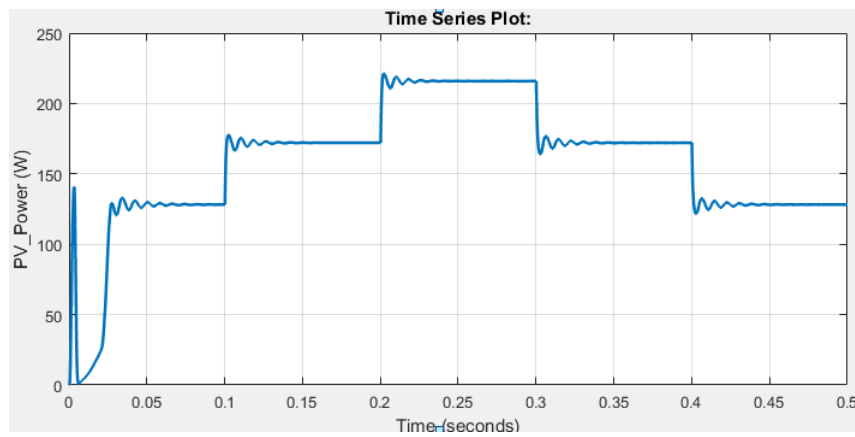


Figure 3.37: PV Power Evolution (in W)

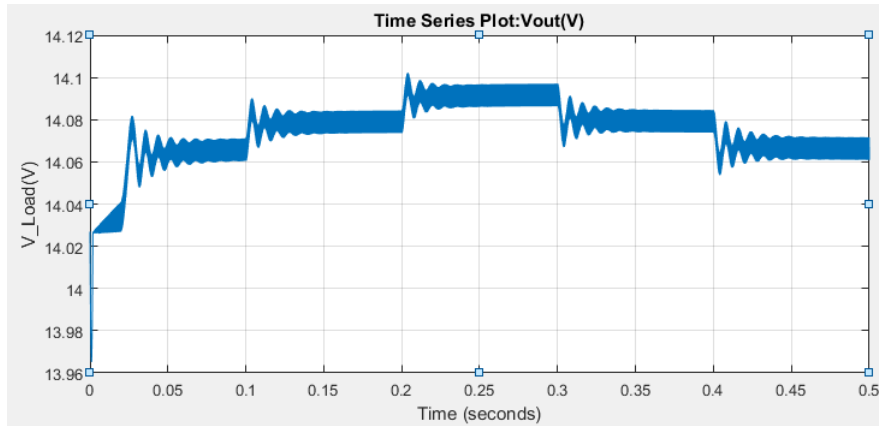


Figure 3.38: Battery Voltage Evolution (in V).

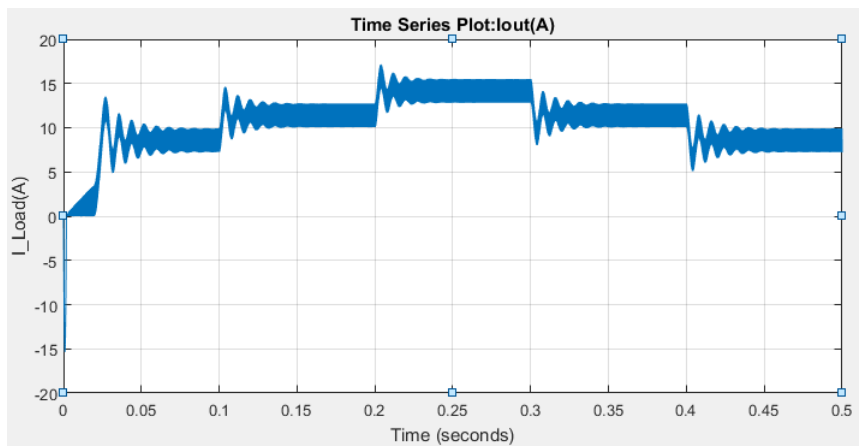


Figure 3.39: Battery Current Evolution (in A).

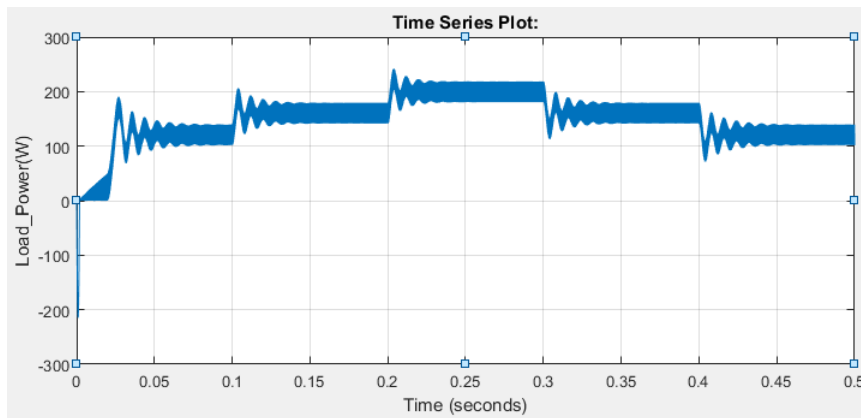


Figure 3.40: Battery Power Evolution (in W)

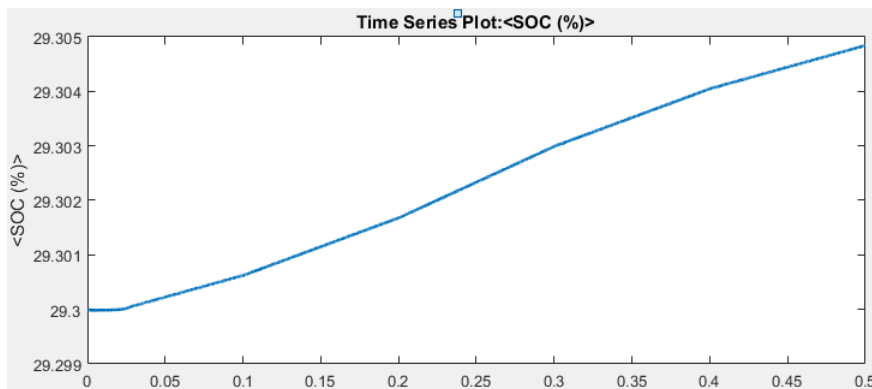


Figure 3.41: State of charge of the battery.

Now by replacing the battery with a resistive load of 1 Ohms we can get the results below:

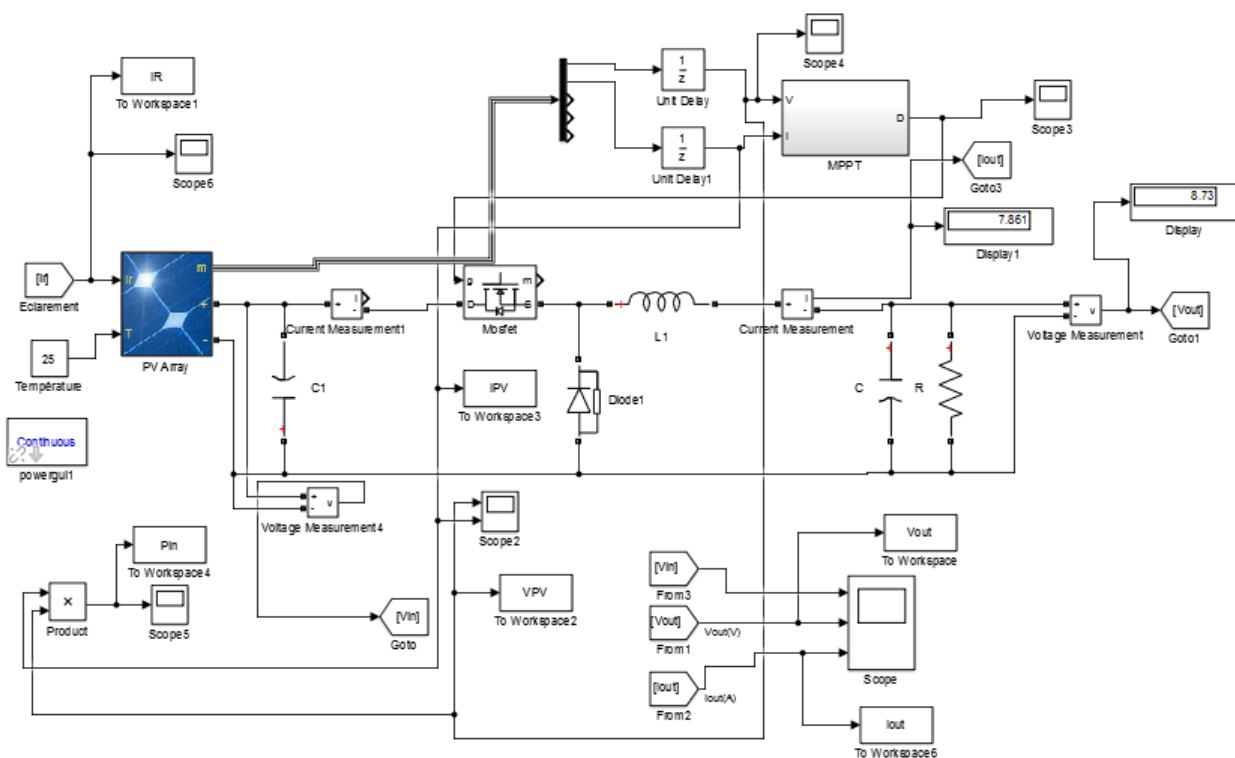


Figure 3.42: Global system simulation with a resistive load.

Simulation results are shown below:

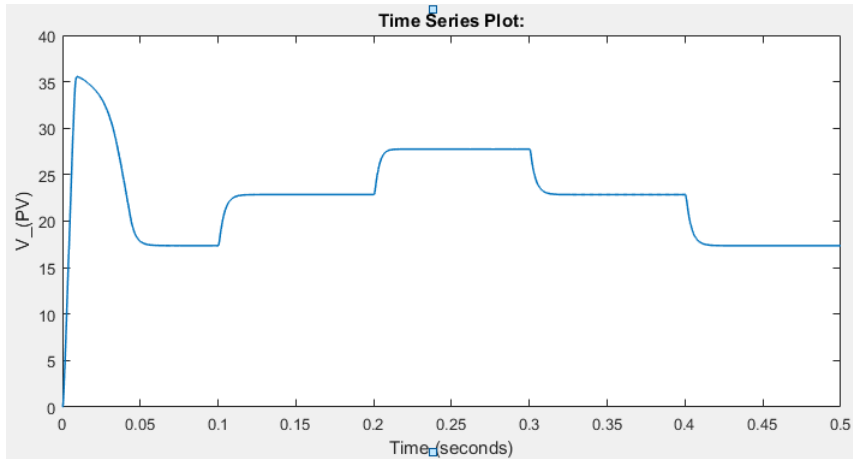


Figure 3.43: PV Voltage Evolution (in V).

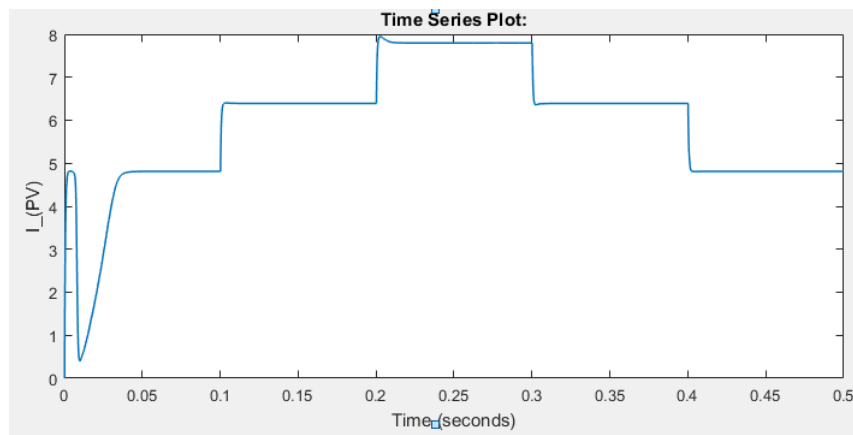


Figure 3.44: PV Current Evolution (in A).

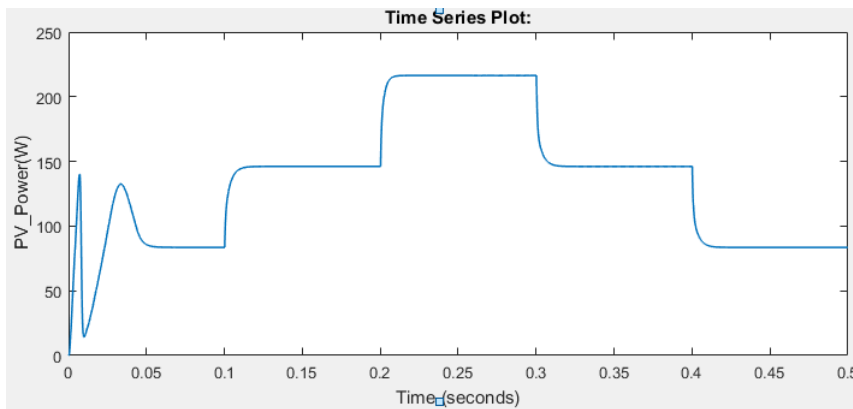


Figure 3.45: PV Power Evolution (in W)

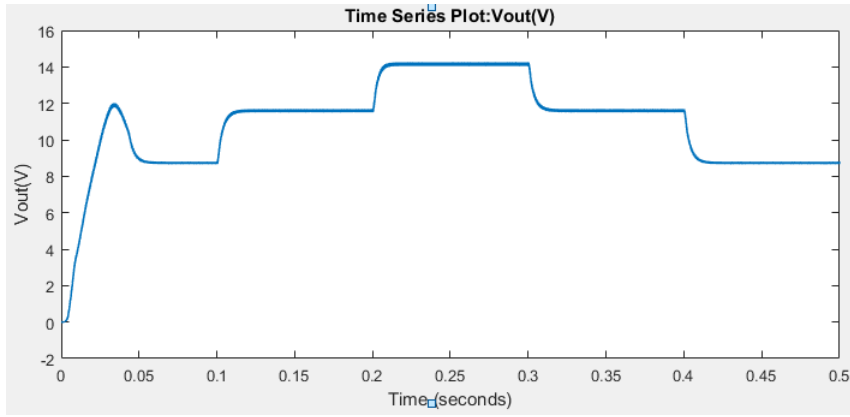


Figure 3.46: Load Voltage Evolution (in V).

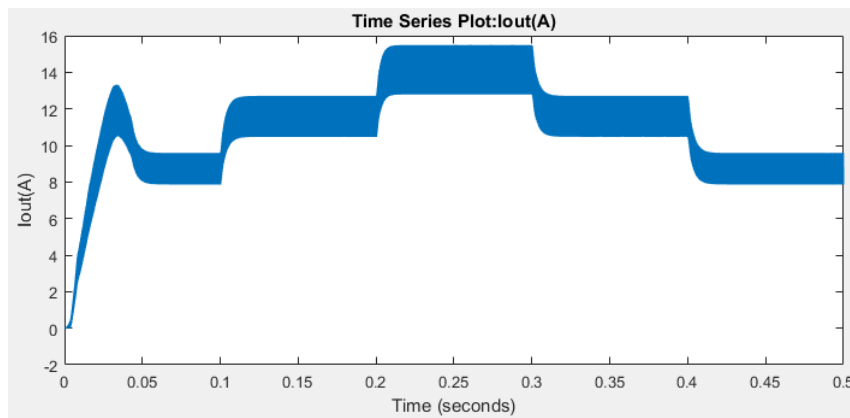


Figure 3.47: Load Current Evolution (in A).

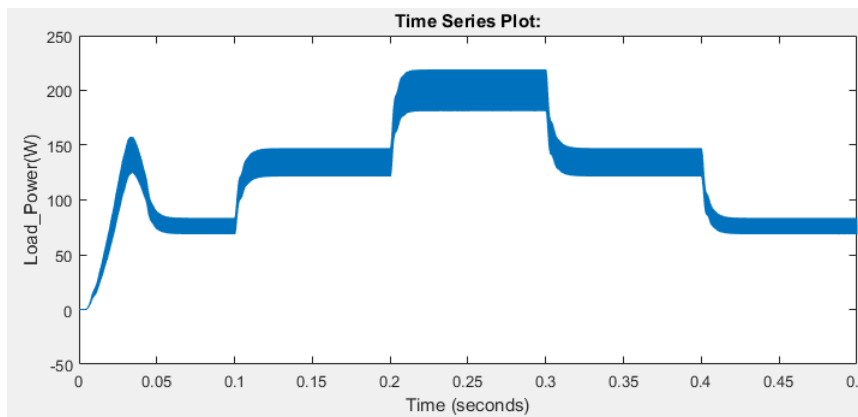


Figure 3.48: Load Power Evolution (in W)

- **Comments:**

In the PV-panel+buck converter+resistive load system without a battery, the objective is typically to regulate the output voltage at a constant level. The buck converter adjusts its duty cycle based on the PO algorithm to maintain the desired output voltage. However, this voltage regulation approach may not be directly aligned with maximizing power extraction from the PV panel.

Without a battery, the buck converter control range is limited by the input voltage from the PV panel. This limitation may prevent the system from effectively tracking and maintaining the MPP, especially during rapidly changing irradiation conditions.

3.7 Conclusion

In this chapter we have seen the simulation of the buck converter with different environments with matlab and protues software, and we observed how can the factors such as power transistor switching losses, inductor and capacitor selection, switching frequency and duty cycle fluctuations can affect the converter's efficiency. Also we have seen The performance of a buck converter connected to a photovoltaic (PV) panel as input and a battery and a resistance as output respectively, controlled by the Perturb and Observe (PO) method for supplying the battery with an optimum power delivered from the panel. Plus the rule of the battery for enhancing control flexibility and energy storage capability enable the PO algorithm to achieve better performance by continuously adjusting the converter's duty cycle to extract maximum power from the PV panel.

In the next chapter we will be looking for an optimum Design and realization of the power circuit for the buck converter.

Chapter 4

Design and realization of the power circuit (Buck converter)

4.1 Introduction:

We will now proceed with the practical implementation of the Buck converter. We will also apply the PWM signals generated by **GBF** to the Buck chopper with the driver circuit: IR2112 MOSFET-DRIVER. Proteus pro 8.13 software is used to design the PCB. But before that we will look at the different factors and elements that can affect the buck converter efficiency such as :

- Choosing the right inductor and capacitor
- Operating Frequency
- Parasitic Elements
- Heat Dissipation
- Load variation
- Control Circuitry

but the switching device element, such as a MOSFET or a transistor, is indeed a major factor influencing the efficiency of a buck converter. When the switch turns on and off, it conducts switching losses, which can contribute to power dissipation and reduce efficiency. These switching losses consist of two main components: Conduction Losses and Switching Losses. Therefore we'll do a test on an existing buck converter designed in «Renewable Energy Development Center(CDER)» using various Mosfets and observe the variation of the average efficiency for each one.

4.2 Testing and observing the results for the tested buck converter:

4.2.1 Description of the board :

The tested buck converter has the same performance requirements that we desire as mentioned in table(3.1). The board components are shown in table below :

Components	Specifications
Diode (D1-PV)	MBR4560WT
Diode (D2-BUCK)	MBR4560WT
Resistance (R1-PV)	10k Ω
Resistance (R3-DRIVER)	47 Ω
Capacitor (C2-PV)	1000 μF
Capacitor (C3-PV)	330 μF
Capacitor (C4-DRIVER)	100 μF
Capacitor (C5-DRIVER)	100 μF
Capacitor (C5-BUCK)	330 μF
Inductor (L1-BUCK)	5 mH
MOSFET-DRIVER	TLP250
MOSFET (Q1-BUCK)	Three technolo- gies

Table 4.1: Components specification

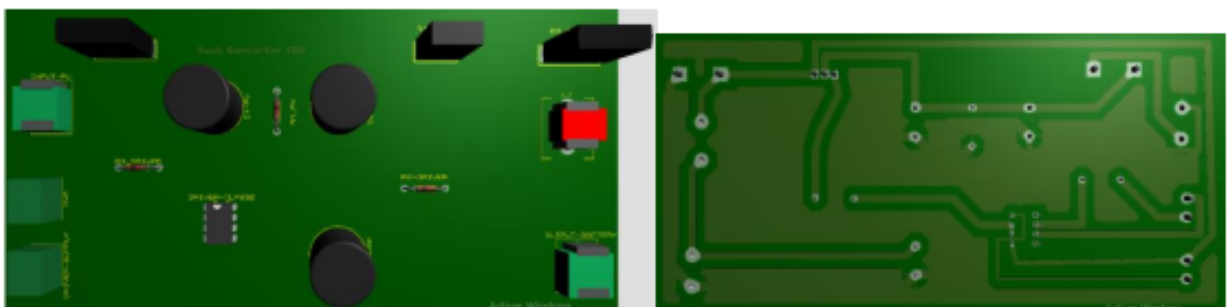
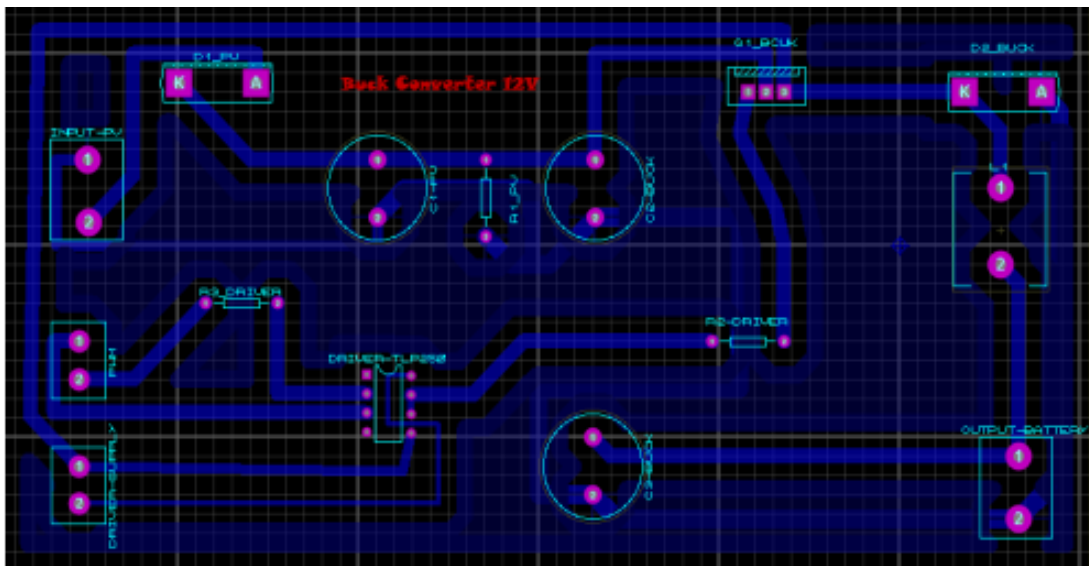


Figure 4.1: TLP250-Buck converter schematic, PCB and 3D view

The mosfets we chose are : IRFP140N , IRFZ44N , IRF2807N Each time we try one and observe the efficiency vs the duty cycle evolution.

IRFP140N-MOSFET :

IRFP140N N-channel MOSFET is designed to handle high power levels. It has a maximum drain-source voltage (V_{ds}) rating of 100 volts and has a maximum continuous drain current (I_d) rating of 33 amperes, The on-resistance ($R_{DS(on)}$) of the IRFP140N is typically around 40 miliohms [27].

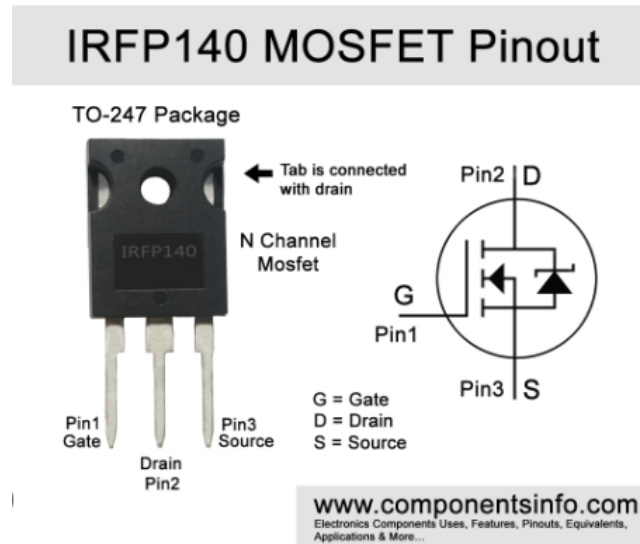


Figure 4.2: MOSFET IRFP140N [27] .

Duty Cycle	Input Voltage (V)	Input Current(A)	Input Power(W)	Output Voltage(V)	Output Current(A)	Output Power(W)	Efficiency (%)
0.95	20	2	40	18.12	2.1	38.052	95.13
0.8	20	1.78	34	15.37	1.91	29.3567	86.34
0.75	20	1.6	32	14.24	1.82	25.9168	80.99
0.6	20	1.13	26	12.21	1.68	20.5128	78.9
0.5	20	1.1	22	10.62	1.55	16.461	74.82
0.4	20	0.9	18	8.64	1.39	12.0096	66.72
0.3	20	0.5	10	5.6	1.09	6.104	61.04
0.2	20	0.2	4	3.57	0.87	3.1059	77.65
0.1	20	0.1	2	1.74	0.64	1.1136	55.68

Table 4.2: IRFP140N results

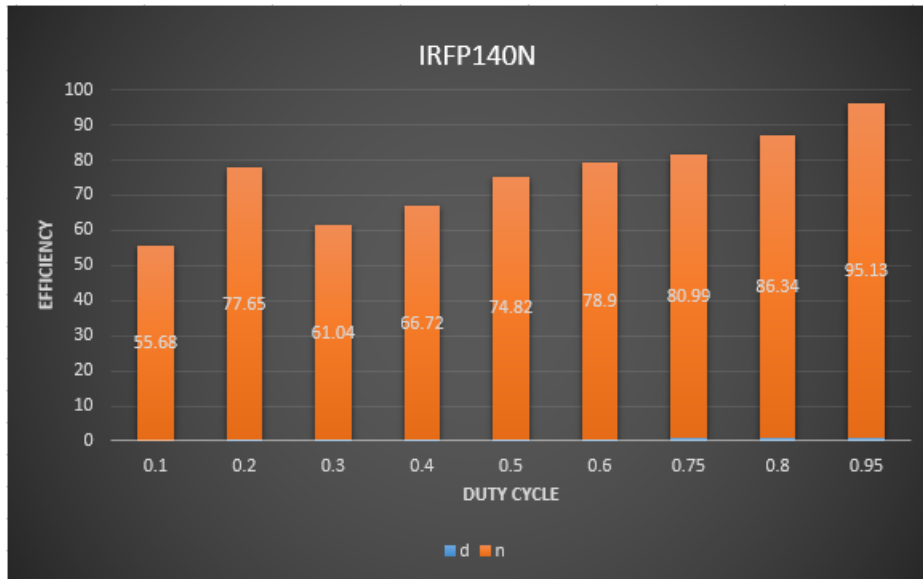


Figure 4.3: Efficiency vs duty cycle for IRFP140N

IRFZ44N-MOSFET :

IRFZ44N N-channel MOSFET is designed to handle high power levels. It has a maximum drain-source voltage (V_{ds}) rating of 55 volts, and it has a maximum continuous drain current (I_d) rating of 49 amperes. The on-resistance ($R_{DS(on)}$) of the IRFZ44N is typically around 22 milliohms [28].

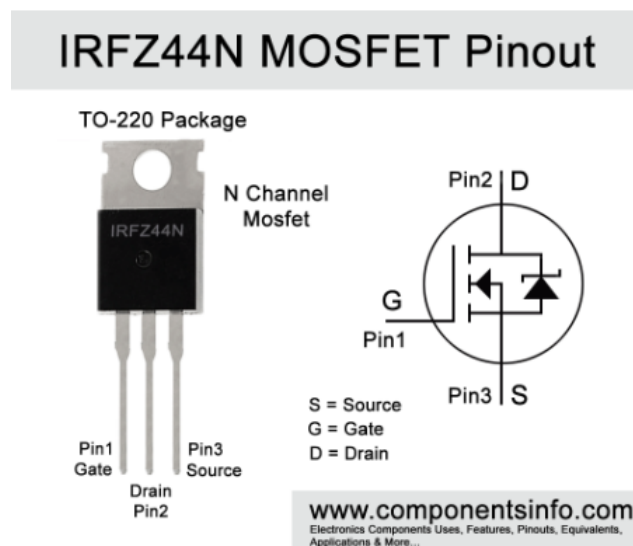


Figure 4.4: MOSFET IRFZ44N [28].

Duty Cycle	Input Voltage (V)	Input Current(A)	Input Power(W)	Output Voltage(V)	Output Current(A)	Output Power(W)	Efficiency (%)
0.95	20	2.1	42	18.15	2.08	37.75	90
0.8	20	1.8	36	16.23	1.96	31.81	88.3
0.75	20	1.5	30	14.31	1.82	26.04	86.8
0.6	20	1.1	22	11.5	1.6	18.4	83.63
0.5	20	0.8	16	9.51	1.47	13.98	87.37
0.4	20	0.6	12	7.45	1.28	9.54	79.5
0.3	20	0.4	8	5.57	1.1	6.127	76.58
0.2	20	0.2	4	3.57	0.87	3.221	80.55
0.1	20	0.1	2	1.69	0.63	1.06	53

Table 4.3: IRFZ44N results

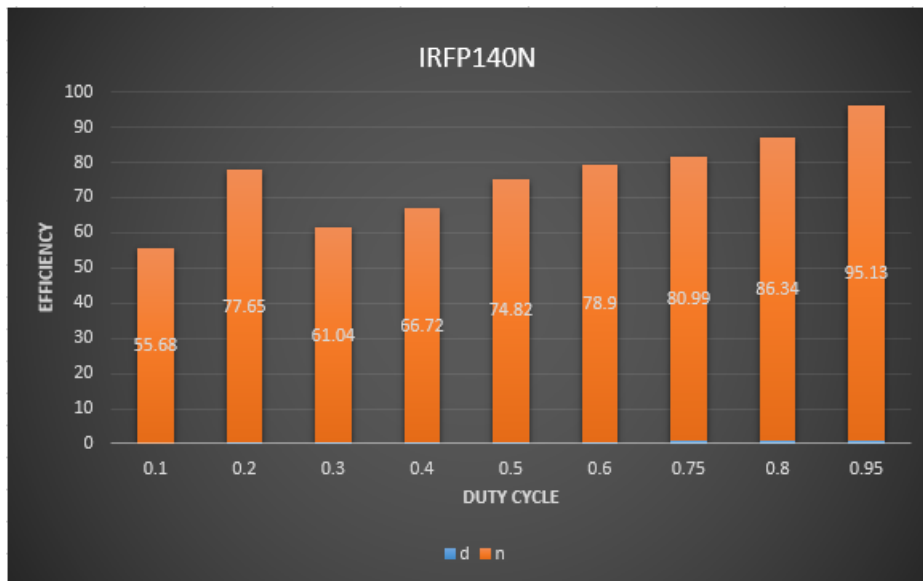


Figure 4.5: Efficiency vs duty cycle for IRFZ44N

IRF2807-MOSFET :

IRF2807 is an N-channel MOSFET, It's designed to handle continuous drain currents of up to 82A (Amperes) and has a maximum drain current of 310A in pulsed mode. It has a maximum drain-source voltage rating of 75V, with maximum on-resistance (RDS(on)) of 13 milliohms [29].



Figure 4.6: MOSFET IRF2807 [29].

Duty Cycle	Input Voltage (V)	Input Current(A)	Input Power(W)	Output Voltage(V)	Output Current(A)	Output Power(W)	Efficiency (%)
0.95	20	2	40	18.37	2.07	38.0259	95.06
0.8	20	1.6	32	15.45	1.9	29.355	91.73
0.75	20	1.4	28	13.53	1.77	23.9481	85.3
0.6	20	1.1	22	11.55	1.62	18.711	85.05
0.5	20	0.9	18	9.71	1.49	14.4679	80.37
0.4	20	0.6	12	7.69	1.3	9.997	83.30
0.3	20	0.4	8	5.73	1.13	6.4749	80.93
0.2	20	0.2	4	3.8	0.92	3.496	87.4
0.1	20	0.1	2	1.93	0.69	1.3317	66.58

Table 4.4: IRF2807N results

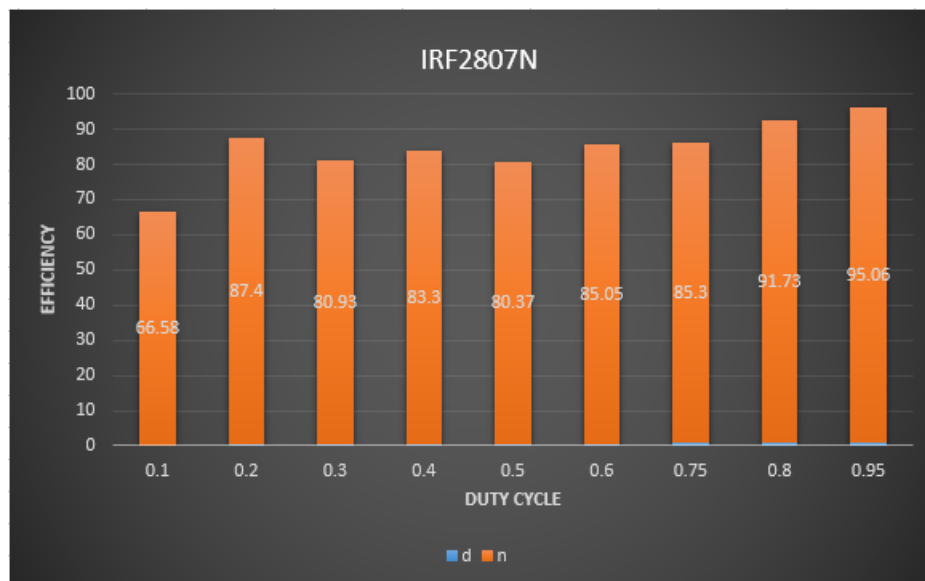


Figure 4.7: Efficiency vs duty cycle for IRF2807N

Comparison between the results :

By calculating the average efficiency for each MOSFET we tested, we got the results shown in the figure 4.8.

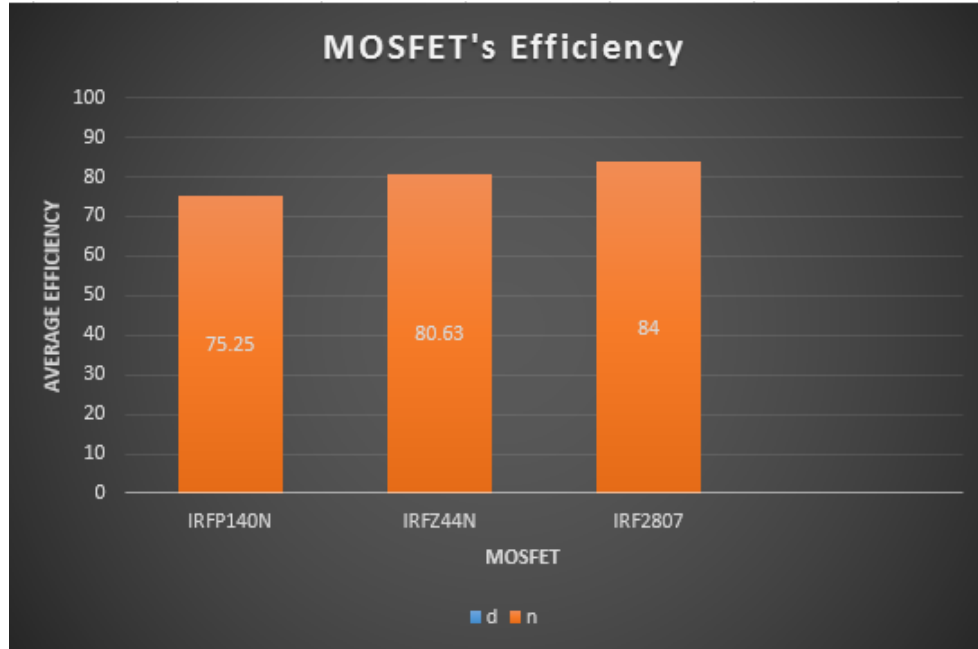


Figure 4.8: Average Efficiency Comparison for IRFP140N ,IRFZ44N , IRF2807

We can notice that IRF2807N has the highest efficiency due to its lowest on-resistance ($R_{DS(on)}$) of 13 milliohms which is less than RDS of IRFZ44N with 22 milliohms and RDS of IRFP140N with 40 milliohms.

The conduction losses(4.1) and switching losses(4.2) can be calculated with the formula below [30] :

$$P_{rDS\max} = d * r_{DS} * I_{s\max}^2 \quad (4.1)$$

$$P_{sw(\max)} = f * C_o * V_{e\max}^2 \quad (4.2)$$

with:

d: Duty cycle

r_{DS} : MOSFET on-resistance

$I_{s\max}$: Maximum output current

f: Switching frequency

C_o : MOSFET output capacitance

$V_{e\max}$: Maximum input voltage.

[30]

4.3 Choice and description of board components:

4.3.1 < MOSFET > switch

Hence its higher efficiency and lower on-resistance We chose IRF2807 an N-channel MOSFET, designed to handle continuous drain currents of up to 82A (Amperes) and has a maximum drain current of 310A in pulsed mode. It has a maximum drain-source voltage rating of 75V, with maximum on-resistance ($R_{DS(on)}$) of 13 milliohms



Figure 4.9: MOSFET IRF2807 [29].

4.3.2 Diode

We chose a fast MBR3060PT diode (Schottky type) which is designed to handle a maximum average forward current rating (I_F) of 30A, maximum peak forward surge current rating (I_{FSM}) of 220A. It has a maximum reverse voltage (V_R) rating of 60V, and has a low forward voltage drop, which means it exhibits low voltage losses when conducting current in the forward direction.

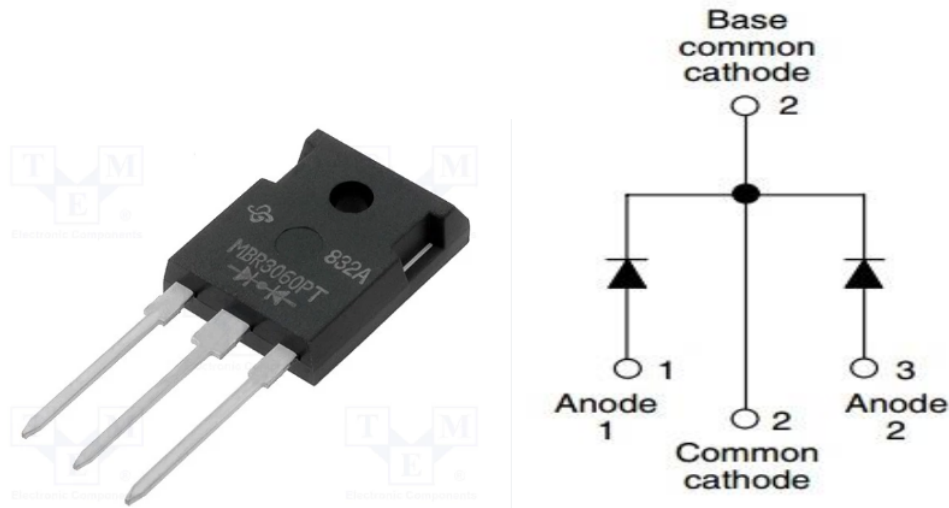


Figure 4.10: Schottky Diode MBR3060PT [31].

4.3.3 Ferrite core coil

A ferromagnetic core coil with an inductance of 5 mH is used. It supports a maximum current of 25A. To do this, we needed a ferrite core with a diameter large enough to pass a specific number of turns. The number of turns : $N = 24$ turns.



Figure 4.11: Ferrite core coil

4.3.4 Capacitors

A C_{2-buck} capacitive storage capacitor with a capacitance of 330 μF and 63V (greater than a $C_{buck-min} = 13.02\mu\text{F}$) is used at the converter's passive filter. It has 63V isolation voltage. Another capacitor (C_{PV} greater than $C_{pv-min} = 714\mu\text{F}$) connected across the PV module to filter the chopper input voltage and reduce input ripple. Its isolation voltage is 63V.

Figure 4.12: Capacitor $330\mu F - 63V$

4.3.5 MOSFET-DRIVER «IR2112»

The IR2112 is a high-speed MOSFET driver integrated circuit (IC) designed for driving power MOSFETs and IGBTs, to provide high-speed switching performance. It features two floating outputs, HO and LO, which are designed to drive the gate of an external power device. The IR2112 incorporates an under-voltage lockout circuit that protects against improper operation when the power supply voltage falls below a certain threshold. This feature ensures reliable operation of the driver and power devices even under low voltage conditions. It also has protection features to prevent damage in case of a short-circuit condition. The IR2112 operates over a wide supply voltage range, typically from 10V to 20V. [32]

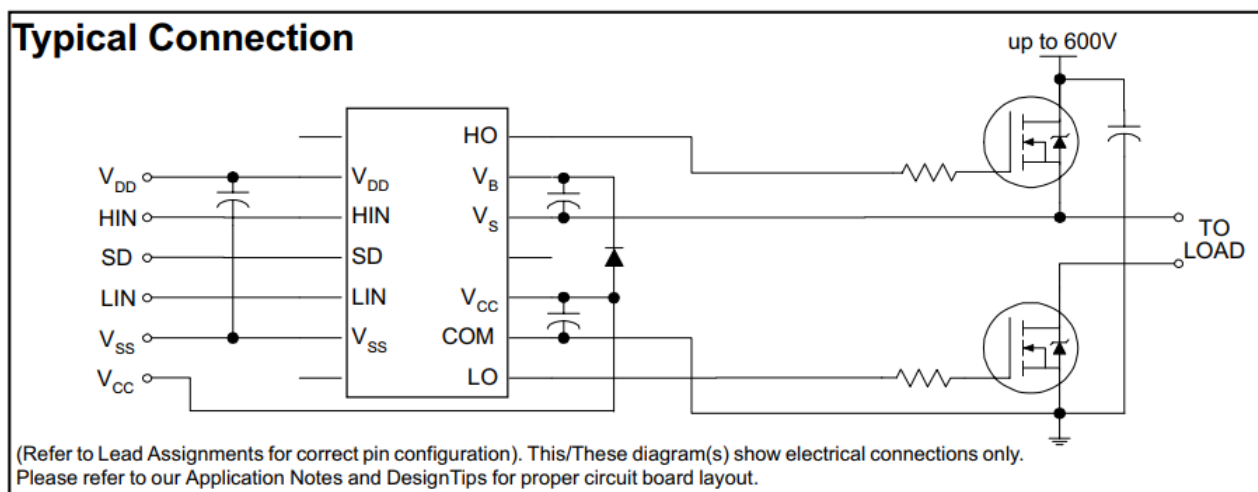


Figure 4.13: IR2112 Functional Block Diagram [32]

- **IR2112-DRIVER electrical characteristics and specifications:**

Supply Voltage (VCC): between 10V and 20V.

Logic high Input Voltage (VIL):2.5V

Logic low Input Voltage (VIL): 1.5V

Floating Output Voltage (VFO): 500mV.

Output Voltage Swing (VOUT): around 0.3V.

Output Current: up to 2A of peak output current

Propagation Delay Time (tPD): around 120ns.

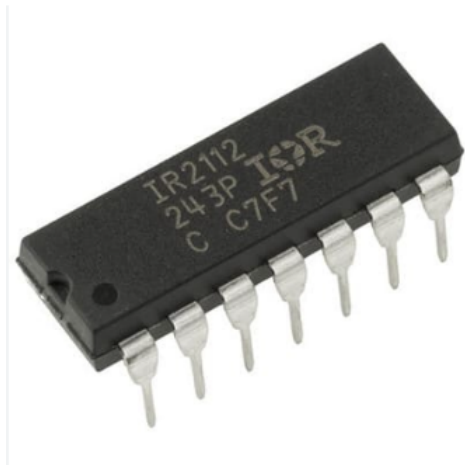


Figure 4.14: IR2112-DRIVER overview [32].

The values of the components associated with the driver IR2112 are as follows:

$$C_{3-DRIVER} = 1\mu F, C_{4-DRIVER} = 47\mu F, R_{2-DRIVER} = 10\Omega$$

And the $D_{2-DRIVER}$ diode we used is the UF4007 diode. ultra-fast rectifier, characterized by the following parameters:

Maximum Peak Forward Surge Current (IFSM):30A

Maximum Reverse Voltage (VRRM):1000V

Maximum Forward Voltage Drop (VF):1V

Reverse Recovery Time (trr):75ns



Figure 4.15: Diode UF4007 [33].

By using the proteus software,with the desired components a design was done shown in the figure 4.16 below :

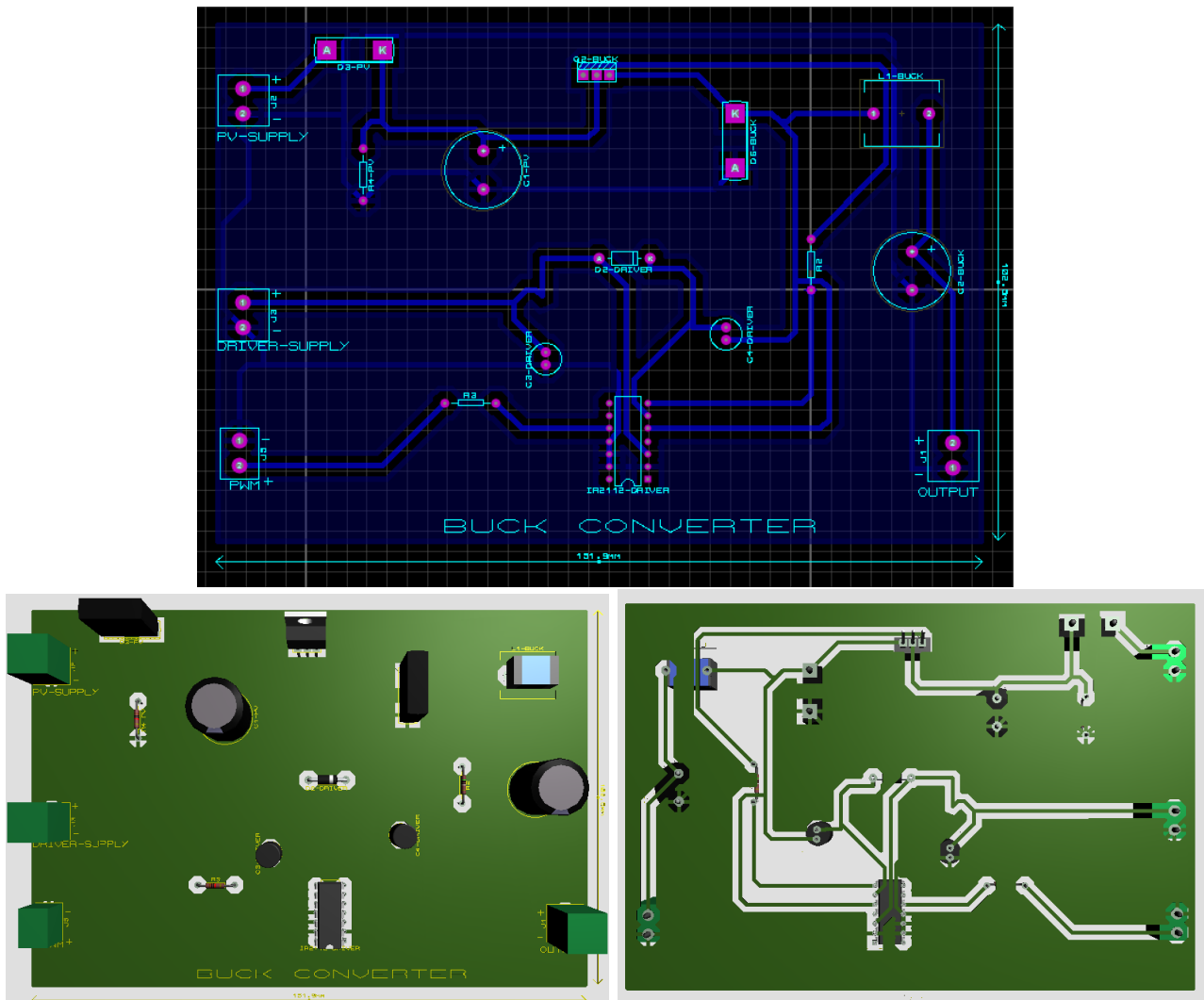


Figure 4.16: Buck converter schematic, PCB and 3D view

4.4 Power Losses and Efficiency of the Buck Converter:

We will consider for calculating the power losses : Duty cycle $d=0.6$, Maximum output current $I_{s\max} = 20A$,Maximum input voltage $V_{e\max} = 30V$,Output resistance 0.6Ω ,Output voltage $V_s=12V$

- The maximum MOSFET conduction power is:

$$P_{rDS\max} = d * r_{DS} * I_{s\max}^2 = 0.6 * 13 * 10^{-3} * 20^2 = 3.12W$$

- The maximum switching loss is:

$$P_{sw(\max)} = f * C_o * V_{e\max}^2 = 20 * 10^3 * 610 * 10^{-12} * 30^2 = 0.011W$$

- The total power dissipation in the MOSFET is:

$$P_{rDS\max} + P_{sw(\max)}/2 = 3.12 + 0.366/2 = 3.1255W$$

- Conduction diode power loss is:

$$P_D = (1 - d) V_F I_{s\max} = (1 - 0.1)0.75 * 20 = 6W$$

- The power loss in the inductor is :

$$P_{rL} = r_L I_{s\max}^2 = 50 * 10^{-3} * 20^2 = 20W$$

- The power loss in the ESR is:

$$P_{rC} = \frac{r_C (\Delta i_{L\max})^2}{12} = 0.05 * 1^2/12 = 0.00416W$$

with:

V_F : MBR3060PT forward voltage drop

r_L : series inductor resistance

r_C : series capacitor resistance [30]

The total power loss is:

$$P_{LS} = P_{rDS} + P_{sw} + P_D + P_{rL} + P_{rC} = 3.1255 + 6 + 20 + 0.00416 = 29.13W$$

The efficiency of the converter for 0.6 duty cycle is:

$$\eta = \frac{P_{out}}{P_{out} + P_{LS}} = \frac{240}{240 + 29.13} = 0.8917 = 89.17\%$$

After testing it with the same condition as the CDER tested converter we got the results shown in the table 4.5 below :

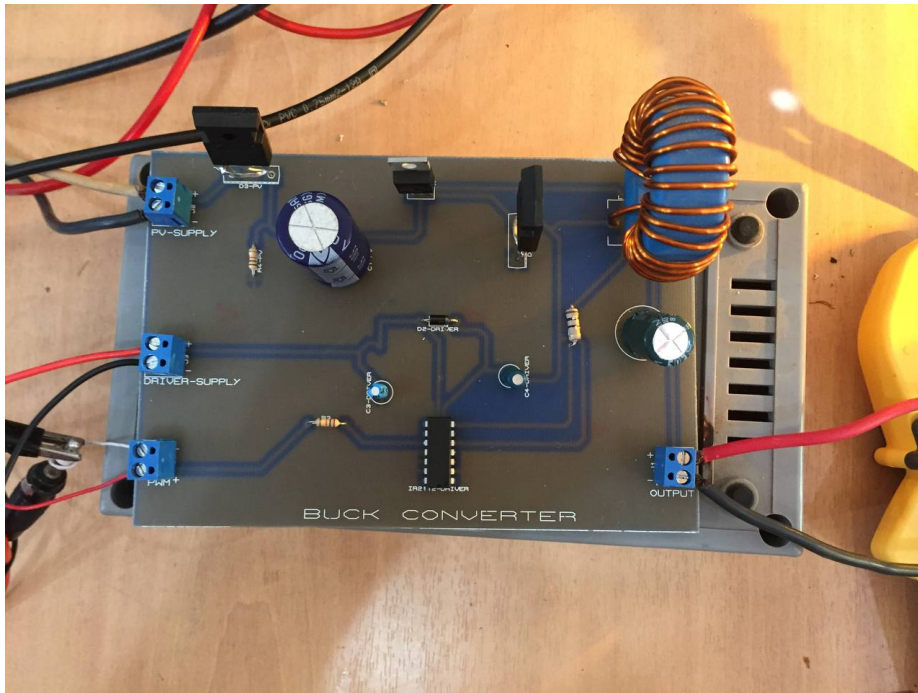


Figure 4.17: Realized buck converter overview

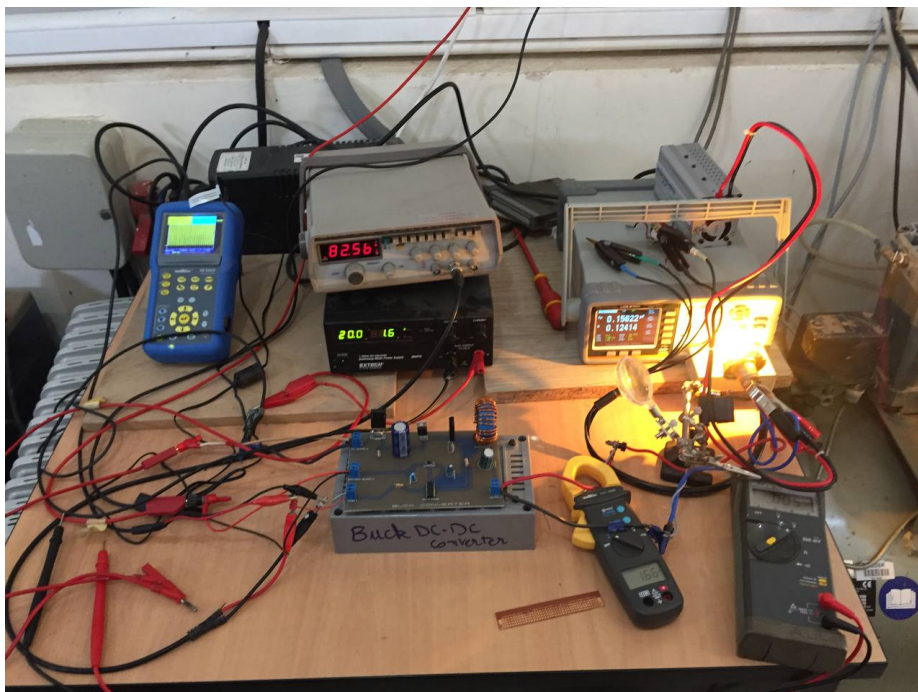


Figure 4.18: Experimental platform

Duty Cycle	Input Voltage (V)	Input Current(A)	Input Power(W)	Output Voltage(V)	Output Current(A)	Output Power(W)	Efficiency (%)
0.95	20	2	40	18.21	2.14	38.9694	97.42
0.8	20	1.6	32	15.6	1.98	30.888	96.52
0.75	20	1.5	30	14.45	1.92	27.744	92.48
0.6	20	1.1	22	11.52	1.68	19.3536	87.97
0.5	20	0.8	16	9.64	1.47	14.1708	88.56
0.4	20	0.6	12	7.6	1.4	10.64	88.66
0.3	20	0.4	8	5.7	1.22	6.954	86.92
0.2	20	0.2	4	3.76	0.95	3.572	89.3
0.1	20	0.1	2	1.78	0.85	1.513	75.65

Table 4.5: Testing results

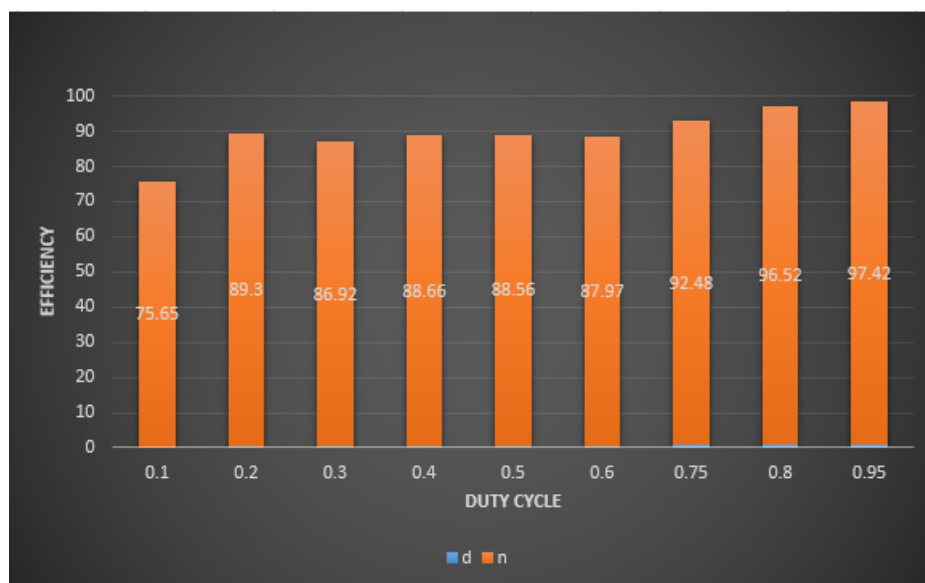


Figure 4.19: Efficiency vs duty cycle for the realization buck converter

The average efficiency is 89.27%

4.5 Conclusion

The efficiency of buck converter can be enhanced by choosing the right components, between them we chose to test the effect of the switch element where choosing a switching device with low on-resistance and fast switching characteristics. Lower on-resistance reduces conduction losses, and faster switching speeds minimize switching losses.

Conclusion and perspectives

Photovoltaic (PV) generators play a crucial role in stand-alone PV systems, providing a sustainable and renewable source of energy. These systems consist of various components, each with its specific role. The key components include PV panels, charge controllers, batteries, and DC-DC converters.

The battery plays a critical role in controlling and storing energy in stand-alone PV systems. It serves as an energy reservoir, allowing for the storage of excess electricity generated by the PV panels. When a battery is included in the system, it introduces additional control possibilities and energy storage capabilities. The battery can act as a buffer, allowing the converter to operate within a wider control range and decoupling the load from the PV panel's instantaneous power generation. This enhanced control flexibility and energy storage capability enable the PO algorithm to achieve better performance by continuously adjusting the converter's duty cycle to extract maximum power from the PV panel while maintaining the battery's state of charge.

To enhance the efficiency of the DC-DC buck converter in stand-alone PV systems, several factors can be considered:

Proper Sizing and Matching: Ensuring the buck converter is appropriately sized and matched to the PV panel's voltage and current characteristics is essential. This helps optimize the converter's performance and maximize energy transfer.

Maximum Power Point Tracking (MPPT): Implementing MPPT algorithms in the system can significantly improve the buck converter's efficiency. More than the PWM control method where MPPT algorithms track the maximum power point of the PV panels, adjusting the converter's operating parameters to extract the maximum power available.

Component Selection: Choosing high-quality components, such as Inductors, Capacitors, and Diodes, Mosfets with low resistance and suitable specifications, can improve the overall efficiency of the buck converter.

Minimizing Losses: Reducing losses in the system, such as minimizing resistive losses in wiring and connections, using appropriate heat sinks for dissipating heat, and optimizing the layout and design of the circuit, can enhance the efficiency of the buck converter.

By considering these factors and implementing appropriate measures, the efficiency of the DC-DC buck converter in stand-alone PV systems can be enhanced, leading to improved energy utilization and overall system performance.

Bibliography

- [1] MECHALIKH-HAMADA, M. N. C. E. (2013). Modélisation et simulation d'un système photovoltaïque en fonctionnement autonome et connecté au réseau, Thèse de Master, UNIVERSITÉ KASDI MERBAH – OUARGLA, 2013.
- [2] BUN, L. Détection et Localisation de Défauts pour un Système PV. Laboratoire G2ELAB dans l'École Doctorale EEATS. L'université de GRENOBLE 2013.
- [3] « Photovoltaic generators structure » available online <https://biblus.accasoftware.com/fr/types-de-panneaux-photovoltaiques-quelles-sont-les-differences/>
- [4] GOAR Nouredine, MAHMOUDI Abdelkader, "Réalisation d'un convertisseur DC/DC dans une chaîne de conversion d'énergie photovoltaïque", Thèse de Master, Université Larbi Ben M'Hidi - Oum El Bouaghi Juin 2017.
- [5] Camara Mohamed Ansoumane, "Modélisation du stockage de l'énergie photovoltaïque par supercondensateurs", thèse de Doctorat, université de Paris 2011.
- [6] « Stand alone photovoltaic system technology » available online <https://learning.edx.org/course/course-v1:DelftX+PV3x+1T2023/home>
- [7] « Diagram block of standalone pv systems » available online https://www.researchgate.net/figure/Block-diagram-of-the-stand-alone-PV-system_fig2_269798897.
- [8] Guy Chateigner, Michel Boës, "Manuel de génie électrique", Dunod, 2007.
- [9] Philippe Barrade, "électronique de puissance méthodologie et convertisseurs élémentaire", press polytechnique et universitaires, 1ère édition 2006.

- [10] Zaouche, Khélil, Etude et développement de différentes méthodes MPPT pour un système photovoltaïque(thèse de Magister Université des sciences et de la technologie Houari Boumediène) 2009.
- [11] « DC-DC Converters » available online <https://www.mongosukulu.com/index.php/contenu/genie-electrique4/electronique-depuissance/550-leshacheurs?showall=1/>.
- [12] S.C. Tan, Y.M. Lai, C. K. Tse, and M.K.H. Cheung, "Adaptive Feedforward and Feedback Control Schemes for Sliding Mode Controlled Power Converters," IEEE Transaction on Power Electronics, vol. 21, no. 1, pp. 182-192, Jan 2006.
- [13] M .Touaref , « Etude et simulation d'un convertisseur AC/DC type BUCK (Abaisseur de tension) », thèse master en génie électrique université de Biskra, juin 2014.
- [14] M. BERROUBI Abdennoure,"Commande par mode de glissement des convertisseurs Buck et Boost intégrés dans un système photovoltaïque",DIPLÔME DE MASTER EN GENIE ELECTRIQUE, M'sila 2015/2016.
- [15] MARIAN K. KAZIMIERCZUK,« Pulse-width Modulated DC–DC Power Converters », Wright State University Dayton, Ohio, USA, 1st edition 2008.
- [16] Sofiane ait chabane ,Romain girard « Dimensionnement des composants passifs d'un convertisseur Buck » UFR PH ITEM - Université Joseph Fourier 2011.
- [17] Hidri.Imed, « électronique de puissance Les convertisseurs DC-DC et DC-AC », Cour d'électronique de puissance, l'ISET de Nabeul.
- [18] A.Ayad, Etude et réalisation d'une commande MLI pilotant un hacheur série, thèse de Master en électrotechnique, Tlemcen: Univercité Abou Bakr Belkaid, 2014.
- [19] Dr. Aissa Oualid, «Cours Régulation Industrielle, Chapitre 04 : Les Régulateurs Standards : P, PI, PD et PID», 3eme année Licence, Spécialités: ELT et ELM.
- [20] SAHRAOUI M, "Contrôle robuste des systèmes non linéaires par les approches de l'intelligence artificielle",DOCTORAT EN SCIENCES, Université d'Oran1 A. Ben Bella,2016.

- [21] Zemouri Azeddine, «étude expérimentale d'un convertisseur DC/DC contrôles par une commande robuste», Thèse de magister, Université Batna.2014.
- [22] M. BERROUBI Abdennoure, Commande par mode de glissement des convertisseurs Buck et Boost intégrés dans un système photovoltaïque, DIPLÔME DE MASTER EN GENIE ELECTRIQUE, UNIVERSITE MOHAMED BOUDIAF-M'SILA 2015 / 2016.
- [23] Akshay Kumar Rathore" Two Loop Average Current Control of Boost Converter" National University of Singapore, www.ece.nus.edu.sg/stfpage/akr, Dernier accès: 28/04/2016.
- [24] A. A. A. ZENAZEL Leila, ETUDE ET REALISATION DES CONVERTISSEURS EQUIPANT LE TRAIN, SIDI BEL ABBES, 2018.
- [25] Proteus interface available online <https://cpge.frama.io/fiches-cpge/Proteus/1-Demarrage/>
- [26] M. A. Elgendy; B. Zahawi; D. J. Atkinson "Evaluation of perturb and observe MPPT algorithm implementation", techniques Conference Paper · January 2012 DOI: 10.1049/cp.2012.0156
- [27] Alldatasheet IRFP140N DATASHEET, available online ,<https://html.alldatasheet.com/html-pdf/67538/INTERSIL/IRFP140N/322/1/IRFP140N.html>
- [28] Alldatasheet IRFZ44N DATASHEET , available online <https://html.alldatasheet.com/html-pdf/17807/PHILIPS/IRFZ44N/246/1/IRFZ44N.html>
- [29] Alldatasheet IRF2807 DATASHEET, available online ,<https://html.alldatasheet.com/html-pdf/68130/IRF/IRF2807/46/1/IRF2807.html>
- [30] M. K. Kazimierczuk and J. Jo´zwik, New topologies of high-efficiency high-frequency zero- ´ voltage switching resonant dc/dc converters. Proc. 29th IEEE Midwest Symposium on Circuits and Systems, Lincoln, NE, 1986, pp. 474–477.
- [31] Alldatasheet MBR3060PT DATASHEET, available online ,https://www.alldatasheet.com/view.jsp?Searchword=Mbr3060pt&gclid=EAIaIQobChMI0cfR806n_wIVVQCLCh2boAWHEAAYASAAEgJt1fD_BwE

- [32] Utmel IR2112 DATASHEET, available online ,<https://www.utmel.com/components/ir2112-driver-ic-circuit-pinout-and-datasheet?id=543#cat1>
- [33] Mouser UF4007 DATASHEET, available online ,<https://www.mouser.fr/ProductDetail/onsemi-Fairchild/UF4007?qs=NwIfwa72Flp1AHiXupLMBA%3D%3D>